Journal of the National Academy of Forensic Engineers®

http://www.nafe.org

ISSN: 2379-3252

DOI: 10.51501/jotnafe.v43i1

Vol. 43 No. 1 June 2026

National Academy of Forensic Engineers®

Journal Staff

Technical Review Process

The Technical Review Committee Chair chooses the reviewers for each Journal manuscript from amongst the members and affiliates of the NAFE according to their competence and the subject of the paper, and then arbitrates (as necessary) during the review process. External reviewers may also be utilized when necessary. This confidential process concludes with the acceptance of the finished paper for publication or its rejection/withdrawal. The name(s) of authors are included with their published works. However, unpublished drafts together with the names and comments of reviewers are entirely confidential during the review process and are excised upon publication of the finished paper.

National Academy of Forensic Engineers®

Board of Directors

President
Tonja Koob Marking, PhD, PE, DFE
Senior Member

President-Elect
Daniel Couture, PEng, DFE
Senior Member

Senior Vice President
Ben Railsback, PE, DFE
Fellow

Vice President
Greg Boso, PE, DFE
Member

Treasurer
Bruce Wiers, PE, DFE
Senior Member

Secretary
Shawn Ray, PE, DFE
Senior Member

Past Presidents
Michael Aitken, PE, DFE
Senior Member

Steven Pietropaolo, PE, DFE
Senior Member

Joseph Leane, PE, DFE
Fellow

Directors at Large
Paul Tucker, PE, DFE
Senior Member

Michael Stichter, PhD, PE, DFE
Member

Executive Director
Amanda Hendley

Journal of the National Academy of Forensic Engineers®

Editorial Board

Submitting Proposed Papers to NAFE for Consideration

Please visit the Journal's author page for submission details.

We are looking for NAFE members who are interested in giving presentations on technical topics that will further the advancement and understanding of forensic engineering at one of the academy's biannual meetings and then developing those presentations into written manuscripts/papers, which will go through a single-blind peer review process before publication. Only papers presented at a NAFE regular technical seminar and that have received oral critique at the seminar will be accepted for review and publication. We recommend that you review the About the Journal page for the journal's section policies as well as the Author Guidelines listed on the Submissions page. Authors need to register with the Journal prior to submitting, or (if already registered) they can simply log in and begin the process. The first step is for potential authors to submit a 150-word maximum abstract for consideration at an upcoming conference into the online journal management system.

Copies of the Journal

The Journal of the National Academy of Forensic Engineers® contains papers that have been accepted by NAFE. Members and Affiliates receive a PDF download of the Journal as part of their annual dues. All Journal papers may be individually downloaded from the NAFE website. There is no charge to NAFE Members & Affiliates. A limited supply of Volume 33 and earlier hardcopy Journals (black & white) are available. The costs are as follows: $15.00 for NAFE Members and Affiliates; $30.00 for members of the NSPE not included in NAFE membership; $45.00 for all others. Requests should be sent to NAFE Headquarters, 1266 W Paces Ferry Rd NW #141, Atlanta, GA 30327 or call (770) 268-0802.

Comments by Readers

Comments by readers are invited, and, if deemed appropriate, will be published. Send to: Ellen Parson, Journal Managing Editor, 3780 SW Boulder Dr., Lee's Summit, MO 64082. Comments can also be sent via email to journal@nafe.org.

Table of Contents

‡ Paper presented at the NAFE seminar held in July 2024 in Ann Arbor, Mich.
ᴗ Paper presented at the NAFE seminar held in July 2025 in Ottawa, Canada
§ Paper presented at the NAFE seminar held in January 2026 in New Orleans, La.

Investigating Effects of Imperfections on Aluminum Stepladder Using Finite Element Analysis

By John Thomazin, PE, DFE (NAFE #1188M), Bill Webster, and Sai Kosaraju, PhD

Abstract

Ladders are a valuable tool, but they can also be dangerous. In 2020, ladder-related falls resulted in more than 100 fatalities and thousands of injuries, particularly in the installation, maintenance, and repair industries [1]. The ANSI A14.2 standard governs the safe construction, design, testing, and use of portable metal ladders, outlining requirements for ladder rung spacing, connections, and angle of inclination. While 15 different load tests are performed to ensure a ladder meets the standard, it's important to note that these tests use statistical tolerances and represent pass/fail criteria. Altering the cross-section of a shape can impact its stiffness, and imperfections can affect a structure's collapse. Understanding the testing limitations is crucial. To reduce ladder-related injuries and fatalities, imperfection-sensitive ladders can be detected, evaluated, and identified using 3D modeling and nonlinear finite element analysis (FEA). This paper presents a technique for using linear-elastic buckling analysis to identify potential failure modes. It is followed by nonlinear static analysis with material plasticity to detect significant decreases in strength when dents or other imperfections are included in the geometry or when the applied load directions are changed.

Keywords

Forensic engineering, finite element analysis, FEA, structural safety, ladder design, fall-related injuries, ANSI standards A14.2, load testing, workplace safety, imperfection sensitivity, 3D modeling, simulation, computer-aided engineering, CAE

Ladder Hazards & Injuries

The stepladder is a mechanical linkage consisting of front and back rails connected with spreaders that are used to lock the front and back rails in the open position. Steps on the front rails are spaced at approximately 1-foot intervals. Once the stepladder is locked in position, the feet form a base along with the four rails, creating two basic triangles that form a rigid, stable framework suitable for climbing.

Ladders, a tool in use for more than 10,000 years, have seen significant advancements in safety. The first practical folding stepladder was invented by John H. Balsley, a skilled carpenter from Pennsylvania. His patent in 1862 marked a significant improvement in ladder safety, as he replaced round rungs with flat steps and added hinges for easy folding and storage when not in use [2].

Ladders are useful tools both at home and at the worksite; however, they can also be dangerous. Many hospital visits result from ladder falls. According to the National Institute for Occupational Safety and Health (NIOSH), ladder-related falls account for more than 100 fatalities and thousands of injuries each year [1]. In 2020, there were 22,710 injuries caused by ladder-related falls, compared with 22,330 in 2019. The installation, maintenance, and repair occupations had the highest ladder-related injuries — with 5,790 incidents reported. Construction and extraction occupations accounted for 5,370 ladder injuries, and service occupations had 3,160 [3]. Despite efforts at improving safety and training, the number of fatalities and ladder-related injuries from falls does not change much from year to year.

John Thomazin, PE, DFE, 1925 Westbourne Dr., Oviedo, FL 32765, (407) 375-1435, jthomazin@outlook.com

Injury and Background

In the late summer of 2019, a homeowner was using a stepladder purchased from a home-improvement retail chain. As the stepladder was being used for household chores, the side rail components of the stepladder's A-frame buckled, resulting in instability, downfall, and collapse. The stepladder was allegedly not overloaded or subject to abuse at the time of the collapse. The homeowner landed on his backside and was injured by the collapse. Settlement terms of the case prevent disclosure of the parties' names and product brands. The subject stepladder was sold throughout the United States and distributed through major home-improvement retail chains. The subject stepladder is made of aluminum and has a rated load capacity of 250 pounds.

ANSI Standards and Certifications

The subject stepladder is marked with the American National Standards Institute (ANSI) A14.2, Occupational Safety and Health Administration (OSHA) certification label. The Metal Ladder Manufacturers Association is responsible for initiating the ANSI standard for portable metal ladders, dating back to May 1951. The ANSI 14.2 standard prescribes rules governing the safe construction, design, testing, care, and use of portable metal ladders of various types and styles [4].

As shown in **Figure 1**, there are five duty ratings and ladder types with working-load limits ranging from 200 pounds to 375 pounds. According to the label on the subject stepladder, the ladder's size was 6 feet, the maximum reach was 10 feet, and the highest standing level was 3 feet, 10 inches. It has a tray for holding tools or one paint can and slots for a roller tray. As such, the subject ladder would be considered "light duty."

Development of ANSI Ladder Standards

The prescriptive standard aims to provide reasonable safety for life, limb, and property. The voluntary standard on portable ladders is one of many American National Standards prepared under the ANSI Accredited Standards Committee on Safety in the Construction, Care, and Use of Ladders (A14). The subcommittee for portable metal ladders is A14.2.

Duty Rating	Ladder Type	Working Load (lb)	Size (ft)
Special Duty	IAA	375	3-12
Extra Heavy Duty	IA	300	3-20
Heavy Duty	I	250	3-20
Medium Duty	II	225	3-12
Light Duty	III	200	3-6

Figure 1
Classification of stepladders by duty rating, type, and size.

Section five of A14.2 outlines portable metal ladders' general safety and performance criteria. The requirements are kept to a minimum to allow for various combinations of metals and design alternatives when designing and constructing the ladders. This section specifies dimensions such as rung spacing, width, and height, ensuring the ladders provide a stable and comfortable climbing experience. Other features, such as rungs, steps, and railings, must comply with safety specifications regarding size and shape. Designers and manufacturers must ensure that ladders are designed and constructed to safely support the loads they will encounter during use, accounting for strength, durability, and stability. The construction materials must be high-quality and appropriate for ladder manufacturing. Furthermore, the design must ensure that the ladder is strong and stiff enough to meet the performance requirements of this standard and is free from structural defects or accident hazards, such as sharp edges or burrs.

The standard outlines the safe construction, design, testing, care, and use of metal ladders. The testing procedures in section seven were developed for three applications: design verification, quality control, and in-service testing. During the original design development of the product, design verification tests are generally conducted as destructive tests. The manufacturer performs quality control tests on an ongoing basis, including both destructive and nondestructive tests.

The standard's remaining sections outline the most appropriate procedures for ladder care, selection, and use. They also specify the required labeling and product data information marks for the different types of ladders.

Investigation and Examination

For the subject incident investigation, the homeowner was available for an interview, and the room where the fall happened was measured, photographed, and 3D-scanned. The subject stepladder was also measured and photographed. The assembled stepladder framework uses rivets to fasten aluminum and plastic components into the finished product. The braced aluminum side rails are open-section C-shaped members joined by steps, rungs, cleats, or rear braces at regular intervals. The thickness of the aluminum side rails connecting the rungs was approximately 14 gauge (0.0747

inches). The aluminum back rails are open-section C-shaped members with unequal legs. The thickness of the aluminum back rails was approximately 13 gauge (0.0897 inches). The diameter of the rivets was approximately $^{3}/_{16}$ inches. The subject stepladder generally met the requirements of Section 5 and the specifications of section 6 of ANSI A14.2. Additionally, it fulfilled the labeling/marking requirements of Section 9.0 in ANSI 14.2.

According to A14.2 requirements, the physical loads on the stepladder, and the homeowners' description of use before the collapse, the ladder should not have collapsed. The stepladder was set up on carpet, and the floor was even and firm. The homeowner weighed approximately 160 pounds — well below the ladder's working load limit. According to the claimant, at the time of the incident, the stepladder was not overloaded, and the weight was centered on its base. As shown in **Figure 2**, the right front side rail of the stepladder buckled near the first rung and braces by the connections. Overall, buckling initiated below the lower rung near the connections along the shorter, horizontal axis of the two front-side rails.

Exemplar Ladder

An exemplar ladder was purchased for comparison. The exemplar and subject ladders were manufactured at the same plant four years apart. The authors photographed, measured, and documented the exemplary ladder and used those measurements to create a 3D CAD model, which could then be used in FEA simulation software.

Manufacturer's Testing

The test requirements in A14.2 Section seven are preferred methods to determine whether a ladder conforms to the standard's requirements. The tests that were developed for the standard use statistical methods. If a single test fails, then the test can be repeated using a sufficient sample size to ultimately determine whether a ladder passes or fails a test. In the case of a stepladder, various loads are placed on it — usually for 1 minute. If the ladder does not collapse or permanently deform after the test, it has passed. In all, there are about 15 different load tests for a stepladder. This analysis addresses only one test: the *Torsional Stability Test*, which is a design verification test.

After the incident, the manufacturer performed physical testing on the exemplar stepladder to recreate the damage and deformation seen in the subject stepladder. The physical testing was video recorded and narrated. The testing consisted of a demonstration and modified A14.2 test cases. In the demonstration, the product tester stepped on the bottom rung of the ladder, gently lifted the front rails of the ladder, and twisted the stepladder at the top to simulate a walking motion. The implied purpose of the demonstration was to show that the stepladder could be misused without collapsing.

FEA vs. Physical Testing

The manufacturer's tests did not replicate the buckling response seen in the subject stepladder. The post-buckling damage observed in the stepladder's side rails implies a torsional loading condition or walking motion before collapse. Desired confidence intervals and error levels establish the necessary sample size for testing [5] [6]. High confidence intervals and low error levels require more test trials, and vice versa (**Figure 3**). The great advantage of computer simulation is that multiple trials can be run at a fraction of the time and labor of a physical test. In addition, the model can predict failure modes before failure. A stepladder response can forewarn of potential failure modes present in the stepladder's structure.

The torsional loading test case in ANSI 14.2 Section 7.5.12 *Rail Torsion and Spreader Test* was chosen for FEA, as shown in **Figure 4**. After the FEA analysis, ANSI physical tests could be performed, and the results compared, if needed. In Section 7.5.12, the test unit should be placed on a level floor, with a 200-pound load applied to the ladder top cap and a horizontal force applied to the top cap. The ladder should withstand the forces without damage. Ladders with a bucket shelf should be tested with

Figure 2
Buckled condition of the front side rails for the subject stepladder.

Error \ Confidence level	99	95	90	85	80	75	70
0.05	664	385	271	208	165	133	108
0.1	166	97	68	52	42	34	27
0.15	74	43	31	24	19	15	12
0.2	42	25	17	13	11	9	7

Sample size needed to meet confidence interval at error level.

Figure 3
Sample size needed for various confidence intervals and error levels.

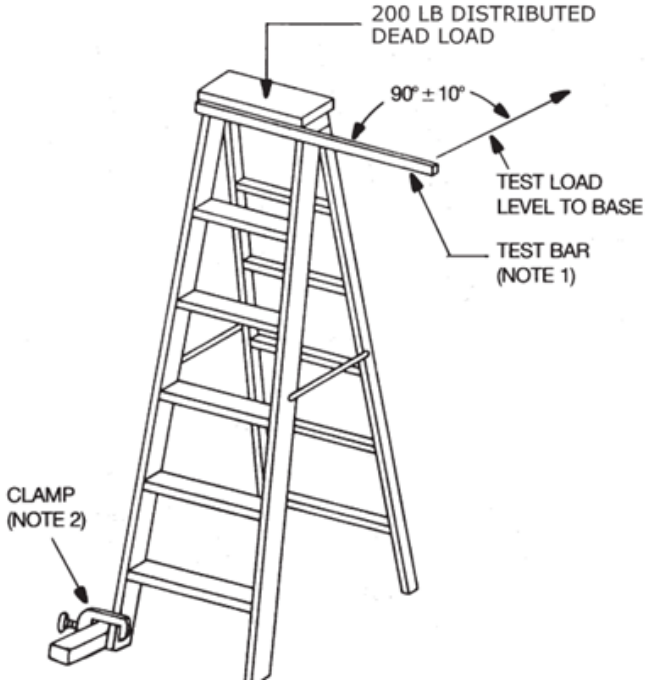

(1) The test bar is clamped to the top cap.
(2) Clamp only used for the rail torsion and spreader tests in 7.5.12.

Figure 4
Setup for rail torsion and spreader test.

the shelf in the in-use position, and step stools are exempt from this test.

The stiffness of a ladder or any framework combines material elasticity, given as Young's modulus, and geometry. The shape of individual components, combined with the overall assembled geometry of the structure, determines the framework's stiffness. Changing the cross-section of a shape can increase or decrease its stiffness. Dimensionally larger cross-sections are generally stiffer than dimensionally smaller cross-sections. To change the stiffness and affect a favorable response, a designer can change either material, geometry, or a combination of both geometry and material. Gaining insight into the response of the stepladder's assembled framework to external loads can start with an understanding of the response of individual components to external loads.

The buckling of bars, frames, plates, shells, or other members is a response to compressive axial loads. Buckling occurs when a member converts membrane strain energy into bending strain energy without changing externally applied loads [7, Ch. 14]. There is no forewarning when conditions become critical — that moment when buckling is imminent — and any slight change in the deformation state triggers an instant conversion of membrane energy to bending energy. Comparatively, a member can store huge amounts of membrane strain energy, but bending strain energy can only absorb the released membrane energy with large lateral deflections and cross-sectional rotations. In other words, buckling occurs without forewarning when compressive forces reduce the bending stiffness to near-zero for some deformation mode, and potential energy rapidly converts to kinetic energy with large lateral deformations.

FEA is a good tool for gaining insight into stress distribution throughout ladder components before the onset of buckling behavior. Both a limit-state analysis and a computer-aided linear-bifurcation buckling analysis may over-predict the failure load of a structure. The goal of the forensic engineer is to understand if the structure loses strength when applied to various loads.

The post-buckling response of a structure becomes nonlinear, and stiffness is reduced. A loss of stiffness can result in large deformations without any increase in load. In that case, the performance of a structure is strongly affected by small changes in the direction of the loads, the manner of support, or changes in the structure's geometry. Changing the geometry of the structure or cross-sectional properties of a member is an effective means for favorably changing the response of a structure to prevent collapse. Accordingly, FEA is an effective technique for modeling the effects of changes.

Finite Element Model and Workflow

The initial step in any simulation process, following thorough research and planning, is generating an appropriate model for analysis. Broadly, this entails creating a finite element mesh, applying relevant material and section properties, modeling connections, interactions, or contact phenomena, and finally, constraining and loading the structure. While the process may appear straightforward, it requires significant expertise and a deep understanding of physics to be executed correctly. The FEA workflow for evaluating buckling sensitivity generally unfolds in four stages, as depicted in **Figure 5**.

Following the creation of a detailed ladder model, a linear buckling analysis was performed to estimate buckling loads, yielding results comparable to those from hand calculations. Although this analysis is relatively simple and based on linear assumptions, it offers several advantages. First, it provides a more efficient method for conducting traditional buckling calculations on complex

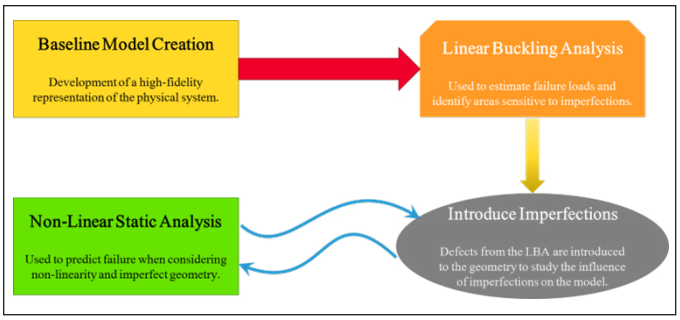

Figure 5
General workflow for FEA buckling model creation and analysis.

structures compared to manual calculations using free-body diagrams and spreadsheets. More importantly, it identifies potential failure locations in the structure and predicts the failure mode or shape. This information empowers engineers to make qualitative design improvements, alter load paths, and adjust boundary conditions to mitigate risks of failure. Additionally, linear buckling analyses are computationally inexpensive, allowing for the rapid evaluation of design alternatives. For reference, each buckling simulation was completed in approximately 3 minutes.

In the subsequent workflow phase, geometric imperfections were introduced to assess sensitivity to various defects. The authors examined thickness and section defects by reducing the thickness of the front leg and shortening the length of the C-channel flange. Shape defects were also explored, although their introduction posed challenges in terms of model implementation. Determining the defect's size, shape, and placement within the model required careful consideration to ensure a meaningful impact on the results. By leveraging the buckled shapes from the linear buckling analysis, the authors ensured that imperfections were properly sized, shaped, and positioned to yield worst-case scenarios.

The final phase involved conducting a nonlinear static analysis on both the baseline geometry and the models with geometric defects. This analysis considers material plasticity, load redistribution, section changes, contact, and stress stiffening, making it more realistic than linear analyses or hand calculations.

Material and Model Discretization

Creating a model for FEA begins with a thorough understanding of the material properties. In the absence of specific material properties for the ladder under investigation, the authors used properties for 6061-T6 aluminum, which are well-documented in existing literature. Aluminum 6061-T6 is recognized for its favorable mechanical properties, corrosion resistance, widespread availability, and relatively low cost compared to other aluminum alloys. They referenced MMPDS-04 [8], a key standard for metal material properties in the aerospace industry (**Figure 6a**), to obtain engineering properties such as Young's modulus, yield strength, ultimate strength, and elongation — necessary for defining the model's material behavior (**Figure 6b**).

The nonlinear stress-strain behavior was approximated using the Ramberg-Osgood equation, which has shown excellent correlation with physical test data for metals such as steel, aluminum, and titanium. This method, developed in 1943, relates strain to stress, Young's modulus, a material-specific strength coefficient, and a material-specific hardening coefficient. These coefficients can be calculated using readily available engineering data, making it a convenient method for approximating nonlinear material behavior without the need for test data.

The ladder model included aluminum components as well as plastic and rubber parts. The top cap was made from ABS plastic, and the ladder feet were made of rubber. Linear elastic material properties were used for the ladder cap, as it was not a primary focus and was not subjected to significant stress. The rubber feet were omitted from the model due to their minimal structural impact.

The modeling approach employed shell elements for the main structural components, a process known as

FEA Material Properties						
Component	Material	Young's Modulus (ksi)	Poisson's Ratio	Yield Strength (ksi)	Ultimate Strength (ksi)	Elongation (%)
Structural Components	6061-T6 Aluminum	9900	0.33	35	42	16
Plastic Cap	ABS Plastic	350	0.37			

Figure 6a
Aluminum 6061 material properties.

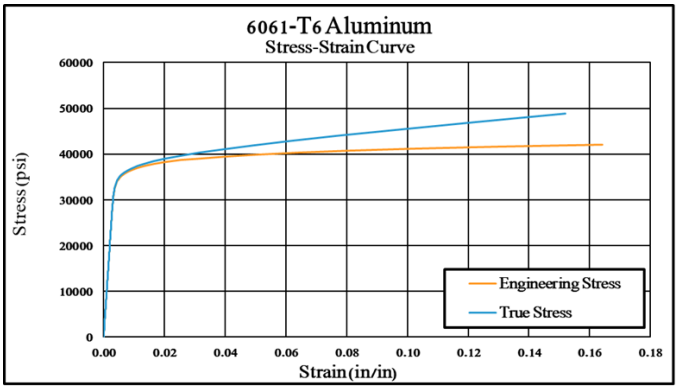

Figure 6b
Aluminum 6061 material behavior modeled by FEA.

midplaning, which involves creating a 2D mesh to represent a 3D structure. While this approach might initially seem counterintuitive, shells provide the most accurate and cost-effective solution for modeling thin-walled structures under bending. A 1-inch mesh size was primarily used, which, although relatively large, was sufficient to generate an accurate stiffness matrix and predict correct displacements. However, the large mesh size may result in non-converged stress values, which were addressed by locally refining the mesh near failure locations. Sensitivity studies determined the appropriate mesh size in these areas, ultimately settling on a 3-millimeter mesh size in regions near the bottom of the front left leg and the proximal angle braces, as shown in **Figure 7**.

The connection of the ladder structure was simplified using TIED constraints (an Abaqus keyword) to bond neighboring components at the overlapping interface, rather than modeling the complexity of rivets and associated contact between components. This level of detail was deemed sufficient because the failure mode was not related to the joints, and the load path could still be accurately captured using TIED constraints. This approach is also supported by St. Venant's principle, which posits that the exact distribution of load near the point of application does not significantly affect the stress distribution at a distance, thereby ensuring global accuracy despite local modeling simplifications.

Boundary Conditions and Loads

With a highly accurate simulation model created, the next step was to constrain and load the model to replicate the test conditions outlined in ANSI A14.2. The front left leg of the ladder was fully clamped to prevent all translation and rotation, while the other three legs were c onstrained only in the downward direction, allowing them to slide or lift off the ground — similar to a ladder on a frictionless surface.

The ladder was loaded according to ANSI A14.2, with a 200-pound distributed dead load applied downward on the ladder's top cap. A rigid bar was clamped to the top cap, and a rearward load was applied to that rigid bar 18 inches from the ladder's longitudinal centerline (**Figure 8**).

FEA Analysis Techniques

Finite element analysis was conducted using Abaqus 2024 [9] to examine the structural response of a ladder under loads similar to those outlined in ANSI A14.2. As summarized in **Figure 9**, the study involved two types of analyses: linear buckling analysis and nonlinear static analysis. Linear buckling analysis is akin to arithmetic, providing

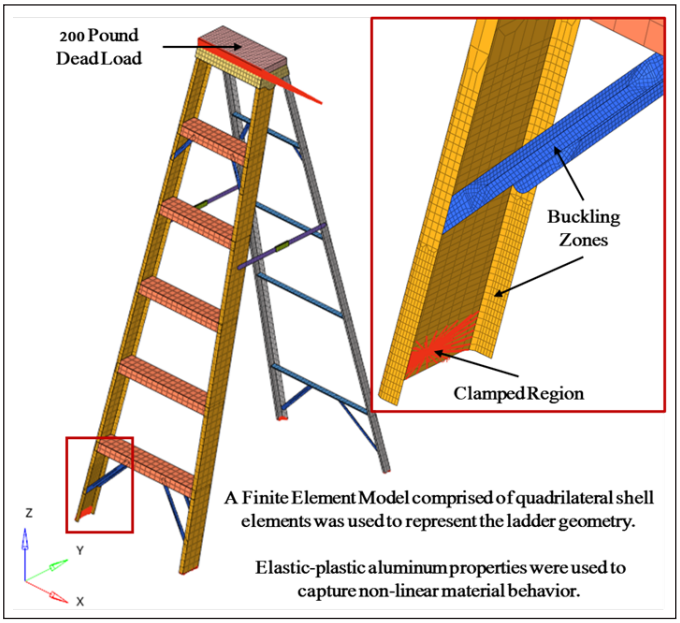

Figure 7
Finite element model of the stepladder.

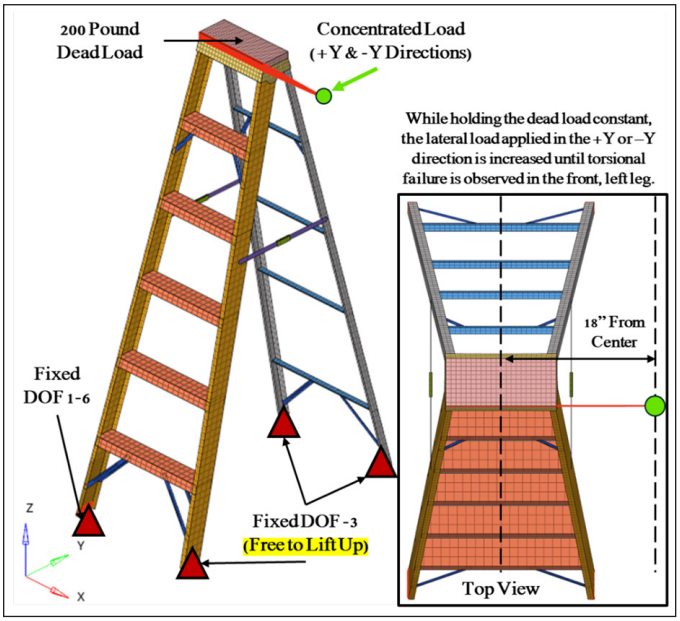

Figure 8
Loading and boundary conditions of the stepladder.

Linear Buckling Analysis	Nonlinear Static Analysis
• Used to estimate the critical bifurcation load of stiff structures.	• Used to evaluate the non-linear structural response to loading.
• Inherently linear: elastic material properties & linear geometry only.	• Considers material plasticity and changes to geometry arising from loading-induced deformation.
• Can be used to extract deformed shapes used in subsequent imperfection sensitivity analyses.	• Used to understand the non-linear force-deflection behavior of a system.
• Useful in identifying collapse mode shapes but can often overestimate failure loads due to inherent linearity.	• Provides a more accurate solution by accounting for non-linearities that may arise prior to elastic buckling.

Figure 9
Summary of analysis techniques used in the FEA study.

a simple and efficient method for estimating critical bifurcation loads in stiff structures. Nonlinear static analysis (comparable to calculus) accounts for material plasticity, load redistribution, and geometric changes, yielding more accurate results for complex scenarios.

Linear buckling analysis predicts elastic buckling by estimating the critical bifurcation load, offering accurate and cost-effective quantitative results for structures experiencing true elastic buckling. However, its inherent linearity limits its accuracy, which fails to account for material plasticity, changes in loading direction, loss of section properties due to deformation, or contact between neighboring bodies. As a result, linear buckling analyses often overestimate the magnitude of buckling failure, particularly in structures that experience significant material yielding.

In contrast, nonlinear static analysis evaluates a system's nonlinear structural response, accounting for material, geometric, and contact nonlinearities. This method provides a deeper understanding of the true physics involved and yields more accurate results than linear analyses.

Linear Buckling Analysis Results

The linear buckling analysis results shown in **Figure 10** revealed several interesting trends. The first buckling mode occurs in the angle brace, a thin, relatively flat piece of metal loaded in compression. However, the buckling of the angle brace does not necessarily lead to the collapse of the ladder, as the front leg is the primary load-carrying member. To assess the potential for ladder collapse, it is crucial to identify the buckling mode affecting the area of interest.

When the ladder is loaded according to ANSI A14.2, the first buckling mode affecting the left front leg occurs at a load of 164 pounds, and Positive Y was applied. Interestingly, when Negative Y was applied, the first buckling mode occurs at a load of only 77 pounds — a decrease of over 50 percent compared to the baseline (**Figure 10**). This discrepancy arises due to the different stiffnesses of the C-channel under positive and negative bending moments. However, despite this discrepancy, the ladder still meets the 30-pound requirement even when loaded in the opposite direction to that which is specified by ANSI A14.2.

Linear Buckling Results				
Buckling Mode	Positive Y (ANSI Standard)		Negative Y (Opposite Direction)	
	Torsional Load (lb)	Buckling Location	Torsional Load (lb)	Buckling Location
1	31.1	Rear Brace	19.8	Forward Brace
2	67.5	Rear Brace	43.9	Forward Brace
3	114.4	Rear Brace	77.4	Leg Below Rear Brace
4	134.6	Rear Brace	80.6	Forward Brace
5	152.4	Rear Brace	81.0	Forward Brace
6	161.3	Rear Brace	83.7	Leg Below Rear Brace
7	163.9	Leg Side Wall	104.7	Forward Brace

Figure 10
Linear buckling modes with red text identifying modes likely to result in ladder collapse.

When loaded in the ANSI A14.2-specified direction, the buckling results can be animated to demonstrate that the first six modes affect the angle braces. Although the angle brace may buckle before the leg, it does not necessarily cause a collapse. However, the buckling of the side wall of the front leg, as shown in **Figure 11**, aligns with the observed failure in the field. With symmetry in the structure, modeling failure on the left front leg would be mirrored on the right front leg, which was the incident failure.

When the load is applied in the opposite direction, the buckling modes follow a similar trend, with the first several modes primarily affecting the angle braces. The third buckling mode, however, occurs at the same location where plastic failure was observed in the subject ladder, as shown in **Figure 12**.

In gathering data for analysis, the author evaluated three types of imperfections. A thickness imperfection was

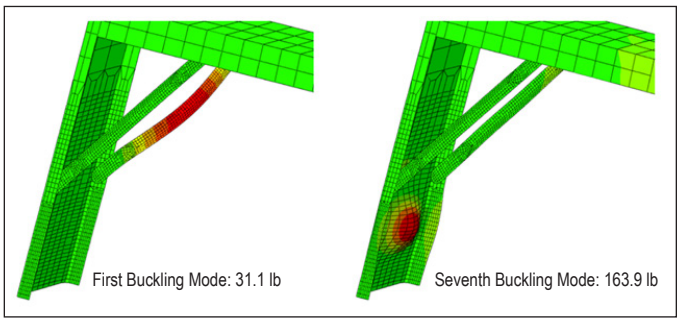

Figure 11
Linear buckling results when loaded in the +Y direction (loaded in accordance with ANSI A14.2).

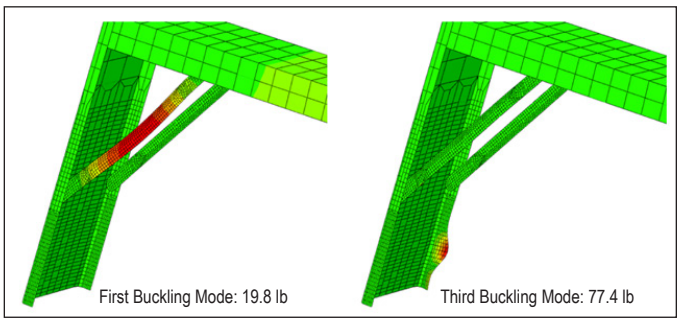

Figure 12
Linear buckling results when loaded in the Y direction (loaded in opposite direction to ANSI A14.2).

simulated by reducing the thickness of the front leg by 0.004 inches — the tolerance for 14-gauge aluminum. Section imperfections were simulated by reducing the widths of each leg flanges — first by ⅛ inches and secondly by ¼ inches. Five shape imperfections extracted from the linear buckling analysis (LBA) were introduced into the modeled geometry, as shown in **Figure 13**.

One of the key applications of LBA is the visualization of deformed shapes on the original geometry. In this research, five shape defects were examined (**Figure 13**). The selected buckling mode shapes were chosen because the modeled failures all occur within the failure zone.

Nonlinear Static Analysis Results

The nonlinear results for the baseline ladder design indicated that the ladder buckles at 62 pounds under ANSI A14.2 loading conditions. However, when loaded in the opposite direction, the failure load is reduced to approximately 23 pounds — about one-third of the forward-loading capacity. As shown in **Figure 14**, while the ladder technically meets the 30-pound ANSI requirement when loaded according to the specification, it falls short when loaded in the opposite direction, highlighting a potential code enhancement concerning buckling collapse.

Further analysis revealed the reason behind the significant difference in results. When loaded according to the ANSI standard, Von Mises stresses showed material yielding initiates on the rear flange and ultimately extends across the side wall of the front leg prior to collapse. In contrast, when loaded in the opposite direction, yielding not only initiates on the rear flange but also collapses in this region (without propagating across the side wall of the front leg).

The Maximum Principal Stress plots provide additional insight into the observed failure mechanisms. Under ANSI A14.2 torsional loading (+Y direction), tensile stresses develop in the rear flange of the front leg, suppressing local flange buckling and allowing continued load transfer. As plastic deformation progresses, stresses redistribute through the side wall of the front leg, ultimately leading to global collapse driven by gross material plasticity. Conversely, when the load is applied in the opposite direction (−Y), the rear flange is placed in compression, promoting flange buckling and precipitating failure prior to significant load redistribution.

The observed behavior is further clarified by examining the ladder's force–deflection response under opposite torsional loading directions. A force–deflection curve provides a concise means of visualizing the global nonlinear response of the stepladder, including initial yielding, post-

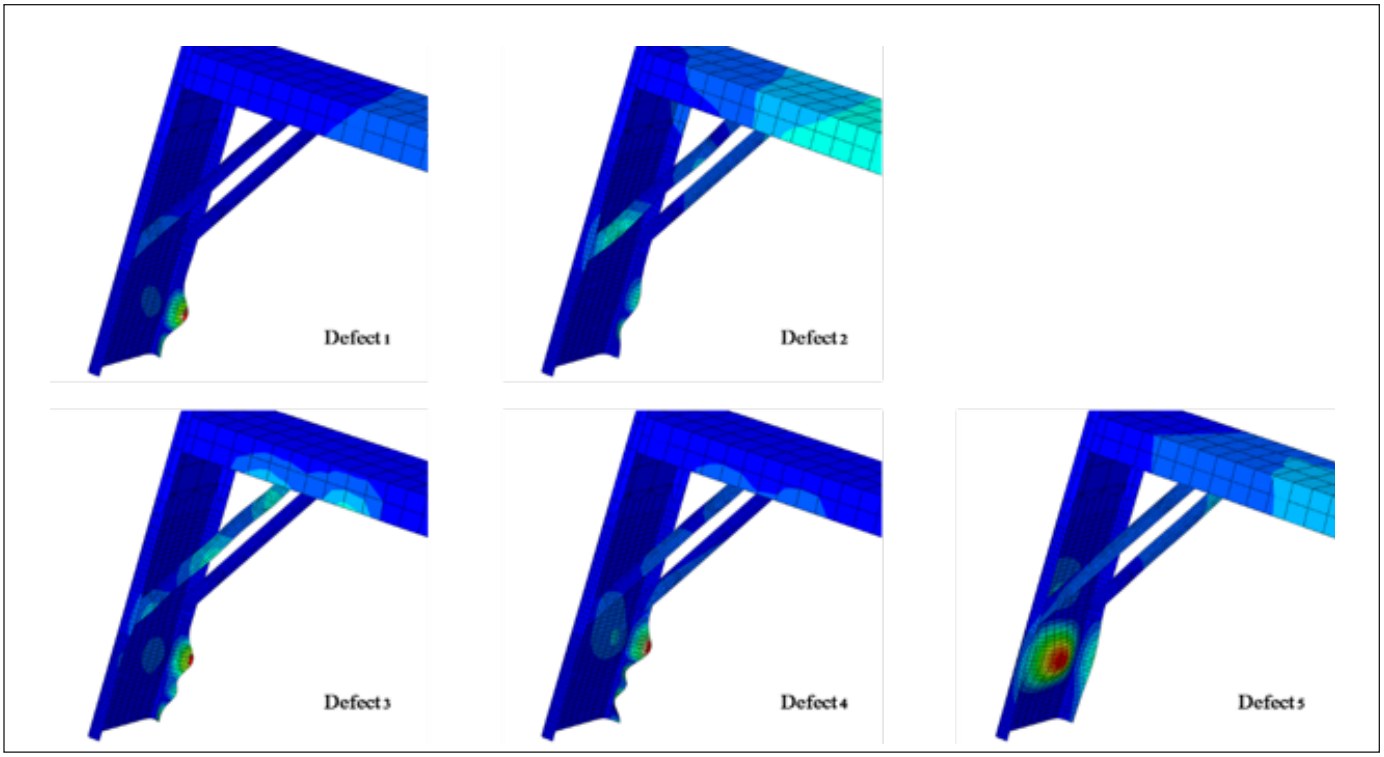

Figure 13
Imperfection definitions.

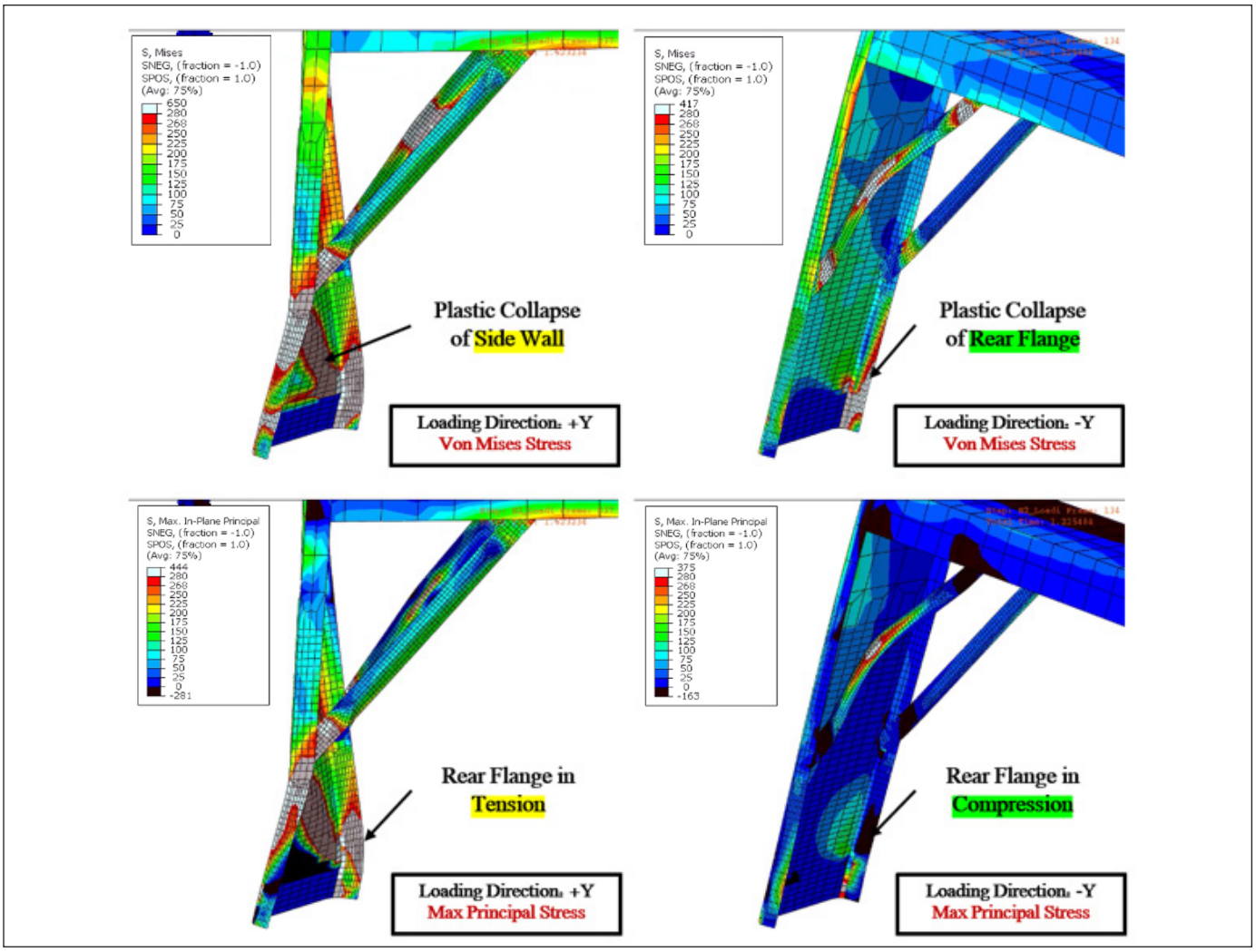

Figure 14
Nonlinear static analysis results for load directions +Y (left) and -Y (right).

buckling behavior, load redistribution, and ultimate failure.

In this study, displacement is defined as the resultant translational displacement in the global x–y plane of the node at which the torsional load is applied; specifically, the node located at the top of the stepladder on the rigid loading bar, positioned 18 inches from the ladder's centerline in accordance with ANSI A14.2. This displacement represents the motion of the rigid load application point relative to the fixed base supports and reflects the cumulative deformation of the stepladder system rather than the local deformation of an individual member. Force is defined as the applied load transmitted through the rigid loading bar at this same node in the corresponding loading direction. Both displacement and applied force were extracted directly from Abaqus as history output at the load application point and subsequently plotted to generate force-deflection curves.

When the ladder is loaded in the direction opposite the ANSI A14.2 specification (−Y direction), the force–deflection curves for the baseline and imperfect models exhibit a similar response: Initial yielding in the rear flange of the front leg is followed by a rapid loss of load-carrying capacity (**Figure 15**, left). This behavior is characteristic of flange buckling and snap-through instability, in which compressive stresses dominate and prevent significant post-yield load redistribution.

In contrast, when loaded in accordance with ANSI A14.2 (+Y direction), the force–deflection response shows a distinctly different progression (**Figure 15**, right). Tensile yielding initiates in the rear flange of the front leg, suppressing flange buckling and allowing the structure to continue carrying load. As plastic deformation develops, load redistributes into the side wall of the front leg, producing a transient stiffening response before the onset of

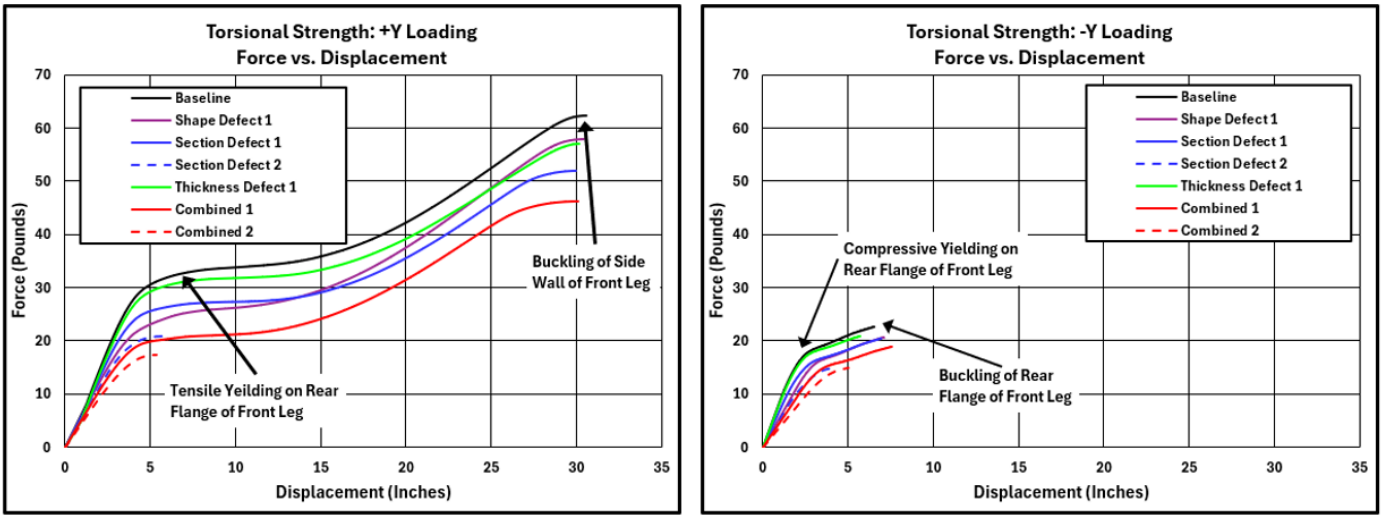

Figure 15

Force-deflection response from nonlinear static analyses for torsional loading applied in accordance with ANSI A14.2, where displacement denotes the resultant in-plane (x–y) translation of the load application node at the top of the stepladder (located 18 inches from the centerline on the rigid torsional loading bar), and force denotes the corresponding applied load transmitted through the rigid loading bar.

global collapse due to gross material plasticity. The larger displacement values observed in these curves reflect continued global deformation of the ladder assembly under sustained load redistribution, rather than excessive deformation of an individual member. For clarity and comparison, all force–deflection plots were generated using consistent axis scales. While this approach introduces unused plot space in some cases, it enables direct visual comparison between loading directions and imperfection cases without rescaling effects.

The Sensitivity of the Structure to Imperfections

The analysis of the ladder's sensitivity to imperfections revealed that nearly all introduced defects negatively impacted performance. As tabulated in **Figure 16**, the combination of multiple defects had a particularly significant impact, with strength reductions ranging from 16 to 72 percent, depending on the severity of the section change and loading direction.

Reducing section properties had the most pronounced impact on strength among the individual contributors. However, the presence of shape defects or dents in the geometry had a similar effect on performance, as did thickness reductions, despite the relatively small size of the introduced dents.

Conclusion

Physical testing is inherently constrained by time, labor, and the limited number of samples. However, FEA offers a robust alternative, demonstrating that variations in load and geometry can significantly reduce the stepladder's stiffness. When utilized correctly, FEA becomes a powerful tool for forensic investigation, enabling far more sophisticated calculations than traditional hand methods. It enables rapid iteration across designs and provides critical insights into weakening behavior that would be difficult (if not impossible) to predict with conventional approaches. Additionally, FEA software can generate compelling animations that often communicate complex information more effectively than technical data presented in spreadsheets.

The key findings of this study include the following:

1. **Loading Direction Sensitivity**: Both elastic and nonlinear analyses revealed a significant variation in performance, depending on the loading direction. Buckling response was more severe when loading was applied in the direction opposite that specified by ANSI A14.2, suggesting that the current ANSI A14.2 specification may not fully predict the buckling behavior of stepladders.

2. **Limitations of Linear Buckling Analysis**: While linear buckling analysis is effective for identifying potential failure points within a structure, it may overestimate the buckling load due to its inability to account for material plasticity, contact, or section changes.

3. **Localized Buckling vs. Structural Collapse**: The presence of localized buckling does not always signal an imminent structural collapse. Individual components can often buckle without compromising the overall stability of the structure, as seen with angle braces versus the front leg.

4. **Impact of Nonlinearities**: The nonlinear static analysis results indicated a significant decrease in performance when nonlinearities, particularly plasticity, were considered, compared to traditional elastic approaches. This underscores the importance of understanding the system's true physical behavior. An inexperienced analyst might overlook these nonlinearities when assessing buckling, potentially leading to under-design for a given load case. In contrast, experienced engineers can interpret these complexities and adapt their approach accordingly.

5. **Effect of Imperfections**: The study demonstrated that imperfections can have a material impact on structural performance.

Non-Linear Static Analysis Results					
Imperfection Type	Design Condition	Torsional Load (lb)			
		Positive Y (ANSI Standard)	% Change	Negative Y (Opposite Direction)	% Change
None	Baseline	62.3		22.5	
Thickness Imperfection	Reduced Gauge (0.004")	57.1	-8.3%	20.7	-8.0%
Section Imperfection	Reduced Section 1 (1/8")	52.0	-16.5%	20.4	-9.3%
	Reduced Section 2 (1/4")	20.8	-66.6%	14.9	-33.8%
Shape Imperfection	Defect 1	57.8	-7.2%	20.7	-8.0%
	Defect 2	59.8	-4.0%	20.8	-7.6%
	Defect 3	58.4	-6.3%	21.2	-5.8%
	Defect 4	57.3	-8.0%	21.9	-2.7%
	Defect 5	66.1	6.1%	22.4	-0.4%
Combined Imperfections	Combination 1 Reduced Gauge + Reduced Section 1 + Defect 1	46.1	-26.0%	18.9	-16.0%
	Combination 2 Reduced Gauge + Reduced Section 2 + Defect 1	17.3	-72.2%	13.8	-38.7%

Figure 16
Tabular summary of nonlinear static analysis results.

Acknowledgments

The authors would like to thank Joe Dexter, PE of Reliability Engineering, LLC, for contributing to this project. He played an important role in creating the 3D CAD model used to discretize the FEA model.

References

[1] "NEWSROOM FEATURE: Ladder Safety NIOSH," 2024. [Online]. Available: http://www.cdc.gov/niosh/newsroom/feature/ladder-safety.html. Accessed: Aug. 23, 2024.

[2] J. H. Balsley, "Improved Step-Ladder," U.S. Patent 34,100A, Jan. 7, 1862.

[3] "Fatal injuries from ladders down in 2020; nonfatal ladder injuries were essentially unchanged," *The Economics Daily*, Bureau of Labor Statistics, U.S. Department of Labor, 2022. [Online]. Available: https://www.bls.gov/opub/ted/2022/fatal-injuries-from-ladders-down-in-2020-nonfatal-ladder-injuries-were-essentially-unchanged.htm. Accessed: Mar. 20, 2024.

[4] ANSI-ASC A14.2 *Ladders — Portable Metal — Safety Requirements*. Chicago, IL, USA: American Ladder Institute, 2007.

[5] W. Hammer, *Product Safety Management and Engineering*, 2nd ed. Park Ridge, IL, USA: American Society of Safety Engineers, 1993.

[6] R. E. Walpole and R. H. Myers, *Probability and Statistics for Engineers and Scientists*, 4th ed. New York, NY, USA: Macmillan, 1989.

[7] R. D. Cook, D. S. Malkus, and M. E. Plesha, *Concepts and Applications of Finite Element Analysis*, 3rd ed. New York, NY, USA: John Wiley & Sons, 1989.

[8] *Metallic Materials Properties Development and Standardization (MMPDS-04)*. Columbus, OH, USA: Federal Aviation Administration and Battelle Memorial Institute, 2008. [Online]. Available: http://app.knovel.com/hotlink/toc/id:kpMMPDSM01/metallic-materials-properties.

Barrel Failure in an Over and Under Shotgun

By Stephen A. Batzer, PhD, PE (NAFE #677F)

Abstract

A 12-gauge over-and-under shotgun experienced a rupture in its lower barrel when firing standard factory ammunition. This incident marked the shotgun's first use in the field, as it had only been test-fired at the factory with regular-pressure shells (not proof loads) prior to this event. The barrel steel split axially ahead of the reinforced chamber, under the polymer fore-end, causing hot gases and plastic debris to violently strike the shooter's left hand, resulting in serious injury. A detailed metallurgical and geometric evaluation of the affected barrel was conducted at an independent third-party laboratory. Chemical analysis confirmed the steel matched SAE 1045 alloy with appropriate hardness for the barrel's intended thickness. Performance testing on a new, identical shotgun using intentionally overloaded shells was also carried out, despite the spent hulls from the incident showing no signs of excessive pressure. The assessment uncovered a distinct manufacturing flaw in the lower barrel, creating a localized weak spot in the barrel wall.

Keywords

Over-and-under shotgun, barrel rupture, factory ammunition, metallurgy, manufacturing defect, forensic engineering

Introduction and Background

The firearm involved in the incident was an imported "value model" over-under shotgun, chambered for 12-gauge, 3-inch shells, featuring 28-inch carbon steel barrels equipped with interchangeable chokes. The shotgun was fitted with polymer furniture. The owner, operating the firearm for the first time during a bird-hunting excursion on open farmland, used factory-loaded 12-gauge steel shot ammunition (predominantly Winchester brand).

On approximately the sixth round fired, which was the first shell discharged through the lower barrel by the owner, a catastrophic failure occurred. The lower barrel ruptured along the left side, resulting in the destruction of the fore-end and severe injury to the shooter's left hand, as depicted in **Figure 1**. Additional evidence available for examination included fragments of the fore-end, the printed owner's manual, three unfired shotgun shells, and five spent shotgun hulls previously fired through the firearm, including the final Winchester shell.

A shotgun barrel functions as a steel open-ended pressure vessel. It comprises a long cylindrical tube designed to channel multiple shots or a single slug, accelerated by combustion gases from the propellant upon cartridge discharge. Unlike rifle and pistol barrels, most shotgun barrels are smoothbore, lacking rifling, except in specialized slug guns. The barrel wall thickness is non-uniform, with the chamber exhibiting the greatest thickness and strength to withstand peak combustion stresses at the breech. The barrel thickness then decreases along the barrel length.

In modern shotguns, fast-burning smokeless propellant, akin to pistol powder, is employed, which combusts rapidly, with peak chamber pressures developed within ~1 to 3 inches of wad and shot travel down the barrel. Bore

Figure 1
Photo of the ruptured carbon steel lower barrel from the left side; red arrows indicate the chamber region welding point to the thinner and longer barrel segments leading to the muzzle.

Stephen A. Batzer, PhD, PE, 8383 M-113 E, Fife Lake MI, (479) 466-7435, batzer@batzerengineering.com

pressure diminishes rapidly past peak manifestation due to increased gas volume from axial projectile movement, adiabatic cooling that is associated with the volume increase, heat transfer to the barrel and shell, and interfacial friction, as illustrated by the representative shotgun barrel pressure trace in **Figure 2** [1]-[4].

The stress distribution within the barrel wall comprises three orthogonal principal components as illustrated in **Figure 3**, expressed in cylindrical coordinates. Isostatic atmospheric pressure is disregarded. The radial compressive stress at the inner wall (σ_r) corresponds identically to the local combustion pressure (p) as measured by the compression gauge. Additionally, axial tensile stress (σ_z) and circumferential hoop tensile stress (σ_θ) are induced.

Experimental evidence indicates that hollow cylinders subjected to excessive internal pressure predominantly — essentially universally — fail due to hoop stress. Failure typically initiates as a near-planar fracture at the inner wall, propagating toward the outer wall with axial and radial progression, resulting in either brittle or ductile surface characteristics. For most shotgun barrels, at axial positions distant from the chamber, the bore radius significantly exceeds the barrel steel thickness, satisfying the condition $r_i > 10t$. In this region, Barlow's hoop stress formula for thin-walled cylinders, given in **Equation 1**, provides sufficient accuracy to evaluate the dominant hoop stress component against the material's tensile yield stress or the designated maximum working tensile stress [5]-[6].

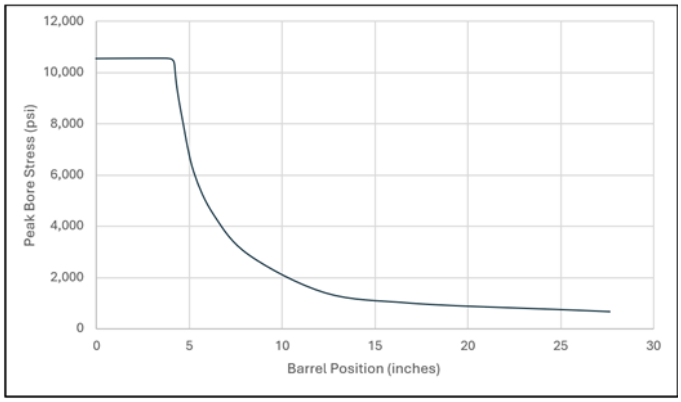

Figure 2
Schematic shape of shotgun barrel maximum bore pressure by axial position.

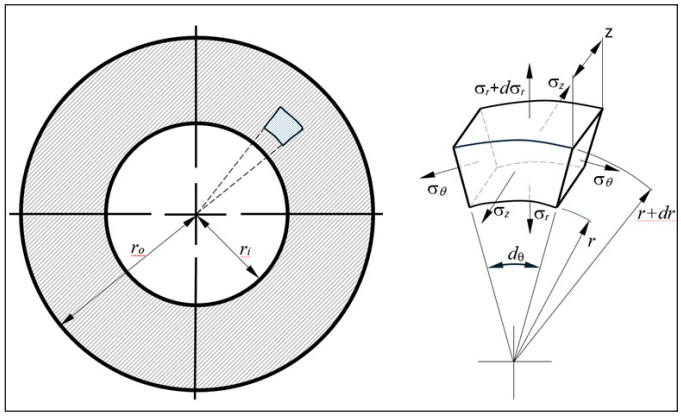

Figure 3
Orthogonal stress components associated with a shotgun barrel cylinder wall describing axial stress σ_z, radial stress σ_r, and hoop stress σ_θ.

Eq. 1: $\sigma_\theta = p * r_i / (r_o - r_i)$
Barlow's equation for pressurized cylinder hoop stress

As a failure criterion, the Barlow equation omits the radial compressive stress on the inner wall and the axial tensile stress, both of which contribute, albeit marginally, to failure in over-pressurized thin-walled cylinders. For internally pressurized cylinders with thicker walls, such as a shotgun barrel where the local condition $r_i < 10t$ is satisfied, the Lamé formulae yield more precise stress analysis results for the maximum stress components at the inner wall surface [7]-[8].

Eq. 2: $\sigma_r = -p$
Lamé equation for cylinder radial stress at inner wall

Eq. 3: $\sigma_z = pr_i^2/(r_o^2 - r_i^2)$
Lamé equation for cylinder axial stress at inner wall

Eq. 4:$\sigma_\theta = p\,(r_o^2 + r_i^2)/(r_o^2 - r_i^2)$
Lamé formula for cylinder hoop stress at inner wall

Equations 2 through **4** apply to linear elastic materials, such as steel. For failure assessment, the Lamé hoop stress equation serves as a conservative estimator and can be compared directly to the material's yield stress. Alternatively, the three orthogonal stress components can be combined using either the Tresca shear yield criterion or the von Mises distortion energy criterion, as outlined in **Equations 5** and **6**, where σ_Y represents the uniaxial tensile yield stress of the barrel material, and τ_Y represents the barrel material shear yield stress, which is conservatively approximated as half of the tensile yield stress [9]-[10].

Eq. 5: $\tau_{max} = (\sigma_\theta - \sigma_r)/2 \leq \sigma_Y/2 \leq \tau_Y$
Tresca shear yield criterion

Eq. 6: $\sigma_{max} = 1/\sqrt{2} * \sqrt{(\sigma_r - \sigma_z)^2 + (\sigma_r - \sigma_\theta)^2 + (\sigma_z - \sigma_\theta)^2)} \leq \sigma_Y$
von Mises distortion energy criterion

Forensic Engineering Analysis & Candidate Barrel Failure Mechanisms

In the examined shotgun barrel, the stresses induced in the barrel wall by the combustion gases of the propellant surpassed the material's local strength, leading to failure [11]. The injury incurred by the shooter resulted in the forensic investigation detailed in this study. The subsequent analysis focused on three key areas to ascertain whether the barrel wall's inadequate strength or excessive combustion gas pressure caused the failure.

- Shooter activities and other circumstances
- Ammunition suitability and peak pressure
- Firearm design, metallurgy, manufacturing

A technical paper by forensic investigator Stanton O. Berg summarized 33 previously published barrel obstruction tests along with their results, performed by multiple researchers [12]. Berg categorized the experiments into six different obstruction types:

1. Bullet lodged in barrel, deliberate placement
2. Bullet lodged in barrel, squib loading
3. Bullet jacket in barrel
4. Cleaning patch in barrel
5. Sand, earth, or mud in muzzle
6. Water in barrel

The results of discharging a normal pressure cartridge with bullet behind the known obstructions included:

1. No detectable damage to firearm
2. Bullet halts and lodges behind obstruction
3. Barrel burst
4. Barrel circumferentially bulged

Testing conducted by Hatcher [13] on bolt-action rifles demonstrated that excessive cosmoline — a thick, waxy grease used as a rust inhibitor — acted as a bore obstruction and resulted in outcomes ranging from no damage to a split barrel, depending on the quantity of cosmoline present. The National Shooting Sports Foundation [14] confirms similar risks for shotguns, stating, "Excessive lubricating oil or grease in the bore can lead to dangerously elevated pressures, potentially causing the barrel to bulge or rupture upon firing, posing injury risks to the shooter and bystanders."

In the case of the well-used pump action shotgun depicted in **Figures 4** and **5**, the owner reported a barrel rupture during the first discharge of the season. According to him, the barrel contained only a factory-loaded shotgun shell and residual oil from the previous season's final cleaning. A circumferential ring, located away from the chamber and formed incrementally prior to the rupture, served as a diagnostic indicator of overpressure caused by an obstruction. The existing literature does not describe a mechanism whereby the peak combustion pressure from fast-burning nitrocellulose powder propagates down a shotgun bore to induce this failure mode. However, numerous reports document secondary explosive effects from underloaded cartridges with slow-burning nitrocellulose powders [2], [15]-[17].

Figure 4
Ruptured pump-action shotgun barrel due to bore obstruction with wad retention observed at the distal end of the fracture.

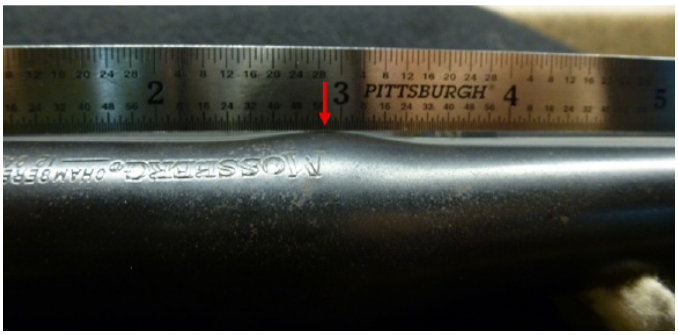

Figure 5
Circumferential ring indicative of local gas stress maximum due to a barrel obstruction in the region of the red arrow.

Shooter Evaluation

The individual involved in the incident was an adult male who had purchased the shotgun new from a local retailer. No drugs or alcohol were involved, and the shotgun was being used for legal hunting purposes — not for criminal activity, competitive shooting, or misuse. The incident occurred during the first outing with the shotgun with the failure occurring upon the initial discharge of a cartridge through the lower barrel.

One potential, though improbable, user error that could have contributed to the overpressure event is the inadvertent insertion of a 20-gauge shotgun shell into the chamber prior to the destructive shot; this barrel contamination would have acted as a barrel obstruction [18]-[19]. To investigate this possibility, a dummy 20-gauge shell was inserted into the lower barrel, and its farthest forward position was recorded. The 20-gauge test shell passed easily through the 12-gauge chamber but was halted by its rim at the forcing cone downstream of the chamber. The face of the 20-gauge dummy shell was positioned 3.4 inches from the breech face, whereas the approximate initiation point of the barrel fracture was approximately 7 inches from the breech face, as shown in **Figure 6** (where the barrel set is depicted inverted from its standard over-under configuration for clarity). Thus, this inadvertent improper ammunition substitution explanation was discarded.

Bore diameter measurements for the upper and lower barrels were obtained using a three-point internal diameter gauge with results tabulated in **Figure 7**.

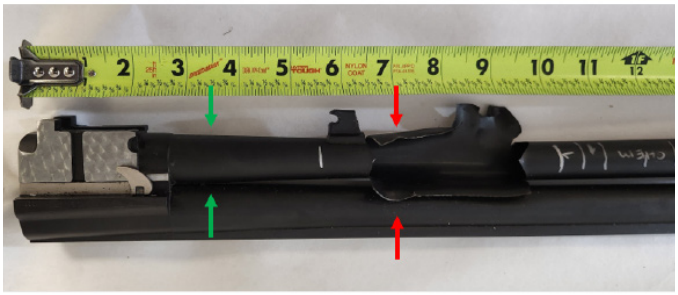

Figure 6
Close-up photo of the inverted barrel pair; green arrows mark the lodging point of the rimmed base of the 20-gauge test round, while red arrows indicate the approximate location of fracture initiation.

As recorded in the table, the inner diameter of the upper barrel is slightly smaller than that of the lower barrel. This design variation may stem from factors such as recoil management, weight distribution, balance considerations, or a perceptual effect influencing the subjective comparison of the top and bottom barrel sizes.

No credible failure causation could be attributed to the shooter in this case. The shooter did not manufacture the firearm, had no opportunity to neglect its maintenance due to the incident occurring during its first use, used ammunition that was appropriate for the firearm and not self-manufactured, and there was no evidence indicating the presence of an obstruction during the discharge.

Incident Ammunition Inspection and Analysis

A standard initial step in investigating a ruptured firearm barrel is to determine whether hand-loaded ammunition was used. Manufacturers predictably void warranties for damage associated with hand-loaded ammunition. Hand-loading is typically associated with high-volume competition shooters or long-range shooters — neither of which applies to this case. However, reloading of expended shotgun hulls is a known practice, supported by commercially available equipment for small-volume operations. “Most blown-up handguns and rifles are caused by improper hand loads. Shotgun ammunition, on the other hand, is not nearly so frequently handloaded” [18]. In this investigation, no evidence was found to suggest that the shell responsible for the rupture of the lower barrel was hand-loaded.

The cardboard box for the incident ammunition involved had been marked with the production lot number on the inner surface of a closing tab. However, this packaging was not preserved by the owner, leaving no lot number information available for the forensic investigation. An online search of the manufacturer’s website and the Consumer Product Safety Commission’s database revealed no

	Barrel Bore Internal Diameter Measurement at Position Past Breech Face (inches)											
Position	**1 – 3**	**4**	**5**	**6**	**6.5**	**7**	**8**	**9**	**10.5**	**11**	**12**	**13**
Upper	Chamber	0.728	0.727	0.728	0.728	0.728	0.725	Dent	Dent	0.728	0.728	0.728
Lower		0.735	0.735	0.736	0.734	RUPTURED			0.734	0.735	0.735	0.735

Figure 7
Measurements of bore diameter for the shotgun barrels involved in the incident.

evidence of recalls for ammunition of this make and load characteristics, either recently or historically. Exemplar ammunition of the same design remains in production, and two boxes were purchased for analysis. Multiple rounds, randomly selected from boxes bearing identical lot numbers, were disassembled to document their construction, as shown in **Figure 8**. The primer was left intact within the brass base. For reassembly of the round of **Figure 8**, the smokeless propellant would first be poured back into the empty hull, settling at the base near the primer flash hole. The white wad would then be positioned above the propellant. The shot would be loaded into the blue cup, and both components would be inserted into the red hull, which would subsequently be crimped at the end to form a star-shaped closure.

The exemplar rounds have the following mass characteristics, based upon an average of four deconstructed shells:

1.	Empty hull with primer	136.6 grains
2.	Smokeless propellant	30.9 grains
3.	White plastic wad disk	13.9 grains
4.	Blue polymer cup	38.0 grains
5.	Steel shot	543.3 grains
6.	**Total**	**762.6 grains**

Figure 8
Components of an exemplar 12-gauge shotgun round displaying decrimped plastic and brass hull, smokeless flake propellant, polymer wad, polymer shot cup, and steel shot.

The total mass of the solid ejecta is 595 grains, equivalent to 0.085 lb or 1.36 oz. The average shot mass was measured at 1.24 oz, closely aligning with the nominal 1.25 oz load indicated on the retail ammunition packaging.

No significant evidence of excessive pressure was observed on the breech face of the receiver of the incident break-action shotgun. The expended shell, which was discharged and resulted in the rupture of the lower barrel, showed no clear signs of overpressure markings. Such markings on a brass casing may include an ejector mark on the base or a flattened or cratered primer. Soot around the primer pocket generally indicates gas leakage due to a loose primer pocket rather than overpressure. As noted by Naramore, “Primers are of very little value in estimating [cartridge] pressures” [20]. For thoroughness, bore ash swabs were collected from the upper and lower chambers and at the site of the barrel rupture. These combustion product samples were preserved but not subjected to further analysis.

Shotgun Inspection, Testing, and Analysis

The owner’s manual claimed that the incident shotgun was subjected to “proof testing” prior to shipment, utilizing “standard factory-loaded ammunition.” Typically, proof testing entails the use of higher-than-standard pressure cartridges to validate a barrel’s construction, encompassing its geometry and metallurgical properties. (See 21 for standard and proof load peak bore pressures for 12-gauge shotgun rounds of various types.)

Successful proof testing is frequently indicated by stamped or engraved pictograms on the barrel, action, or both. The absence of such markings on the incident firearm suggests that the manufacturer’s assertion of “proof testing” in the owner’s manual may be misleading. A more precise description would be that the firearm underwent successful functions testing before being shipped to the distributor. Inspection of two exemplar shotguns of the same make and model, performed by swabbing their bores with clean cotton patches, detected ash residue, consistent with these firearms being functions-tested at the factory using standard-pressure 12-gauge ammunition.

To evaluate the durability of the incident shotgun design, one of the two sample shotguns acquired for this study was tested with a double propellant charge, mirroring the destructive event outlined by Lee [22]. A single round with a double propellant charge was created by combining components from two disassembled shotgun rounds. Due to space constraints, the test round’s hull

could not accommodate both the doubled propellant and all the original shot, as factory rounds lack extra space or compressible parts.

Consequently, the quantity of shot was diminished, yet the polymer case mouth still failed to form the neat star crimp seen in the original rounds. Such a visibly imperfect and underweight round is unlikely to leave a modern ammunition factory. The test was conducted by remotely firing the double-propellant round from the lower barrel of the sample shotgun in an open area, using a fixture and trigger lanyard for safety. The shotgun fired without issue, showing no cracks, bulges, dimensional changes in the barrel, or damage to other components. **Figure 9** juxtaposes the primers of the incident round and the double-propellant round. Notably, the incident primer appears flatter than the double-propellant round's primer, supporting Naramore's [20] view that primer shape analysis is unreliable. These rounds likely came from different production lots. While both used type 209 shotgun Boxer primers, their designs may not be identical.

A metallurgical analysis was conducted at a commercial laboratory to examine the barrel's properties. The barrel was marked for sampling and then sectioned using a diamond saw, as shown in **Figure 10**. The upper barrel exhibits significant compression deformation, resulting from the impact of hot combustion gases during the rupture of the lower barrel.

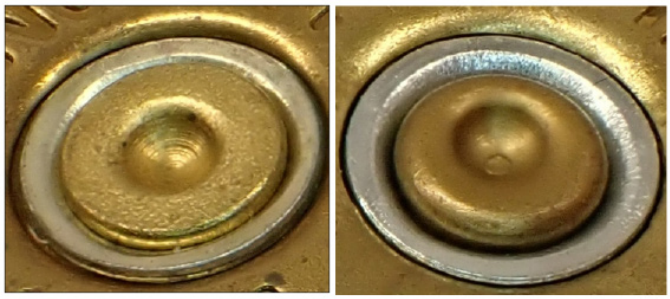

Figure 9
Primers of two shotgun shells; ruptured barrel final round at left, double-propellant exemplar test round at right.

Figure 10
Segments of the lower barrel post diamond sawing and the deformed area of the upper barrel.

Once cut free, the fracture surface was analyzed using a scanning electron microscope, as shown in **Figure 11**. The examination revealed a ductile fracture surface without undesirable features such as porosity, inclusions, or laps.

A barrel segment underwent optical emission spectroscopy (OES) to analyze its composition [23], as shown in **Figure 12**. The elemental fractions are consistent with SAE 1045 carbon steel [24].

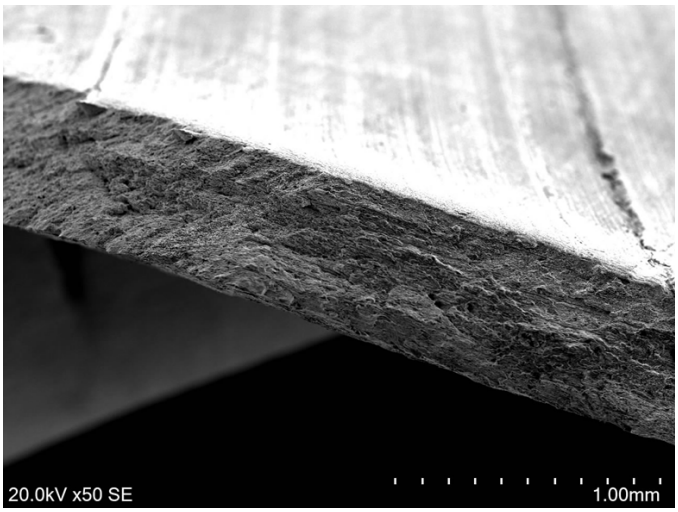

Figure 11
Scanning electron microscope image of fracture surface of the ~0.020" barrel local wall thickness with bore interior surface visible showing circumferential machining marks.

Element	Sample Chemistry (Wt %)	SAE Grade 1045 Chemistry (Wt. %)
Carbon	0.47	0.43 - 0.50
Manganese	0.61	0.60 – 0.90
Silicon	Silicon	Silicon
Phosphorous	0.025	0.04 Max
Sulfur	0.012	0.05 Max
Iron	Balance	Balance
Aluminum	0.02	Trace
Chromium	0.03	Trace
Cobalt	<0.01	Trace
Copper	0.03	Trace
Molybdenum	<0.01	Trace
Nickel	0.01	Trace
Niobium	<0.01	Trace
Titanium	<0.01	Trace
Vanadium	<0.02	Trace

Figure 12
Results of optical emission spectroscopy elemental analysis of the incident barrel.

Two barrel specimens were cut and sectioned — one perpendicular and one parallel to the axial plane. They were encased in polymer for metallographic examination. Both were ground, polished, and etched, revealing a hypoeutectoid microstructure of pearlite grains within a ferrite matrix. Hardness was assessed using a diamond Vickers indenter in the perpendicular specimen with findings presented in **Figure 13**. These measurements were taken midway between the barrel bore and exterior and evenly distributed angularly with ~72° of separation between hardness indentations.

Measured Barrel Hardness (Vickers, HV)
242
242
247
236
239
Avg 241.2

Figure 13
Barrel hardness measurements using a Vickers micro-indenter on plane cut perpendicular to the bore axis.

The hardness measurements showed a maximum-to-minimum range of 11 HV, which is not remarkable. The measured hardness is equivalent to 22 HRC (Rockwell C), 99 HRB (Rockwell B), and 233 HB (Brinell). This suggests a yield strength of the 1045 steel barrel of approximately 105,000 psi or 720 MPa.

Cutting the barrel downstream from the fracture exposed the critical defect responsible for the barrel rupture. The barrel was incorrectly bored using a damaged or misaligned reamer or gun drill, resulting in uneven wall thickness. The right side of the barrel was visibly thicker than the left side due to a collinearity machining error. This produced a region near the chamber with abnormally high local tensile wall stress during firing. The defect is visually evident in the mounted specimen shown in **Figure 14**, which gives the local thickness of the barrel in the text boxes. This specimen is the short cylindrical specimen nearest the rupture in **Figure 10** marked with a rightward-facing arrow.

Caliper measurements of the barrel thickness near the fracture were recorded, with a representative measurement shown in **Figure 15**. The wall thickness, as thin as cardstock paper, was uniform across several inches of the ruptured area.

For thoroughness, a calculation of the barrel's strength and localized bore stress was conducted. Since the ammunition manufacturer does not disclose pressure trace data, the bore pressure at the approximate failure point during discharge was estimated using representative barrel bore pressure values from Butler [3], as tabulated in **Figure 16**.

At a barrel position where the load had traveled 4 inches, the distance from the breech face was 7 inches with a wall thickness of ~0.015 inches. According to data shown in **Figure 16**, the bore pressure at the point of rupture

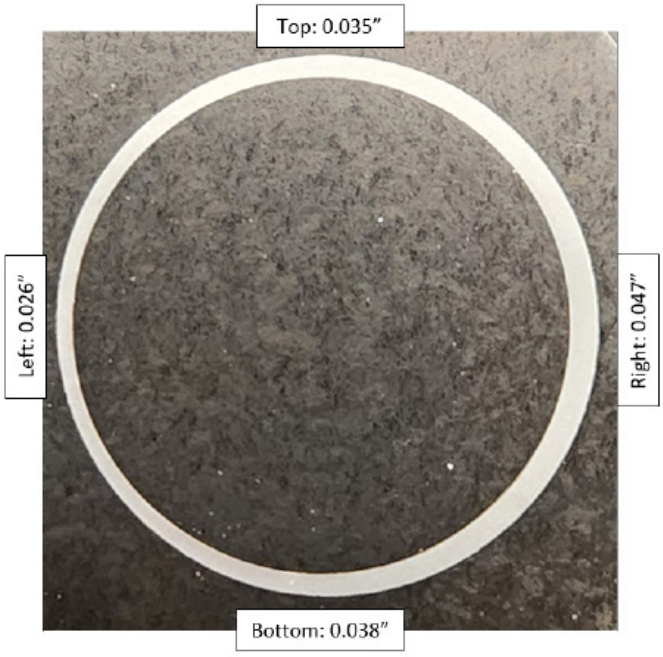

Figure 14
The polished and mounted barrel cross-section sample was taken forward of the rupture, documenting an improperly bored interior wall.

Figure 15
Barrel thickness measurement at the region of rupture propagation.

Representative 12-gauge Barrel Bore Pressures [Butler, 1973]					
Page	**12 Gauge Load**	**Load Travel / Pressure**	**Load Travel / Pressure**	**Load Travel / Pressure**	**Load Travel / Pressure**
203	XPERT 3-1-4	0.65 inches 11,018 PSI	4.91 inches 3,479 PSI	6.05 inches 2,899 PSI	7.25 inches 2,406 PSI
218	Super Speed 3 ¾-1-1 1/4 -6	0.38 inches 11,416 PSI	5.02 inches 4,636 PSI	6.17 inches 3,882 PSI	7.37 inches 3,268 PSI
221	Mag. Mark V 4 ½ - 1 ½ - 2	0.39 inches 12,512 PSI	5.05 inches 4,336 PSI	6.15 inches 3,742 PSI	7.30 inches 3,188 PSI

Figure 16
Pressure data for 12-gauge shotgun loads, giving peak bore pressure as a function of shot position in the barrel.

initiation can conservatively be estimated at 4,000 psi, and it could be higher when considering the steep pressure curve slope illustrated in **Figure 1**. The inner radius of the lower barrel at this location was 0.367 inches — over 24 times the barrel thickness — making Barlow's formula for hoop stress appropriate and simplified as Equation 7:

Eq. 7: $\sigma_{\theta} = 4{,}000 \text{ psi} * 0.367" / 0.015" \approx 98{,}000 \text{ psi}$

This estimated hoop stress minimum at the time of discharge as given in **Equation 7** is very close to the calculated yield stress of the barrel's SAE 1045 steel, 105,000 psi. This estimated yield stress of 105 ksi is based upon the measured barrel material hardness and represents yielding at a quasi-static strain rate. Discharge of a firearm produces strain rates significantly above quasi-static, which is reliably expected to increase the yield stress of the carbon steel alloy 1045 as it is a strain-rate sensitive material. This strain rate strengthening is countered by geometric weakening due to the roughly machined bore of the incident shotgun, which manifests as stress concentrations. The balance between the strengthening and weakening aspects of the barrel was beyond the scope of this investigation.

As a further check of this forensic analysis, the C.I.P. standard regarding Material Quality and Wall Thickness of Barrel and Chamber of Small Arms (Recommendation) was consulted [25]. The C.I.P. is a SAAMI-affiliated organization for European manufacturers and importers. This standard indicates that for 12-gauge shotguns with barrels manufactured from Category 1 steel (200-249 HB hardness, perlite + ferrite microstructure), at 200 mm = 7.9" past the breech face, the minimum wall thickness of the barrel is 1.90 mm = 0.075". At the 7.9" position of the incident barrel, the wall thickness on the mis-bored left side measured 0.015", 20% of the C.I.P. safety recommendation.

Summary and Conclusions

The investigation examined three potential causes of the barrel rupture: shooter error, ammunition defects, or weapon deficiencies. No evidence of shooter error or ammunition irregularities was found. The rupture mechanism was clear — a defectively thin barrel at the point of rupture initiation due to a drilling or reaming error.

During function testing using a standard pressure round at the factory prior to shipment, the lower barrel of the incident shotgun probably bulged without bursting. This initial deformation, of unknown extent, could have signaled a defect but was concealed by the polymer handguard, making it undetectable to the user. Since the shotgun failed on its second normal-pressure discharge, the defective barrel could likely have been identified at the factory using high-pressure "proof" rounds, which would have either caused a rupture on this first shot or created a noticeable ring. Prior to proof testing at the factory, there would be reason to not install the polymer handguard. After a nominally successful proof-load discharge, the technician could simply visually inspect the barrel pair and/or run a hand down the barrel, checking for any irregularity. A substantially bulged barrel would also make installation of the tight-fitting polymer fore-end difficult.

References

[1] G. Kolbe, *Classical Internal Ballistics for the Digital Age*. Newcastleton, Scotland, U.K.: Pisces Press, 2025.

[2] R. A. Rinker, *Understanding Firearm Ballistics: Basic to Advanced Ballistics Simplified, Illustrated & Explained*, 6th ed. Clarksville, IN, USA: Mulberry House Publishing, 2009.

[3] D. F. Butler, *The American Shotgun*. New York, NY, USA: Galahad Books, 1973.

[4] Hodgdon/IMR, "Relative burn rates from fastest to slowest," revised Feb. 2024. [Online]. Available: https://hodgdonpowderco.com/wp-content/uploads/2024/02/2024-Smokeless-Relative-Burn-Rate-Chart-WEBSITE.pdf. [Accessed: May 16, 2025].

[5] P. Barlow, "On the force exerted by hydraulic pressure in a Bramah's press; and the best forms for the piston and the plug, so as to combine strength with economy of metal," *Philos. Trans. R. Soc. Lond.*, vol. 126, pp. 231–247, 1836.

[6] ASME, *B31.8: Gas Transmission and Distribution Piping Systems*, 2024.

[7] G. Lamé, "Mémoire sur l'équilibre intérieur des corps solides homogènes," *Mém. Acad. Sci. Inst. Fr.*, vol. 4, pp. 465–562, 1833.

[8] T. Baumeister, Ed., *Marks' Standard Handbook for Mechanical Engineers*, 7th ed. New York, NY, USA: McGraw-Hill, 1978, p. 5-66.

[9] H. Tresca, "Mémoire sur l'écoulement des corps solides soumis à de fortes pressions," *C. R. Acad. Sci.*, vol. 59, pp. 754–758, 1864.

[10] R. E. von Mises, "Mechanik der festen Körper im plastisch-deformablen Zustand," *Nachr. Ges. Wiss. Göttingen, Math.-Phys. Kl.*, vol. 1, pp. 582–592, 1913.

[11] D. Aliya, *Constructing Competence in Failure Analysis: A Technical and Human Factors Guide*, 1st ed. Clackamas, OR, USA: Koho Pono, LLC, 2024, pp. 291–292.

[12] S. O. Berg, "Rifle barrel obstruction tests and experiments," *AFTE J.*, vol. 23, no. 4, Oct. 1991.

[13] J. S. Hatcher, *Hatcher's Notebook*, 3rd ed. Harrisburg, PA, USA: The Telegraph Press, 1952, pp. 194–197.

[14] National Shooting Sports Foundation, "Firearm safety – 10 rules of safe gun handling." [Online]. Available: https://www.nssf.org/safety/rules-firearms-safety/. [Accessed: May 19, 2025].

[15] R. Lee, *Modern Reloading*, 2nd ed., 2010, p. 106.

[16] P. O. Ackley, *Handbook for Shooters and Reloaders*. Salt Lake City, UT, USA: Publishers Press, 1962, p. 91.

[17] United States Naval Institute, *Naval Ordnance: A Textbook Prepared for the Use of the Midshipmen of the United States Naval Academy*. Annapolis, MD, USA: United States Naval Institute, 1939, sec. 357, pp. 86–87.

[18] J. S. Hatcher, F. J. Jury, and J. Weller, *Firearms Investigation, Identification and Evidence*. Harrisburg, PA, USA: Stackpole Books, 1957, pp. 429–432.

[19] Sporting Arms and Ammunition Manufacturers' Institute (SAAMI), "Unsafe firearm-ammunition combinations," SAAMI Tech. Data Sheet, Aug. 2020.

[20] E. Naramore, *Principles and Practices of Loading Ammunition*. Harrisburg, PA, USA: Stackpole Publishing, 1954, p. 836.

[21] Sporting Arms and Ammunition Manufacturers' Institute (SAAMI), *Voluntary Industry Performance Standards for Pressure and Velocity of Shotshell Ammunition for the Use of Commercial Manufacturers*, SAAMI Z299.2-2019. Shelton, CT, USA: SAAMI, 2019.

[22] R. Lee, *Modern Reloading*, 2nd ed., 2010, p. 110.

[23] ASTM International, *ASTM E415-21: Standard Test Method for Analysis of Carbon and Low-Alloy Steel by Spark Atomic Emission Spectrometry*. West Conshohocken, PA, USA: ASTM International, 2021.

[24] "1045 steel," MatWeb Material Property Data. [Online]. Available: http://www.matweb.com. [Accessed: Nov. 20, 2024].

[25] Commission Internationale Permanente pour l'Épreuve des Armes à Feu Portatives (C.I.P.), "Material quality and wall thickness of barrel and chamber of small arms (recommendation)," 2007. [Online]. Available: https://www.scribd.com/document/168156659/C-I-P-Material-Quality-and-Wall-Thickness-of-Barrel-and-Chamber-of-Small-Arms-Recommendation. [Accessed: May 21, 2025].

The Importance of Human Perception in Incident Reconstruction and Potential for Misleading Interactive Reconstructions

By Henry "Hank" V. Mowry, PE, DFE (NAFE #1195M) and David W. Ridder

Abstract

A common and key component of forensic engineering and incident investigations is the "reconstruction" component. Reconstructions allow the investigator to build and analyze the incident based upon objective information such as video cameras (including dash cameras, surveillance cameras, and more), post-incident photographs (such as from first responders, eyewitnesses, etc.), physical data (including evidence such as skid marks in a roadway, damage patterns to involved objects such as vehicles, buildings, etc.), and even physical injuries. As reconstructions, software, and technology advance over time, "interactive" reconstructions are becoming increasingly beneficial and prevalent in investigations, allowing the reconstructionist to control and adjust the reconstruction as it is shown. Interactive reconstructions allow the controlling individual to move cameras, start and stop the reconstruction, adjust parameters or variables, and allow analysis of the incident from static and omniscient perspectives. However, such interactive reconstructions can also be misleading. This paper will discuss the often disregarded or misrepresented portion of a reconstruction — what the individual(s) in question "saw" or "perceived" during the incident — as well as demonstrate the potential for misleading interactive reconstructions.

Keywords

Reconstruction, perception, cognition, visualization, interactive, photogrammetry, videogrammetry, forensic engineering, field of view, vision fovea, foveal, macula

Introduction and Background

As defined by the National Academy of Forensic Engineers (NAFE), forensic engineering is "the application of the art and science of engineering in matters which are in, or may possibly relate to, the jurisprudence system, inclusive of alternative dispute resolution." Often, a key component of the "application of the art and science of engineering," particularly as it relates to the jurisprudence system, is incident reconstruction (often called "accident reconstruction").

Incident reconstruction is performed by the investigating engineer to document, compile, and ultimately illustrate the incident, allowing for analysis and demonstration of how it occurred. The reconstruction allows the investigating engineer to formulate and arrive at conclusions or opinions about the incident. Such opinions often include matters of liability, or what an individual (or individuals) "knew or should have known." However, when used improperly, reconstructions may present misleading (or even wrong) information about the incident, such as what information was visually available to the involved party (or parties). Therefore, it is necessary that the investigator understand what questions are being asked, what information is desired, what the investigator can truthfully and reliably reconstruct and represent in the reconstruction, and avoid misleading reconstructions that could be unfairly prejudicial to the trier of fact.

Law enforcement was called to an apartment complex on a report of suspicious activity occurring within a vehicle parked in the parking lot of the complex. Due to high call volumes, law enforcement was not immediately dispatched. A second call was placed to law enforcement, reporting an escalation of suspicious activity within the same vehicle, including a potential physical altercation

Henry "Hank" V. Mowry, PE, DFE, 12503 E Euclid Dr., Ste 80, Centennial, CO 80111, (303) 970-8853, hmowry@knottlab.com

with a second occupant. Law enforcement again did not immediately dispatch officers due to higher priority matters. A third call was placed to law enforcement, where the caller stated that the suspicious individual had a weapon. Law enforcement was then immediately dispatched to the location. The dispatched officers involved more than five police cruisers, a police helicopter, and numerous uniformed law enforcement agents. Upon arrival, law enforcement blocked the sole entrance/exit to the parking lot, formed a perimeter, and began issuing commands. The suspect exited the vehicle, raised his hands, and began communicating with law enforcement. After unsuccessful negotiations, law enforcement fired a less-lethal beanbag round. The suspect entered his vehicle. After a brief period in the vehicle, the suspect started the vehicle, drove forward, and turned away from law enforcement. One law enforcement officer discharged his service rifle into the vehicle as it pulled forward and made its turn. The driver was shot and killed. The law enforcement officer was charged with homicide.

The prosecution's expert produced an interactive visualization that depicted what the law enforcement officer "saw." Tasked by the defense counsel for the law enforcement officer, the authors' firm produced a reconstruction that was developed in conjunction with the expertise of a professor of psychology from a local university. The reconstruction and the testimony of the professor showed that the prosecution's reconstruction was misleading and misconstrued what was "visible" to the defendant. During the criminal trial, both the prosecution (the state) and the defense produced reconstructions of the incident.

Understanding the Question

Though it may seem obvious, the question the investigating engineer is ultimately trying to answer is often overlooked or taken for granted. The investigator often intrinsically and correctly understands what question is to be answered and how a reconstruction must proceed to answer it. However, it is worthwhile to evaluate the ultimate question in greater detail, and — as absurd as it may seem — further ask the question: "But what does that question mean?"

As an example, the authors were recently asked to assist with the reconstruction of an officer-involved shooting (OIS) that had been captured on multiple cameras including numerous dash-mounted cameras (dash cams), body-worn cameras (BWCs), a law enforcement helicopter, and a civilian cellular phone. The OIS matter involved an individual who was shot and killed during an interaction with law enforcement as the individual attempted to flee from law enforcement in a vehicle. The officer who fired the fatal shot was ultimately tried for murder. The question posed was, "What did the officer see?" This question was posed as the jury would ultimately need to decide whether the officer was justified, or at least was not criminal, in firing the fatal shots. The prosecution argued that the responding law enforcement officer should have seen that the victim attempted to flee the scene by turning his vehicle's wheels away from the responding officers to drive down a dead-end drive lane in the apartment complex and therefore posed no hazard to them. If that was true, the officer was not justified in shooting the victim. However, as will be discussed in greater detail, the prosecution's reconstruction was misleading and did not accurately represent what was visible to the officer — let alone the intricacies of what the officer "saw" or "perceived."

Though a seemingly obvious question, one which many forensic reconstructionists may claim to be able to answer through routine and reliable reconstruction methodologies, the ultimate answer to the question is simply incapable of being visually represented. Revisiting the definition of forensic engineering, representing what the involved officer "saw" extends far beyond the application of the art and science of engineering. Human visualization, the anatomy and movement of the human eye, the transmission of information from the eye to the brain, and the analysis and interpretation of that information by the brain are beyond the scope of engineering and require specialized education, training, and experience to evaluate.

Trusted, reliable, and court-accepted methodologies were applied to reconstruct the incident using available information. However, to be able to answer the question of what the officer saw — and therefore how it informed the officer's decision — required very specialized education and knowledge. The defense counsel was aware of this specialty and engaged a professor of psychology at a local university, with the education, knowledge, and practical experience in human vision and perception, to assist in answering this question. The authors worked with the professor to provide a visual representation that approximated what the involved officer could "see" as the officer aimed down the reticle of the department-issued rifle at the victim. However, even with the representation provided, it was still necessary for the professor to provide testimony regarding human sight and perception, as reconstructions are simply incapable, at this time, of accurately depicting innately human physiological matters, such as perception and cognition.

While the request was for a reconstruction of the incident to answer the question of what the officer saw, the prosecution also retained a reconstructionist to reconstruct the incident and present it from the officer's perspective. In response, the prosecution's reconstructionist developed an interactive reconstruction of the entire incident. The interactive visualization allowed for viewing of the reconstructed shooting incident from the perspective of all the other involved officers and the victim. The interactive reconstruction allowed starting and stopping of playback in the virtual reconstruction of the incident, as well as free movement around the shooting scene, enabling the individual running or viewing the reconstruction to "walk" through the incident and start and stop the incident at any time.

At trial, the prosecution represented a first-person perspective from the officer who fired the fatal shot, thus presenting to the jury what the officer "saw." However, the first-person perspective from the officer did not evaluate or take into consideration the myriad factors involved in human sight — let alone human perception — and thus provided a misleading representation to the jury of what the officer saw. Given the prosecution's claim that the officer should have "seen" that the victim was turning away from law enforcement and therefore did not pose a hazard to the responding law enforcement officers, accurately representing what the officer could have seen and perceived was the critical question to be answered.

Therefore, the question of "What did the officer see?" cannot simply be answered, or represented, by a typical forensic engineering reconstruction. The investigating engineer must understand and appreciate their limitations. The investigating engineer must ensure their client understands the limitations of the reconstruction and the areas in which the engineer may opine. It behooves the investigating engineer to set clear limitations on what the reconstruction accurately portrays and to inform the client if additional expertise is necessary to provide opinions on matters outside the reconstructionist's knowledge and expertise.

Reconstructing the Incident

When a forensic engineer is asked to reconstruct the incident, the engineer often relies upon industry-accepted, court-accepted, reliable, and repeatable methods. The purpose of this paper is not to present previously developed, published, and accepted methodologies [1]-[2]. However, in evaluating the limitations of reconstructions, particularly interactive reconstructions, this paper will discuss the reconstruction of the aforementioned OIS and provide comparison to the prosecution's interactive reconstruction to demonstrate the propensity for misleading reconstructions.

When performing a reconstruction, it is imperative that the reconstructionist use meticulous, scientifically proven and reliable methodologies. When an incident is captured on photographs or recorded footage, the art and science of photogrammetry and videogrammetry is often utilized. Photogrammetry is the art and science of obtaining useful, three-dimensional (3D) information from two-dimensional (2D) photographs. Videogrammetry is, in essence, the application of photogrammetry to a recorded video, as a video consists of still images (photographs) captured in rapid succession [3]-[4].

Often, the first step of conducting photogrammetry is to obtain a to-scale, three-dimensional representation (digital clone or model) of the incident location. Regarding the OIS matter discussed previously, the author's firm utilized a Leica RTC360 laser scanner to capture the geometry and configuration of the location where the shooting incident occurred. The laser scanner captures millions, even hundreds of millions, of individual data points measured with very high accuracy (±1.9 mm at a 10 m distance) and density. Once the laser scans are compiled, the resulting product is a three-dimensional model comprising millions to hundreds of millions of individual data points. This three-dimensional model is referred to as a "point cloud."

The incident location was inspected and photographed (**Figure 1**). A total of 12 scans of the incident location were captured (**Figure 2**). Following the shooting incident and prior to the authors' engagement, an independent law enforcement agency also conducted laser scanning of the incident location utilizing a Leica RTC360 laser scanner. The

Figure 1
A general overview of the incident location.

Figure 2
A general overview of the incident location as viewed from the point cloud of the incident location captured through laser scanning.

law enforcement agency captured a total of eight scans. The prosecution's reconstructionist relied upon the scans captured by the law enforcement agency.

After the incident scene was captured with the laser scanner, the authors then utilized the same laser scanner to document two police cruiser SUVs, one of which was involved in the incident and captured dash camera footage during the incident. The prosecution's reconstructionist did not perform this step, which resulted in inaccuracies in the way the police vehicles were represented and in the way/manner in which the defendant was standing and holding his firearm.

The authors then inspected the subject rifle and optic that was utilized by the officer that fired the fatal shots. The rifle was retained in evidence storage. Access to the rifle was provided while the retaining law enforcement agency and evidence specialist oversaw the authors' actions.

It is worth restating that the question to be answered was, "What did the officer see?" The rifle that was utilized by the responding officer was a Smith & Wesson M&P-15 rifle equipped with an Aimpoint PRO (Patrol Rifle Optic) red-dot optic. Given that the rifle and optic would be seen, in part, by the officer who had shouldered (readied) the rifle, it was critical to inspect the subject rifle and obtain an accurate representation of it.

To obtain an accurate and to-scale representation of the subject rifle and optic, the scientific process of "photo-scanning" was performed. Photo-scanning is a photogrammetric process whereby numerous photographs are captured of the object in question. Specific software can then orient the photographs in three-dimensional space utilizing common reference points in the photographs. The software then generates a point cloud from the photographs by, again, utilizing common and identified features within the photographs. This is the same process by which topographical and three-dimensional images can be created using drone footage, satellites, etc. Two-dimensional images are captured of an object. With a sufficient number of two-dimensional images, three-dimensional representations can be created through projective geometry (photogrammetry).

Utilizing the photo-scan of the subject rifle and optic, a point cloud was then generated by the software (**Figure 3**). The point cloud was then "solidified" into a solid, three-dimensional model of the subject rifle and optic (**Figure 4**). The model lacked fine details, but provided a to-scale representation, or digital clone, of the subject rifle and optic. The prosecution's reconstructionist did not inspect the subject rifle or optic, which again resulted in inaccuracies in the representation of the rifle, and, in particular, misrepresentations of the optic. Given that the assertion was made that the officer should have been able to see the front wheels of the victim's vehicle turning away from the officer, what portion of the officer's view/vision would be obstructed by the optic housing, and what

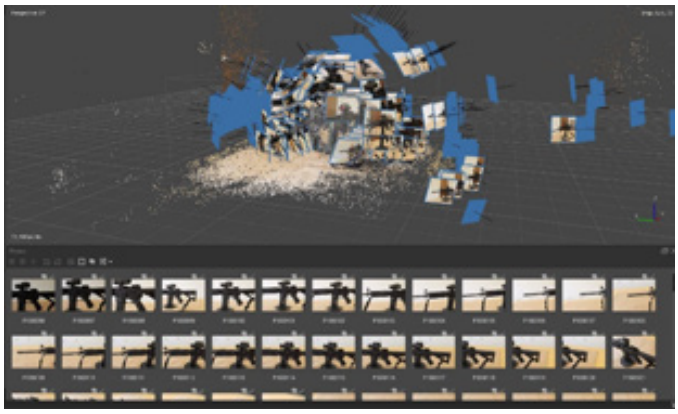

Figure 3
View of the development of a three-dimensional model of the subject service rifle through use of the photo scanning process.

Figure 4
Computer-generated three-dimensional model of the incident service rifle generated from photoscanning.

was visible to the officer through the optic, are of critical importance.

Given the actions described above, the investigation then had accurate, three-dimensional representations of the incident location, the involved police cruisers, and the subject rifle and optic. The next step was to utilize pre-created digital assets (models) of a similar Ford Explorer police cruiser and Smith & Wesson rifle. The pre-created digital assets provided visually accurate representations without requiring the reconstructionist to generate entirely new, labor-intensive models based upon the captured laser scans. However, the digital assets were not accurate in scale or details (e.g., decals, ride height, bumper guard, spotlight, rifle optic housing, etc.). Utilizing the three-dimensional models captured by the laser scans or generated through photo-scanning, the digital assets were scaled and edited to provide accurate, representative three-dimensional models of the involved police cruisers, rifle, and rifle optic.

In addition, the investigation inspected the view afforded to the responding officer through the optic. As previously mentioned, the optic that was mounted to the subject rifle was an Aimpoint brand PRO red-dot. The view through the optic was photographed, and various focal lengths were documented when looking through the optic as it was mounted on the subject rifle. Various focal lengths were photographed to document the change in the size and opacity of the red dot depending on the focal length. In addition, the view down the optic was photographed to document the size and shape of the optic housing (**Figure 5**).

Figure 5
View of the reticle of the Aimpoint brand PRO red-dot optic as viewed from the wielder of the rifle.

To obtain reliable, accurate information from the footage, and therefore to conduct an accurate photogrammetric analysis utilizing the footage, all footage that was relied upon was undistorted. This process has been previously published in multiple articles regarding this process, which will not be detailed at-length in this paper; however, the point cloud of the incident location was then utilized in conjunction with the provided footage to conduct "match moving" or "camera tracking" [12].

In reviewing the footage provided, three cameras were identified that provided the best perspective of the incident (**Figure 6**). The three cameras were identified as coming from two dash cameras from the two police cruisers located nearest to the victim, as well as the civilian cell phone footage. Once the cameras were identified, fixed reference points in three-dimensional space (or "trackers") that were captured in real-life by the laser scan, were identified in the three cameras of interest. Scientific software then "tracked" the reference points throughout the two-dimensional videos. As the points were tracked from the perspective of the cameras of interest, the software solved for the location of the camera that captured the footage. The dash cameras, while fixed, were still tracked to obtain the solved position. However, the cell phone moved throughout the incident; therefore, the position of the cell phone camera was tracked throughout the incident.

At this point, both the prosecution's and the author's reconstructions were largely in agreement. To accurately

Figure 6
Aerial view of the "solved" camera positions throughout the photogrammetric, videogrammetric, and object matching process.

conduct a photogrammetric analysis, a virtual camera must be calibrated and located in three-dimensional virtual space through the aforementioned process. Both reconstructions accurately conducted the camera matching process, resulting in agreed-upon and scientifically validated camera matches.

Once the positions of the virtual cameras were "solved for," the next step in the photogrammetric process was object matching, which is a process where three-dimensional models are placed into the virtual scene by utilizing the calibrated (undistorted) reference footage to match and locate the three-dimensional objects with what is observed within the two-dimensional footage. Utilizing the cell phone footage, dash camera footage, and police helicopter surveillance footage, the scaled three-dimensional representations (digital clones) of the police cruisers were inserted into the virtual scene.

Previously, the prosecution had hired a ballistics expert to evaluate the entry and exit points of the shots fired into the vehicle by the defendant. As part of the ballistics expert's work, the vehicle the victim was driving, a Toyota Prius, was laser scanned with a Leica RTC360. These laser scans were evaluated and determined to be sufficient to scale a pre-created digital asset, similar to what was performed for the police cruisers. A three-dimensional model of the Prius was also inserted into the virtual reconstruction.

Both the defense's and prosecution's reconstructions generally agreed upon the positions of the cruisers and Prius. The positions of the cruisers could be further verified by comparing the "solved for" positions of the dash cameras with where the dash cameras were physically located within the occupant compartment of the police cruisers.

The authors were able to obtain greater accuracy in its reconstruction than the prosecution's expert due to having inspected and scanned the police department's cruisers. Inspection of the department's cruisers allowed for establishment of the actual physical location of the dash cameras in the cruisers, thereby matching the position of the dash cameras with the solved for positions and verification of the solved for positions by comparison of the corrected camera footage. Because the prosecution's expert did not inspect the police department's cruisers, the actual location of the dash cameras within the cruisers could not be verified in the prosecution's reconstruction, resulting in slight differences between the cruiser positions.

Because of the relatively small size of the officer's service weapon, object matching was not primarily relied upon; however, it was utilized to crosscheck placement of the service weapon based upon the BWC footage. The BWC footage from two additional officers was utilized for placement of the service weapon within the reconstructed scene. The BWC footage captured the position and location of the defendant, as well as the position and location of his service weapon, throughout the shooting incident. Reference points within the BWC footage were utilized to place the digital clone of the defendant's rifle within the reconstructed scene. Once the digital rifle clone was placed, the position was further evaluated by examining the undistorted reference footage. The placed digital clone closely matched what was visible in the cell phone footage.

It is worth repeating that a reconstruction of the incident from the officer's perspective was requested to determine what the defendant "saw." To ensure the highest accuracy possible, the officer's "eye relief" was measured. Eye relief is a term utilized to describe the distance between the back of the firearm's optic housing and the shooter's eye when the weapon is shouldered and ready to be fired. The defense counsel obtained and provided an image of the defendant shouldering the subject firearm. For this test, the firing mechanism was removed from the rifle to render it safe and incapable of being fired, and the adjustable stock was adjusted by the defendant to match the extension at the time of the incident. The defendant then shouldered the rifle, and a scale was placed along the rifle to measure the distance between the defendant's eye and the rear of the optic housing. Once this information was provided, a virtual camera could then be placed at the same distance behind the digital rifle clone to provide a view (not vision) down the optic that would be representative of the defendant's view when aiming down the subject rifle and optic. The prosecution's reconstructionist did not account for eye relief or the subject optic.

Misleading Interactive Reconstructions

It is at this point that the prosecution's reconstruction and the authors' reconstruction drastically diverged. The prosecution's expert reconstructed the incident, including from the perspectives of multiple law enforcement officers, and provided an interactive reconstruction (**Figure 7**). The interactive reconstruction allowed the incident to be viewed at varying playback speeds (including slow-motion and paused), at varying angles, from differing perspectives, and allowed the "operator," or individual interacting with the reconstruction, to walk around the incident virtually as the virtual reconstruction was played,

Figure 7
Aerial view of the prosecution's interactive reconstruction.

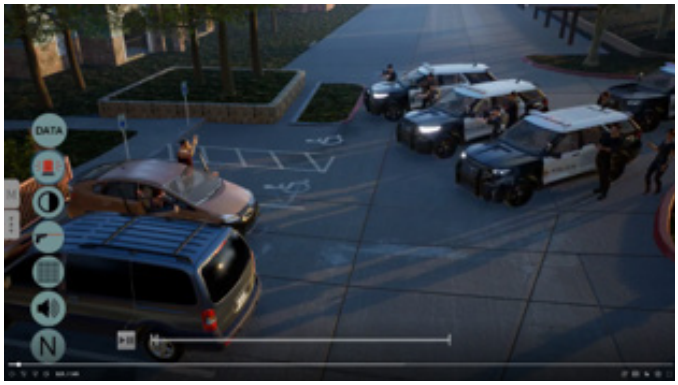

Figure 8
View of the prosecution's reconstruction as viewed from an angle not available to the defendant.

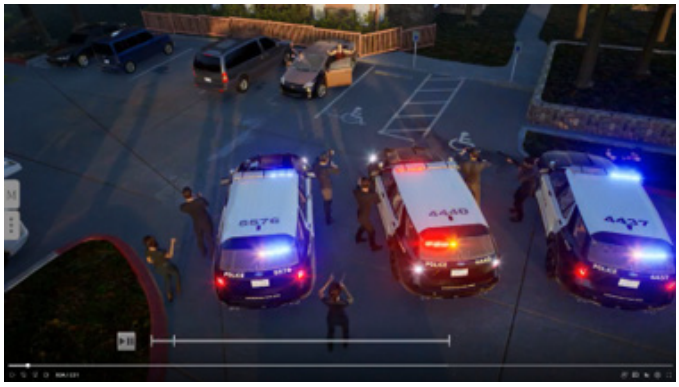

Figure 9
View of the prosecution's reconstruction as viewed from an angle not available to the defendant.

providing unlimited information and perspectives that were not available to the defendant (**Figures 8** and **9**).

Ultimately, the question posed to the jury was whether the defendant was justified in shooting. As such, the matter is best evaluated from the perspective of the individual who acted, not as an omniscient being with a litany of information that was unavailable to the defendant. Although the interactive reconstruction could prove invaluable in answering questions other than what had been asked, such as whether or not the department's response met department guidelines and policies or if the responding officers had positioned themselves appropriately given their training. However, such a reconstruction is neither helpful nor impartial when evaluating the actions of the individual involved if it does not investigate the matter from that individual's perspective. Recall, it was the defendant on trial, not the department; therefore, it is misleading to evaluate the actions of the defendant with omniscient views and information that was not available to the defendant.

The prosecution's reconstructionist did provide first-person perspectives, including from the perspective of the defendant and the victim. However, what was presented was lacking in crucial and critical detail; namely, how human vision functions, what a human "sees," and what that human perceives. Human vision and human perception quickly escape the bounds of engineering and enter the realm of physiology and psychology — a field that requires unique and extensive education and training far beyond the field of forensic engineering.

Representation of Human Vision in a Two-Dimensional Proxy

There are several key problems faced when trying to represent three-dimensional human vision in a two-dimensional proxy. These key issues include:

- Field of view
- Attempting to accurately represent peripheral vision
- Lack of the third dimension
- Determining what the subject was looking at
- Accounting for the viewer's additional perspective

Human vision provides a nearly 180° field of view with both eyes open [5]-[6]. During the reconstruction, a series of images was created with fields of view ranging from 130° down to approximately 20°, with 40° representing the primary visualization presented to the jury. A field of view of 40° is the approximate field of view represented by a 50mm lens on a full-frame camera, which has historically been used by photographers to represent "normal vision."

While images rendered at a much higher field of view are technically more accurate representations of the human field of view, they look very odd to a third party, external viewer because the rifle and optic were hardly visible in these representations. This is partially exacerbated by the viewer's perspective, since they are observing a 2D representation of a compressed 130° view. In other words, what the reconstruction represents is, in essence, a 130°, three-dimensional view of what the officer saw, compressed down to a computer monitor or TV screen, thus resulting in a perceived dramatization of the human field of view, with central objects appearing minimized and distant from the viewer. While technically accurate, viewing such a wide field of view on such a small, targeted surface results in a visualization that appears misleading or distorted.

Another challenge when trying to represent what a subject "saw" or perceived is the lack of the third dimension. Currently, we are limited to two-dimensional images and videos, which don't allow the viewer to clearly determine depth. However, in this case, the subject had stated that he had one eye closed during the event, which allowed the reconstructionist to largely ignore the challenges present while trying to accurately represent dimensional vision/perception in a 2D medium.

Due to the constant scanning nature of human vision, it can be difficult for a reconstruction to accurately determine what specifically the subject was looking at during an incident. This can significantly affect the accuracy and usefulness of these types of exhibits. However, based on testimony, the BWC footage, and the additional circumstances of the case, the reconstruction was performed under the assumption that the subject was looking through the rifle optic and focused primarily on the vehicle and its occupant.

This is a somewhat unique situation. We must recall that, typically, the human eye is constantly moving, shifting from one point of interest to another. For example, when reading this paper, the reader is not just focused on the page, with all words in clear view; the reader's eyes are moving from word to word to word. Therefore, rather than ask, "What did the subject see during the incident?" The question must often be changed to, "What would have been possible to see from a specific point in space and time?" This is consistent with the prosecution's reconstruction, but was not consistent with what the officer saw.

Fortunately, in the situation described above, the authors had the added benefit of knowing the subject was aimed through a rifle scope and that the focus was narrowed on the vehicle and its occupants. This analysis further benefited from working with an expert in human vision, perception, and cognition to aid in analyzing what an individual would be focused on when in a situation such as that faced by the defendant (e.g., aimed down a rifle optic, one eye closed, and focused on a perceived threat).

The authors used relatively simple methods to visually represent and model the "blurriness" (or "lack of focus") and lack of contrast present in peripheral vision. Based on information presented in published literature [5]-[6] and with feedback from the professor, a field of view of approximately 40° was selected as a primary representation for the visualizations. As previously discussed, 40° has historically been used by photographers and other visual artists to represent "normal" vision. With this in mind, the authors employed the use of Adobe After Effects' suite of effects and a black and white gradient map to control the application and falloff of those effects.

The effects were added in two parts — the first part being the "blurriness" of the image, and the second part being the contrast and saturation adjustments.

The blur was applied using the "Camera Lens Blur" effect in Adobe After Effects. This effect can use a black-and-white image to control the amount of blur applied to the affected layers, applying no blur where the black-and-white image is black and fully blurring parts of the image that are white. This black and white image, which will be referred to as a "luminance matte," was generated by using the Gradient Ramp effect and adjusted with Curves effect to control and shape the falloff. The center of the luminance matte was set to pure black to prevent any blurring at the center of the image where the subject's vision would be clear, then slowly transitioned to white near the edges of the frame where the vision would be the least clear.

The amount of blur applied was based on published literature and experimental data [5]-[6] in conjunction with feedback from the psychology expert. Ultimately, the authors' final visualizations were conservative and on the side of creating clearer images with less blur to account for minor eye movements and scanning, even though the subject could be reasonably assumed to have maintained full focus on the vehicle and its occupant. In other words, the visualization contained greater clarity than it would actually be for the human eye in the specific instance reconstructed and experienced by the defendant.

To implement the contrast and saturation adjustments, a secondary adjustment layer was used. The contrast was controlled by another Curves effect, and the saturation was lowered by using a Color Balance effect. The adjustment then used the same luminance matte to gradually apply the adjustments to the outer bounds of the frame. The specific values were chosen to allow clear detection of motion but not allow easy distinction of specific colors or forms, which is consistent with the capabilities of human peripheral vision.

Human Visual Field and Perception

The human eye is a biologically and physiologically complex organ. The back of the human eye is composed of the retina, which is a light-sensitive membrane [7]-[9]. Within the retina are photoreceptors, which are comprised of "rods" and "cones." Rods are photoreceptors (i.e., light-sensitive cells) that are highly sensitive to light and therefore assist with low light vision and excel at motion detection; however, rods lack color discernment. Cone cells process color and provide sharp, acute visual focus and are concentrated near the center of the human field of view.

The rear of the human eye contains an area referred to as the "macula." The macula is a small area at the back of the eye where light is focused and is responsible for our "central" vision [8]. Located within the macula is the "fovea," which is derived from the Greek word meaning "small pit." The fovea is a small depression within the macula. It is within the fovea that the majority of the retina's cone cells are concentrated. The human eye has significantly more rod cells than cone cells; however, it is within the fovea that cone cell density is at its highest. Another area that is often defined is the "perifovea," which is an area of the eye that extends from the foveal rim (i.e., the edge of the rod-free boundary of the center of the fovea) out to approximately 5° eccentricity.

As previously discussed, the human field of view is quite large, extending nearly 180° with both eyes open [5]-[6]. Each eye can see approximately 155° horizontally, 60° vertically up, and 75° vertically down [10]. While most humans are unaware, even with such a large field of view, only a very small portion of the human field of view is in sharp, acute focus and at its highest contrast. A general "rule of thumb" is that what is in sharp, clear focus is approximately the size of a thumbnail when the arm is extended to its full length.

Prior studies have determined that the fovea is only approximately 1° eccentricity. That is, only approximately 1° of the human field of view consists purely of cone cells and is where human visual resolution is at its highest. The perifovea extends only to approximately 5° eccentricity [5]-[6]. Beyond the perifovea — or beyond that approximately 5° central field of view — is defined as "peripheral vision." It is within the peripheral field of view that density of cone cells drops dramatically, with the vast majority of photoreceptors comprised of rod cells. In other words, beyond approximately 5° eccentricity of the human field of view, visual acuity drops dramatically, with objects becoming increasingly "blurred" or "out of focus" with increasing eccentricity (i.e., with increasing angular departure from central focus) [11].

Due to the limited central view of the reconstruction that is in focus, it often appears to an outside observer to be an inaccurate representation of what the average person sees. However, a simple experiment can be performed. If an individual focuses solely on one word of this paper and does not move their eyes from that one word, only one to two words beyond that word of focus can be clearly discerned. It is because of additional human physiology that this narrow field of view is overcome.

The human eye is not static. As we go about our daily lives, it is constantly scanning and is rarely ever stationary. The human eye naturally shifts to the item of concern or focus. Utilizing the previous example, as we read, our eyes move from word to word. The eye is typically not stationary as we read but instead moves across the pages. Likewise, as we drive our vehicles, our eyes constantly scan the road ahead, our speedometer, and the world around us. Therefore, it is not apparent that the sharp and clear focus area of our field of view is very narrow or limited. However, for the subject incident, the law enforcement officer was focused on the vehicle and its occupants as viewed through the rifle scope, thus limiting the likely range of eye movement and object focus.

As our field of view expands into our peripheral vision, objects become increasingly "blurred" or lack definition and clarity. Studies have shown that at approximately 40° eccentricity (or 40° from our central focus), the world is "90% blurred" [11]. One visual scientist from 1976 described peripheral vision as, "When I look at something it is as if a pointer extends from my eye to an object. The 'pointer' is my gaze, and what it touches I see most clearly. Things are less distinct as they lie farther from my gaze. It is not as if these things go out of focus — but rather it's as if they somehow lose the quality of form" [5]. It is this loss

of "quality of form" that becomes critical when attempting to present or reconstruct what is viewed by an individual. Thus, the central question to be answered for the shooting trial necessitated, by its very nature, an understanding and representation of human field of view.

Utilizing the procedure and process described above, the authors were able to reconstruct the incident and place a virtual camera at the same position as the defendant's eye. It is at this point that the forensic engineering and reconstruction begins to end and collaboration with the professor of psychology increases and becomes more important. Prior to working with the professor, the authors utilized methods within their suite of software tools to represent the loss of visual acuity described in various medical journals and articles.

Figure 10
Still image from the reconstruction and visualization demonstrating a 130° field of view.

Figure 11
Still image from the reconstruction and visualization demonstrating a 40° field of view.

The Final Reconstruction

Following the process described above, and with the assistance, refinement, knowledge, experience, and expertise of the professor, the authors produced three final visualizations that aided with answering the question of what the responding officer "saw." The final visualizations included varying fields-of-view presented at 130° (**Figure 10**), 40° (**Figure 11**), and 20° (**Figure 12**). As discussed above, the human field of vision is very large. The 130° field of view was presented; however, due to the seemingly inaccurate representation of such a wide field of view on such a narrow medium (i.e., a computer screen or television screen), and due to the lack of the third dimension, this visualization was not presented at trial.

The 20° field of view was also provided based upon the very limited portion of the human field of view that is in sharp, clear contrast, as well as the fact that the defendant had one eye closed and was focused down the service rifle optic. However, like the 130° field of view reconstruction, this visualization was not presented at trial because most average individuals would claim they can "see more" than what is shown in the 20° reconstruction. While it is accurate to say the human field of view extends well beyond 20°, what is in sharp and clear focus is even less than would be shown in the 20° reconstruction. Therefore, the 40° field of view reconstruction was presented to the jury. As discussed above, a 40° field of view has been historically presented as being "typical" or "normal"

Figure 12
Still image from the authors' reconstruction and visualization demonstrating a 20° field of view.

Figure 13
Side-by-side comparison of the prosecution's reconstruction (left) and the authors' reconstruction (right).

for human vision. Furthermore, a 40° field of view is the approximate field of view presented by the prosecution's reconstruction, thus allowing for a side-by-side comparison (**Figure 13**).

As can be seen from the still images of the reconstructions, the question of what the officer "saw" is not as simple as it may seem. Even with the reconstruction performed, the question of what the officer "saw" is still not easily answered, requiring the expertise of individuals such as the professor of psychology. And even while the professor can provide insight into human perception and cognition, it is impossible to know precisely what the officer "saw," "perceived," or "understood" at the exact moment the shots were fired. However, a thorough, accurate, meticulous reconstruction, with the help of highly specialized and trained experts, can help in working toward that answer.

Summary

Although the reconstruction performed by the prosecution's expert was an involved, labor-intensive, and scientifically accurate reconstruction of the positions of law enforcement officers, law enforcement vehicles, and the defendant, their reconstruction was misleading as presented to the jury about what the defendant "saw." The interactive reconstruction provided by the prosecution would have been valuable in evaluating the law enforcement agency's response with regard to positioning of officers, procedures, policies, and a review of the totality of the incident. However, their reconstruction was not a fair representation of the case being presented by the prosecution's claims of what the defendant "saw" or what he should have seen that informed his decision of whether to fire his service weapon or not.

The prosecution argued that the law enforcement officer should have been able to identify that the victim had turned the front wheels of his vehicle away from the officer and down a dead-end drive lane; therefore, the victim posed no threat to the responding law enforcement officers. However, as can be seen from the author's reconstruction, and with the aid of the professor of psychology, what was visible to the officer, and therefore what he "saw" or "perceived" was not accurately represented by the prosecution's reconstruction.

What a human "sees" involves specialized areas that extend beyond the expertise of a typical engineering reconstruction. Human perception and cognition are highly specialized fields that require the guidance and expertise of individuals trained and educated in psychology and human physiology. The reconstructionist must be aware of their limitations with regard to their expertise and technological representation of uniquely human functions such as vision, perception, and cognition. When the question is asked, "What did they see?" careful consideration must be given to ensuring what is presented is accurate and representative of what is possible within human anatomy and psychology. While interactive reconstructions can provide valuable information, such interactions must not be misconstrued as presenting something the interaction simply cannot scientifically support.

Conclusion

Forensic engineering incident reconstruction is invaluable in understanding, evaluating, and investigating an incident. The three-dimensional reconstruction can provide insight into the totality of an incident, thus allowing the investigator to apply rigorous forensic engineering investigation methodologies. However, it is crucial that the investigator understand their limitations, particularly as it relates to what the reconstruction shows, or what questions the reconstruction can answer. Furthermore, interactive

reconstructions can provide an even broader analysis and view of an incident, allowing the incident to play out "in real time" and allow a frame-by-frame understanding of the incident. However, such reconstructions also have the immense capacity to be misleading and prejudicial.

A seemingly innocuous question, "What did someone see?" couldn't be further from innocuous. Human vision, cognition, and perception are immensely complex and complicated matters that extend far beyond the purview of a forensic engineering investigation. Such matters as what someone "sees" requires very esoteric experience, education, and training. Thus, it is imperative that the forensic engineer understand their knowledge and experience limitations. It is also imperative that the forensic engineer understand the limitations of their reconstruction, what their reconstruction is truly showing or representing to the triers of fact, and limit the conclusions and opinions that they can formulate and arrive at.

References

[1] R. M. Ziernicki, A. G. Leiloglou, T. D. Spiegelberg, and K. Twigg, "Forensic engineering application of the matchmoving process," National Academy of Forensic Engineers Journal, vol. 35, no. 2, Dec. 2018.

[2] R. M. Ziernicki and R. L. Nguyen, "Forensic engineering analysis of fatal overhead crane accident," National Academy of Forensic Engineers Journal, vol. 37, no. 1, Dec. 2020.

[3] R. M. Ziernicki, M. E. Gordon, S. Knapp, and A. G. Leiloglou, "The applications of matchmoving for forensic video analysis of a fatal sprint car accident: Part I," National Academy of Forensic Engineers Journal, vol. 38, no. 1, Jun. 2021.

[4] R. M. Ziernicki, M. E. Gordon, S. Knapp, and A. G. Leiloglou, "The applications of matchmoving for forensic video analysis of a fatal sprint car accident: Part II," National Academy of Forensic Engineers Journal, vol. 38, no. 1, Jun. 2021.

[5] H. Strasburger, I. Rentschler, and M. Jüttner, "Peripheral vision and pattern recognition: A review," Journal of Vision, vol. 11, Dec. 2011.

[6] A. M. Larson and L. C. Loschky, "The contributions of central versus peripheral vision to scene gist recognition," Journal of Vision, vol. 9, Sep. 2009.

[7] A. Sprabary, "Fovea centralis," All About Vision. [Online]. Available: All About Vision. [Accessed: May 18, 2026].

[8] "Macula," Cleveland Clinic. [Online]. Available: Cleveland Clinic Macula Page. [Accessed: May 18, 2026].

[9] "The function of the normal macula," BrightFocus Foundation. [Online]. Available: BrightFocus Foundation. [Accessed: May 18, 2026].

[10] "Visual field," Vision and Eye Health. [Online]. Available: Vision and Eye Health Visual Field Page. [Accessed: May 18, 2026].

[11] A. Kostermann, C. Vater, R. Kredel, and E.-J. Hossner, "Perception and action in sports: On the functionality of foveal and peripheral vision," Biomechanics and Control of Human Movement, vol. 1, 2019.

[12] R. M. Ziernicki and R. L. Nguyen, "Application of matchmoving for forensic video analysis with recorded event data," National Academy of Forensic Engineers Journal, vol. 40, no. 1, Jun. 2023.

Wind Damage vs. Storm Surge Damage: Case Studies from Hurricane Helene

By Manuel Matus, PhD, PE, Ziad Azzi, PhD, PE, DFE (NAFE #1343S), and Krishna Sai Vutukuru, PhD, PE, DFE (NAFE #1384M)

Abstract

Between 1980 and 2024, natural hazards have resulted in approximately $2.9 trillion in economic losses across the United States. Tropical cyclones represent the most damaging hazard type, accounting for approximately 53% of total losses, and are classified as multi-hazard events due to the combined impacts of wind loading and storm surge inundation. In the contiguous United States, coastal regions comprise only 10% of the total land area yet contain approximately 40% of the population, making these communities particularly susceptible to damage from hurricane-induced wind as well as storm surge-related forces. Following major events, post-disaster damage assessments conducted by federal agencies (such as FEMA) and by private-sector entities (including insurance carriers) are tasked with distinguishing between wind-related and storm surge-related damage. This forensic differentiation is critical for structural failure analysis, accurate insurance claims adjudication, and equitable allocation of recovery resources. Misattribution can lead to substantial disputes and financial discrepancies. This paper presents a case study for both pre-event vulnerability assessments and post-event forensic evaluations aimed at identifying and differentiating wind-induced versus storm surge-induced damage to residential buildings. The methodology described in this document integrates civil engineering principles and forensic investigation techniques to provide guidance for improving damage attribution accuracy and post-disaster decision-making.

Keywords

Hurricane season, insurance claims, site assessment, wind damage, storm surge damage, forensic engineering

Introduction

Coastal zones, mainly located in the Southeast of the United States and the Gulf of Mexico, constitute inherently multi-hazard environments, where built infrastructure and communities are simultaneously exposed to interacting or sequential natural hazards such as tropical cyclones accompanied by extreme winds, storm surge, and wave loading [1]. In the United States, hurricanes represent one of the most recurrent and destructive hazard agents, generating annual economic losses of tens of billions of dollars [2]. However, individual events can produce far more catastrophic impacts: The 2004-2005 Atlantic hurricane season exceeded $150 billion in total damages [3], and Hurricane Harvey in 2017 incurred losses estimated at more than $100 billion initially [4] — a figure that was later revised to more than $158 billion [5].

Despite the destructive potential of tropical cyclones and severe wind events, flooding remains the costliest weather-related hazard nationwide in terms of property and infrastructure losses [1], [6]. The magnitude of future hurricane- and flood-related impacts is expected to escalate due to population expansion in high-risk coastal regions, shifts in demographic distribution, and the intensification of climate-driven hazards (e.g., hurricanes). Currently, more than half of the U.S. population resides in coastal counties, and long-term projections by the National Oceanic and Atmospheric Administration (NOAA) indicate that these regions will continue to experience high population growth, further amplifying exposure and vulnerability to weather-related hazards [1], [7]-[8].

In recent years, significant advancements have been made in addressing natural hazard design requirements, and code updates have demonstrated measurable benefits. For instance, post-event assessments following Hurricane

Ziad Azzi, PhD, PE, DFE, Director of Engineering, DDA Forensics, Miami, FL, (786) 772-5643, ziad@ddaforensics.com

Ike showed that residences built after 1987, in accordance with the updated standards, exhibited a substantially higher likelihood of structural survival [1], [9]-[11]. In post-hurricane forensic and structural engineering assessments, accurately distinguishing between wind-induced and storm surge-induced structural damage is critical, primarily because insurance coverage frameworks treat these hazards separately. Standard property insurance generally covers wind-related losses while explicitly excluding flood damage, which is instead addressed under dedicated flood-insurance policies.

In such situations, the forensic engineer becomes a focal point in resolving disputes that may arise between insurance carriers and homeowners. As such, it is imperative that the engineering consultants preserve professional independence, exercise unbiased technical judgment, and rigorously apply established engineering methodologies, principles, and standards [12]-[13]. Additionally, because many coastal structures experience complex interactions between wind and surge-related forces during a hurricane, determining the dominant damage mechanism typically requires comprehensive on-site forensic assessments. Such evaluations are especially relevant to forensic engineers, design professionals, insurance adjusters, building code authorities, floodplain managers, and emergency management officials alike, who rely on accurate hazard attribution for technical, regulatory, and financial decision-making to improve current practices [13].

Literature Review

The distinction between wind-induced and storm surge (or flood)-induced damage has evolved into a specialized field within forensic engineering. Historical and recent hurricanes, including Katrina, Ida, Harvey, Irma, Ian, Helene, and Milton, have provided insights into how these forces impact structures, as illustrated by engineering surveys, forensic assessments/reconnaissance, and published literature [14]-[20].

Field surveys after major storms, such as those by the Federal Emergency Management Agency (FEMA), Haag Engineering, and the United States Geological Survey (USGS), reveal that the extent of surge damage is evident from mud/sediment lines, aligned debris, and relatively undisturbed roof and upper wall structures. The timing and sequencing of wind and water impacts documented using NOAA, National Hurricane Center (NHC), FEMA flood maps, and high-resolution aerial/satellite imagery are critical to accurately determine causation. Modern investigations also utilize mobile instrumentation, aerial imagery, and radar, but direct field evidence remains a key factor in determining the cause of damage and discerning whether the failure occurred from excessive wind pressures or from elevated storm surge levels.

On one hand, wind damage commonly follows a top-down progression [9].

- The highest forces (or pressures) are concentrated at roof ridges/corners, eaves, gable ends, and upper wall features, resulting in the removal of claddings, shingles, and occasionally whole roof structures [21]-[25].

- A breach at the roof or walls increases the internal pressure, accelerating the outward force upon building elements and sometimes generating rapid failure of the structure [26]-[29]. It is worthwhile mentioning that ASCE 7-22 [26] directly relates the internal pressure inherent inside a building, depending on the building's classification as enclosed, partially enclosed, open, or partially open. More information on the internal pressure coefficients and the enclosure classification of buildings is available in Chapter 26 of ASCE 7-22 [26].

- The Enhanced Fujita Scale and Saffir-Simpson Hurricane Wind Scale provide empirical correlations between observed building damage and estimated wind speeds, enabling forensics to back-calculate likely wind forces through damage observed during the on-site assessments [30]-[33]. Note that the correlations are very site-specific, and it is highly recommended to cross-check with meteorological data as well as structural analyses.

- Field assessment methods include documenting the presence or absence of debris flow lines or scour at foundations, cataloging damage to windward vs. leeward components, and comparing neighboring structures [34]-[37]. Note that, due to the nature of hurricane winds and their cyclonic rotation, different portions of a building may alternate between windward and leeward conditions over time as the storm translates and winds change direction. Therefore, accurate site-specific meteorological data are key in making field assessments.

On the other hand, surge and flood-related damage commonly follows a bottom-up progression.

- Storm surge exerts hydrostatic (or stationary water) and hydrodynamic (moving water) forces that are vastly greater than those from wind. As a small example, a body of water traveling at 10 feet per second (ft/s) exerts about 200 pounds per square foot (psf) of pressure on a vertical elevation such as a residence wall compared with roughly 25 psf of pressure emanating from 100-mile-per-hour (mph) winds. This assumes a fluid dynamic pressure equal to half the density times the velocity squared, which is a measure of the kinetic energy of the moving fluid per unit volume acting against the wall. Note that, at sea level, the density of water is about 800 times greater than the density of air [26]. Although the respective forces and points of application of water and air fluids on a vertical surface are drastically different, this simple example illustrates how much impact changes in fluid density and velocity can have on the magnitude of hydrodynamic and aerodynamic loading on structures (e.g., wind vs. water flows).

- Characteristic damage includes the undermining of foundations, displacement of entire structures, severe damage to ground-level walls, and evidence of buoyancy (e.g., wood-framed buildings entirely floated off foundations) [34], [36], [38], [39].

- Moving water, wave action, and debris battering typically devastate lower building elements while upper levels may remain relatively undisturbed [40], [41].

- Identification of high-water marks, sediment and debris lines, scoured soil, and comparative analysis of surrounding vegetation/buildings are standard investigative tools [42], [43].

Field Assessment Methodology to Differentiate Wind from Storm Surge Damage

Determining whether structural damage resulted from wind or storm surge is a critical component of post-hurricane forensic assessments. Differentiating between these two mechanisms requires a systematic inspection methodology, informed by the physical characteristics of each peril, the timing and progression of damage, and corroborating climatological and hydrological data.

Site Documentation and Preliminary Observations

Assessment begins with comprehensive site documentation [44], [45]. The forensic engineer should develop a sketch plan noting building orientation, nearby obstructions, water bodies, terrain elevations, and cardinal directions. Evidence of flood levels (such as debris lines, water staining, and sediment marks) should be documented both externally and internally, as evidenced in **Figure 1**. Importantly, flood debris lines identify the maximum inundation height, which, in turn, helps define the application points for wind and water forces in a typical engineering analysis.

High-resolution photographs should capture both overview and close-up details of affected areas. Field notes should identify the material types, construction methods, and the precise elevation of observed damage. This information allows differentiation between zones influenced by wind and those influenced by water, and can also provide valuable information for estimating structural strength and/or gravitational forces. Note that ASCE 7-22 [26]

Figure 1
Flood debris lines: (A) exterior wall and (B) interior column.

provides guidance and guidelines for flood loads, wave loads, and wind loads on structures, as well as load combinations involving the aforementioned in conjunction with other loads. Although the thrust of the paper is to differentiate wind damage from storm surge damage, in reality, the structure experiences a combination of loads from both sources during a severe wind event. As such, one cannot exclude a damage source based solely on visual assessment. Therefore, an analysis involving load combinations is necessary to attribute the degree of damage caused by each source, if applicable.

Wind Damage Indicators

Wind-related damage typically initiates at the upper elevations of a structure, such as the roof, gable ends, and eaves, where aerodynamic uplift forces are greatest and pressure differentials are most pronounced [12], [13], [21]-[23], [38], [46]-[51]. The initial signs of wind distress often include dislodged or uplifted roof coverings, ridge shingles or tiles, and cladding materials, particularly at roof edges and corners where turbulent flow separation occurs. Examples of failed roof covering components are shown in **Figure 2**.

As wind continues to act on the structure, breaches in the building envelope, such as failed roof sheathing or openings in windows and doors, can result in internal pressurization, producing additional outward forces on walls and roof systems that accelerate structural deformation and potential failure of the roof structure. These progressive failures typically manifest as outward displacement of wall assemblies or complete loss of envelope components. Examples of damage to wall assemblies are shown in **Figure 3**. Importantly, the absence of scour,

Figure 2
Failed roof covering components from excessive wind pressures: (A) hip cap shingles and (B) ridge cap tiles.

Figure 3
Failed building components: (A) window struck by windborne debris and (B) dislodged wall siding.

sediment deposits, or water staining near the foundation distinguishes damage from wind forces rather than storm surge.

Storm Surge Damage Indicators

Storm surge damage is generally characterized by distress concentrated at the lower portions of a structure, reflecting the powerful hydrostatic and hydrodynamic forces exerted by storm surge and wave action [12], [52]. Typical indicators include severe damage to the lower levels, such as foundation scour, undermining of support systems, and collapse of walls near grade. Evidence of wave impact is often visible in the form of broken cladding, displaced wall panels, or structural deformation occurring near the stillwater level and the wave runup height. Additionally, battering debris can bring down siding components, and walls typically fail with a hinge point, facing the water: the force of the water pushes in the seaward walls, forming a hinge line at the top of the wall. This is opposite the location of the hinge line for wind (which would be the bottom of the wall). Typical examples of storm surge damage to buildings and building components are showcased in **Figure 4**. Note that some of the observations shown in **Figure 4** could be the result of wind damage depending on the severity of the wind event itself and the local climatological conditions including the proximity of the structure to the eye of the storm. However, due to the nature of the failure concentrated toward the lower portion of the elevations, and since wind speeds tend to be minimal near ground level, the likelihood of failure due to severe wind pressures alone is unlikely, unless there is a deficiency in the element or in the connection to its surroundings. As such, a comprehensive forensic assessment coupled

Figure 4
Typical indicators of storm surge damage: (A) toppled masonry wall on ground level, (B) displaced wall siding, (C) seaward wall pushed inward (formation of hinge line at the top of the wall), and (D) battering effects on garage door.

with an engineering analysis is recommended to differentiate the resulting effects of wind and wave pressures.

In many cases, entire buildings exhibit lateral displacement or buoyant uplift of substructures due to the upward and horizontal forces imposed by moving water. Additional diagnostic features include residual debris fields and sediment deposits oriented consistently with the flow direction, which confirm the influence of sustained water movement. Frequently, the upper portions of structures remain intact and are found resting on the ground or transported inland, a condition that strongly indicates buoyant displacement from storm surge rather than progressive wind-induced failure (**Figure 5**). When structures remain standing, damage below the stillwater line or debris line is typically attributed to flooding, while damage above this elevation, without corresponding lower-level distress, suggests wind effects.

Last but not least, structures subjected to intense wave loading action and recurrent impacts from floating debris may experience the failure of load-bearing walls, ultimately leading to partial or total roof collapse. As storm surge waters advance inland, the most severe structural damage typically occurs along the façade directly exposed to the incoming water, where hydrodynamic forces and wave impacts are concentrated. Post-storm reconnaissance studies have consistently documented buildings exhibiting a characteristic "pitched-down" orientation toward the shoreline, indicating that the primary failure mechanism was water-induced loading rather than wind pressure effects [35], [52], [53]. This distinctive structural response is illustrated in **Figure 6**. Notably, the roof covering systems in the remaining sections show little to no evidence of wind-related damage.

Integration of Meteorological and Hydrological Data

The correlating field observations with climatological and hydrological records is critical to establishing event chronology. Meteorological datasets from NOAA, NHC, and USGS should be analyzed to identify the timing and magnitude of peak wind velocities relative to maximum inundation levels [45]. These

Figure 5
Storm surge effects: (A) battering effects on seawall and (B) scouring and erosion of soil below sidewalk.

Figure 6
Aerial photographs: (A) intact building prior to the passing of Hurricane Ian and (B) "pitched down" building after the passing of Hurricane Ian. (Figures courtesy of Eagleview) [54].

incremental datasets allow the assessor to determine whether flooding preceded, coincided with, or followed peak wind events.

In addition, the Post Storm Data Acquisition (PSDA) reports from the National Weather Service (NWS) provide wind speeds, surge stillwater elevations, and measurement annotation results. These data sets are of high importance to help in determining whether the damage was caused by wind and/or storm surge [12], [45]. Similarly, the FEMA Flood Recovery Maps document surveyed waterline elevations and is invaluable for establishing the depth of inundation. As such, forensic engineers must distinguish between stillwater height and total wave height, the latter extending up to 50% to 55% higher than the stillwater level due to wave and debris action. This is illustrated in ASCE 7-22 [26] and shown in **Figure 7**. Note that "ds" is the stillwater level and **Figure 7** contains two diagrams: one with the space behind the vertical wall dry and one where flooding has already occurred in the space behind the vertical wall.

Forensic Correlation and Comparative Analysis

To confirm preliminary conclusions, forensic engineers are highly urged to conduct comparative analysis of surrounding structures and vegetation. The degree of wind-related damage to nearby roofs, trees, and claddings can help estimate local wind intensities. Conversely, uniform low-level destruction or debris patterns aligned with flow direction reinforce the likelihood of surge impact. Even when only the foundation remains, telltale evidence persists. Therefore, determining whether a structure was damaged by wind or storm surge requires a holistic forensic approach combining:

- Damage pattern recognition: Distinguishing between wind and storm surge damage begins with identifying characteristic damage patterns. As noted previously, wind-related damage typically exhibits a top-down progression, with failures initiating at the roof, upper walls, or windward openings as uplift and lateral pressures increase. However, as previously noted, storm surge damage follows a bottom-up pattern, with structural distress starting near the ground or lower elevations due to hydrostatic and hydrodynamic forces, debris impact, and scour.

- Elevation-based analysis: Evaluating the vertical distribution of damage is helpful to establish whether the forces originated from wind or surge-related forces. By comparing observed damage to the elevations, such as documented stillwater levels, debris lines, and high-water marks, forensic engineers can determine if the observed damage aligns with surge-related forces or excessive wind-induced forces. Damage observed below the established flood line is typically associated with storm surge damage (or flooding), whereas damage observed to the higher components of a structure (above the

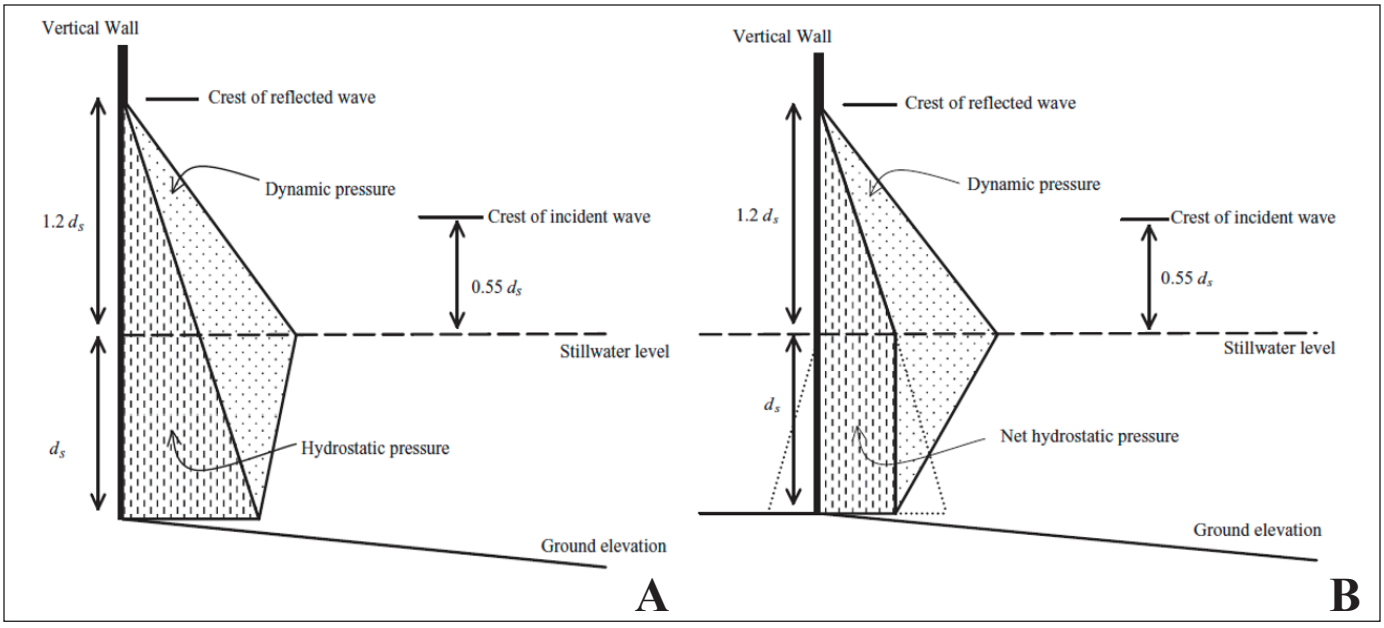

Figure 7
Schematic of breaking wave pressures against a vertical wall: (A) space behind vertical wall is dry and (B) stillwater level is equal on both sides of wall (courtesy of ASCE 7-22 [26], Chapter 5: Flood Loads).

established flood line) is associated with potential impacts from excessive wind-induced forces, if there is any.

- Corroborating Data: Meteorological and hydrological data serve as critical evidence to validate the physical observations obtained during the forensic investigation. Wind speed, predominant wind direction, location of the structure with respect to the eye of the hurricane, location of the hurricane at different times (pre- and post-landfall) are analyzed in conjunction with available nearby tide gauge data, surge hydrographs, and rainfall intensity to establish the timing and magnitude of each hazard. Assessing the structural damage and/or failure with the aforementioned evidence enables a more defensible determination of whether the observed damage corresponds with peak wind loads or the advancing storm surge, or a combination of both.

- Comparative Evaluation: The effect of tropical cyclones can affect vast areas of land simultaneously. Consequently, assessing the damage to neighboring civil infrastructure and vegetation provides valuable contextual evidence. Structures of similar design, elevation, and orientation often exhibit consistent patterns of wind or surge damage under comparable exposure conditions. Additionally, examining fallen trees, displaced debris, and erosion patterns help confirm the dominant force mechanism. This comparative evaluation strengthens forensic conclusions by correlating individual observations with broader, community-scale impact trends, typically associated with tropical cyclones.

In summary, in order to accurately differentiate between wind and surge-related damage, the forensic engineer should document the dimensions of the structure, the location of the structure to obtain flood zones and required base elevations, the roofing components, the wall components, the types of materials that make up the subject structure, the structure's orientation, the damage progression (top-to-bottom or bottom-to-top), flood lines (if any), neighboring structures, surrounding vegetation, and verifiable weather conditions. The forensic engineer should base their findings and conclusions on corroborating that excessive loading, due to wind and surge-related forces, indeed affected the area of the subject structure.

Case Study from Hurricane Helene (2024)

The subject property selected for this case study is located in the city of Keaton Beach, Florida, about 20 miles south of the city of Perry and lies directly along the Gulf of Mexico coastline, facing westward towards the open water. This geographic positioning places the structure in a highly exposed area, classified as Exposure Category D per ASCE 7-22 [26]. The residence itself is a two-story, elevated, wood-framed structure supported by a series of timber posts (or stilts) embedded in the ground, constructed in 1987. The architectural layout includes a partially enclosed lower level, herein referred to as the "first floor," which functions primarily as an open parking and storage area. Approximately 50% of the perimeter of this level is open. The upper level, herein identified as "second floor," is enclosed with conventionally framed wood walls covered with vinyl siding. The roof structure consists of a gable roof type covered with metal panel roof system, as shown in **Figure 8**.

After the passing of Hurricane Helene on September

Figure 8
Front elevation of the residence: (A) prior to Hurricane Helene (courtesy of Google Street View[55] — dated 4/2021) and (B) after the passing of Hurricane Helene (dated 10/2024).

Figure 9
Remnants of stilts used to support the structure before failure (dated 10/2024).

26, 2024, the subject property underwent two post-loss site assessments: the first was conducted by the field adjuster assigned by the insurance company in October 2024, and the second was performed by a forensic engineer in May 2025 as part of a detailed structural evaluation. Findings from both site visits revealed that the entire structure had been completely displaced and removed from its original foundation. No portions of the residential structure remained in situ, as exhibited in **Figure 8**, besides a few limited portions of the stilts that were supporting the main structure in addition to some debris.

The only elements observed at the time of each inspection were the lower segments of the first-floor timber posts, which formerly supported the structure above the ground in accordance with typical coastal elevation practices in addition to a concrete monolithic slab-on-grade. Photographic documentation from both assessments revealed discernible signs of age-related deterioration in the exposed timber elements, including weathering, surface degradation, and biological decay, all consistent with prolonged exposure to moisture (**Figure 9**). Additionally, during the assessment performed by the forensic engineer and his interview with the homeowner, it appears that the structure's exterior cladding system (building envelope) had been upgraded to a vertical board-and-batten finish prior to the reported date of loss.

As the structure itself was no longer present and therefore could not be physically inspected, several dimensional estimates were derived using photographs obtained from publicly available street-level imagery, specifically Google Street View [55]. Based on the visual analysis of these images and the identification of the exterior cladding materials, it was determined that the height of the first-floor, up to the lowest horizontal member of the residence, was "approximately" 7.5 feet above grade. This estimation was derived by identifying the use of standard vinyl siding on the exterior walls, which typically features an exposed height of approximately 5 inches per course. A visual count of the vertically stacked siding sections yielded an estimated total of 18 individual courses, resulting in the calculated overall height. This method, while approximate, provides a reasonable estimate in the absence of direct site measurement, as portrayed in **Figure 10**.

On another note, the subject residence is located within a FEMA-designated "AE" flood zone with a Base Flood

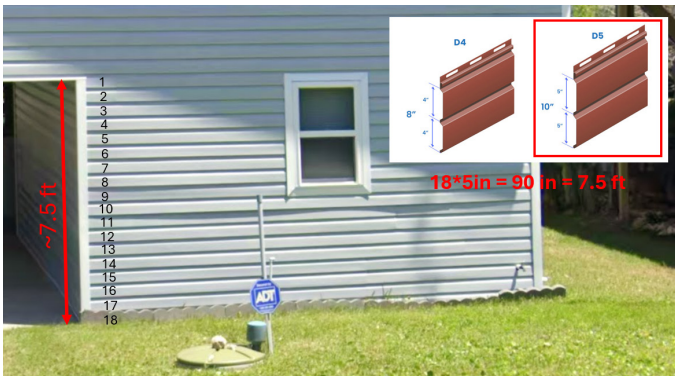

Figure 10
First floor height estimation (about 7.5 feet to lowest horizontal member), courtesy of Google Street View [55] — dated 4/2021.

Elevation (BFE) of 16 feet (EL 16) above NAVD88 datum (North American Vertical Datum of 1988), indicating a coastal high-risk and high-hazard area subject to wave action, storm surge, and velocity flow during major storm events (**Figure 11**).

Note that NAVD88 consists of a leveling network on the North American continent, ranging from Alaska through Canada, across the United States, affixed to a single origin point on the continent. According to FEMA's designation, structures in AE zones are required to have the lowest finished floor elevated at or above the base flood elevation (BFE), allow unobstructed flow of water beneath the building, and use any enclosed area (below the BFE) as parking, building access or storage area only. Being in an area with a BFE of 16 feet, the residence living spaces must be elevated above grade, with the lowest finished floor situated at or above the BFE, in compliance with current floodplain management regulations, regardless of the site's elevation with respect to the mean sea level. Given its location in an AE zone, the residence is particularly vulnerable to storm surge (hydrostatic forces), high-velocity wave impact (hydrodynamic forces), and erosion-related foundation undermining during extreme coastal storm events such as hurricanes. Please note that the structure may have been built following the current standards in the year of the construction of the subject structure. However, based on current FEMA flood elevations, the structure is vulnerable to storm-surge damage.

It must be noted that the BFE is the computed elevation to which floodwater is anticipated to rise during a base flood (a flood having a 1% annual chance of occurrence, also known as the 100-year flood) from the NAVD88 datum. Additionally, the elevation of the structure is estimated to be approximately 7 feet (above NAVD88). As such, the structure's estimated elevation of the second floor, the lowest horizontal structural member (about 7.5 feet above ground level) was insufficient to comply with the regulation provided by the FEMA flood maps (BFE of 16 feet – NAVD88) and did not meet the minimum flood hazard mitigation standards at the time of the date of loss. However, it must be noted that the house was built in the late '80s, and it is possible that it was built for the requirements set forth at the time of the construction of the subject structure.

Hurricane Helene Storm Surge

According to NOAA, Hurricane Helene made landfall in the Big Bend region of Florida on the evening of September 26, 2024, as a Category 4 hurricane according to the Saffir-Simpson Hurricane Wind Scale, bringing severe destruction to coastal communities in the vicinity of the landfall and across the west coast of Florida [57]. Hurricane Helene's path and wind circulation are both presented in **Figure 12**. Furthermore, Hurricane Helene's path made landfall approximately 14 miles northwest of the subject structure as showcased in **Figure 13**, where the yellow pin locates the residence, the red pins locate the position of Hurricane Helene's eye at landfall, and the green

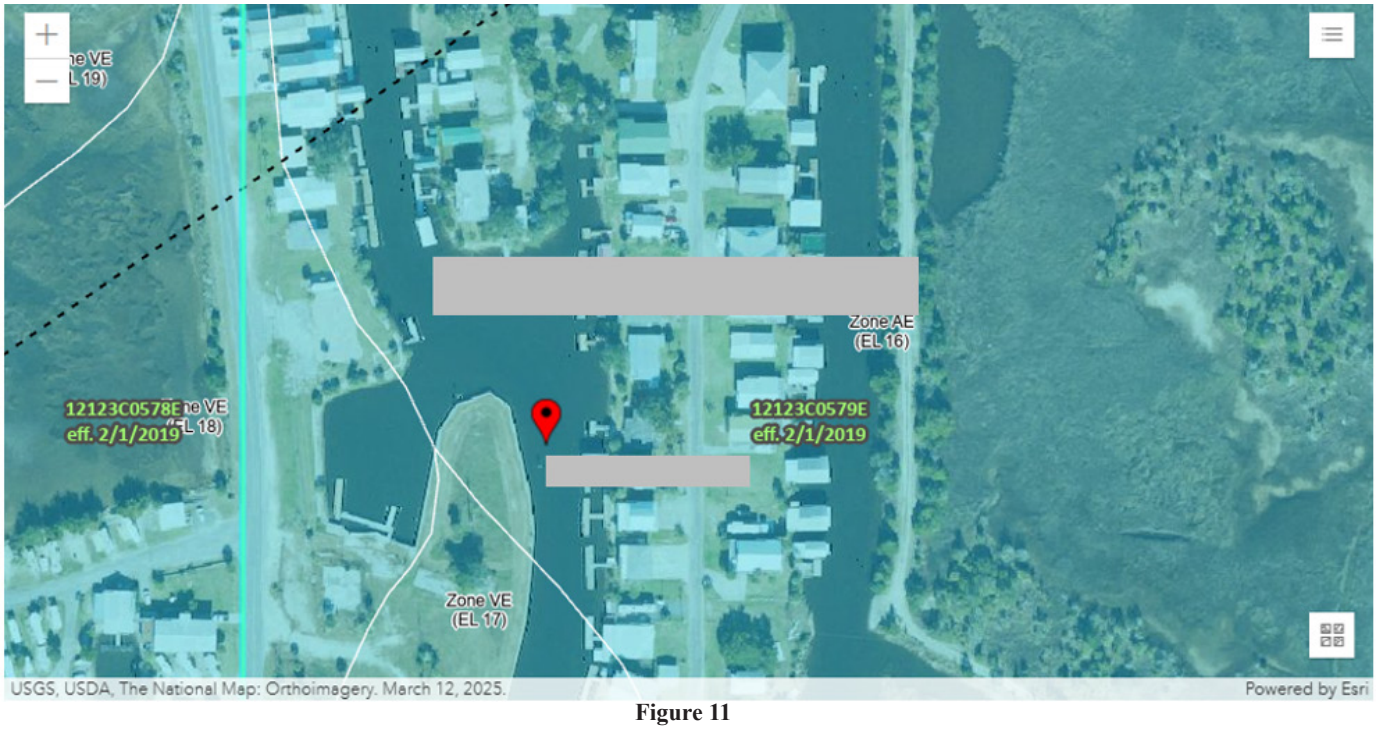

Figure 11
FEMA flood zoning for the subject residence (courtesy of FEMA Flood Maps [56]).

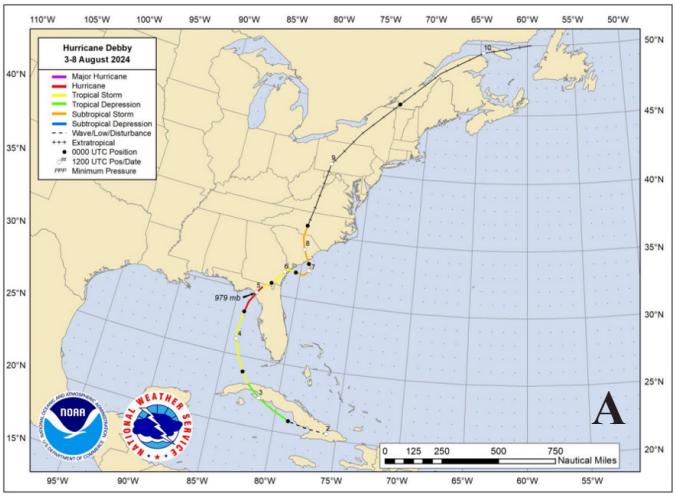

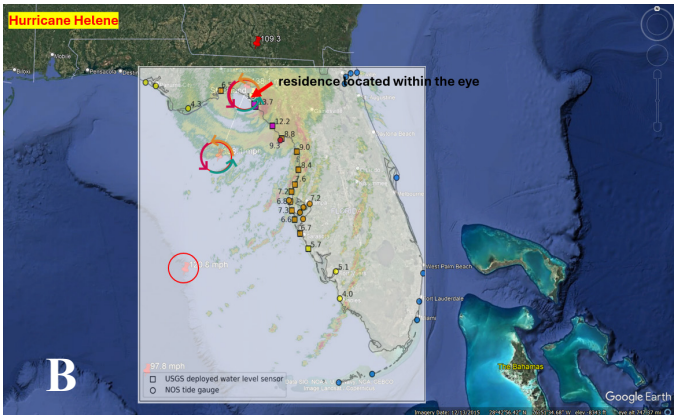

Figure 12
Hurricane Helene's: (A) path and (B) wind direction (both figures are courtesy of NOAA [57]).

pin locates the path of Hurricane Debby (south of the residence). On a side note, Hurricane Debby was a Category 1 hurricane that made landfall near Steinhatchee, Florida, on August 5, 2024. This hurricane and its path were analyzed due to their proximity in terms of time and geographical location at landfall with respect to the subject structure prior to the passing of Hurricane Helene.

Due to the size of Hurricane Helene's wind field along its path, storm surge impacts were amplified across a broad area with effects reaching as far south as Naples and impacting densely populated areas including the Tampa Bay and Sarasota regions. According to data collected by the USGS water level sensor network, the peak surge inundation within the remote stretch between Keaton Beach and Steinhatchee reached 12 to 16 feet above ground level (AGL) as shown in **Figure 13**. It must be noted that the National Hurricane Center storm surge analysis provides water rises Above Ground Level (AGL) measured from the Mean Higher-High Water (MHHW) datum — this is approximately 1.65 ft above NAVD88 datum.

For verification purposes, two independent water level sensors were analyzed to assess storm surge conditions in proximity to the subject property. The first sensor, operated by NOAA at station # 8727520 and located in Cedar Key, Florida, recorded a peak water level rise of approximately 10 feet (**Figure 14**). The graph indicates that the rise in water up to a height of approximately 7.5 feet level occurred on September 26, 2024, at approximately

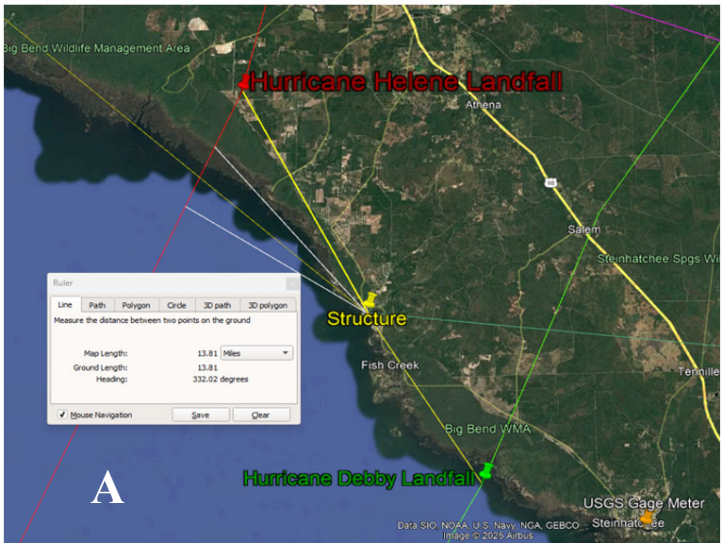

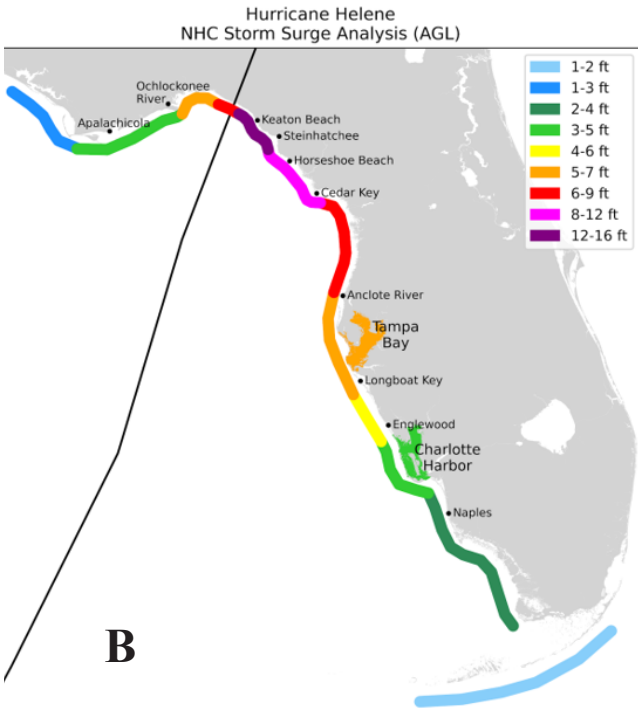

Figure 13
Hurricane Helene's path and landfall with respect to: (A) distance (in miles) to the subject property (courtesy of Google Earth [58]) and (B) storm surge analysis on the west coast of Florida (courtesy of Google [58] and NOAA [57]).

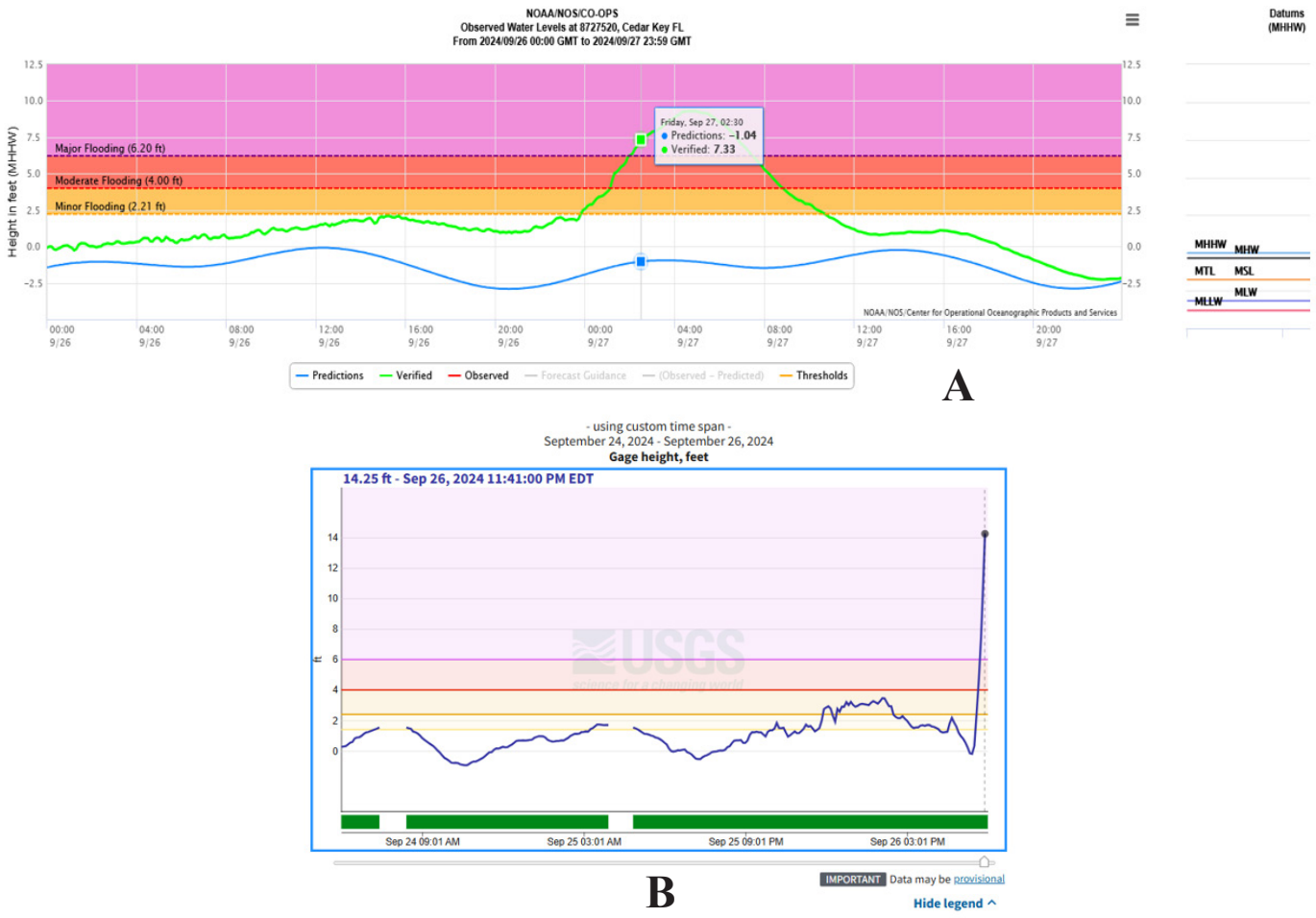

Figure 14
(A) Cedar Key, FL water level (in feet) (NOAA) [59] and (B) Steinhatchee, FL gage height (in feet) (USGS) [60].

9:30 PM (EST). It is important to note that Cedar Key is located approximately 60 miles southeast of the subject property and thus, this sensor may reflect surge behavior in a more southern region of the storm's impact zone. The second sensor, operated by USGS at gage station # 02324170, was located near the Steinhatchee River delta, approximately 15 miles southeast of the subject property. This gauge recorded a peak water level rise of approximately 14 feet before data transmission ceased due to unknown causes (**Figure 14**). The time-history data from this sensor indicated that the water level reached 14.25 feet (above ocean surface mean sea level) at approximately 10:41 PM (EST) on September 26, 2024. The recorded time at which the 14.25-foot water level was reached was used as a reference to estimate when floodwaters were already affecting the lowest horizontal structural member of the subject property, as estimated earlier in **Figure 10**.

Based on the previously discussed data that was collected from the NOAA and USGS sensors and gauges, the approximate sequence of events is outlined as follows:

- The tidal gage at Cedar Key reported water level measurements in GMT. According to the recorded data, the storm surge reached a height of 7.5 feet (above Mean Higher High Water – MHHW) at approximately September 27, 02:30 GMT (or September 26, 21:30 EST). Analysis of the tidal curve indicates that storm surge inundation had already begun prior to the landfall of Hurricane Helene (**Figure 14**). Note that the MHHW datum is defined as the average of the higher high water height of each tidal day observed over the National Tidal Datum Epoch. For stations with shorter series, comparisons of simultaneous observations with a control tide station are made to derive the equivalent datum of the National Tidal Datum Epoch.

- Similarly, data from the Steinhatchee River water level sensor indicated a water level rise reaching 14.25 feet at approximately September 26, 23:41 EDT (or September 26, 22:41 EST). This confirms

that the onset of storm surge preceded the hurricane's landfall at this location as well (**Figure 14**).

- In their report [57], the NHC provided the hurricane eye position data in UTC. According to their tracking, the eye of Hurricane Helene was located just offshore on September 27, 00:00 UTC (or September 26, 19:00 EST). Landfall occurred shortly thereafter, with the eye positioned approximately 5 miles inland by September 27, 03:10 UTC (September 26, 22:10 EST).

The previous findings confirm that storm-surge conditions were already underway before Hurricane Helene's official landfall. This indicates that many of the surge-related impacts developed independently of the intense wind forces typically associated with the passage of the storm's eye. Moreover, the observations align with earlier studies showing that surge height is driven more by the storm's overall size and the shallowness of the continental shelf than by pre-landfall wind strength [61], [62]. In particular, long, gently sloping seabeds tend to amplify storm-surge levels, a defining bathymetric feature of Florida's Big Bend region [63].

Hurricane Helene Wind Direction

In the Northern Hemisphere, hurricanes exhibit a counterclockwise rotation due to the Coriolis effect [64]. Throughout Hurricane Helene's approach and eventual landfall, the storm's core remained consistently west of the subject property. As a result, the most intense wind forces affecting the site would have been from the southwest, consistent with the forward-right quadrant of a landfalling hurricane, typically the region associated with the strongest winds and surge impacts. The southwest winds, combined with the concave configuration of Florida's Big Bend coastline, would have funneled water inland in the same general direction as the wind vectors, amplifying storm surge effects along vulnerable low-lying areas, as demonstrated in **Figure 15**. An analysis of wind circulation patterns in the immediate vicinity of the subject property reveals that tangential wind components, around the storm's center, would have directed water and wave energy toward the northeast. This wind-driven water movement would have resulted in significant lateral hydrodynamic forces acting on coastal structures, particularly those with limited elevation and exposure along the Gulf-facing shoreline, such as the subject property. This is portrayed in **Figure 15**.

Based on the estimated wind circulation patterns, tangential wind velocities, and the projected direction of storm surge flow, a targeted survey was conducted to evaluate the displacement and distribution of debris resulting from Hurricane Helene's combined wind- and surge-induced forces. Given the storm's orientation and dynamics, it was anticipated that debris originating from the structures located in Keaton Beach would have traveled in a generally northeast direction, as shown in **Figure 16**. This projected debris path was subsequently validated through

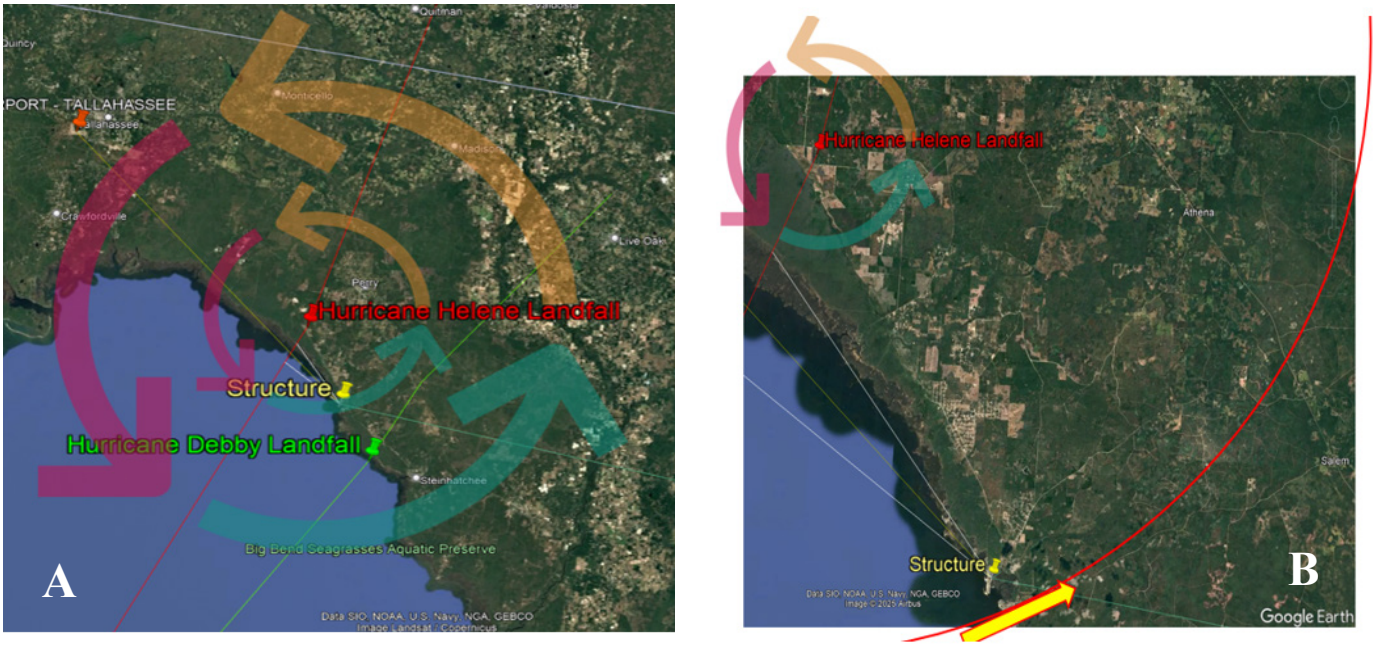

Figure 15

(A) Hurricane Helene circular pattern and (B) Hurricane Helene tangential winds (in yellow) (figures courtesy of Google Earth [58]).

a detailed analysis of high-resolution aerial satellite imagery, which confirmed that the structure had indeed been displaced along the estimated trajectory. Specifically, the entire building was located approximately 1,780 feet northeast of its pre-Hurricane Helene location, aligning with the modeled direction of wind and water forces during the storm event (**Figure 16**).

Displaced Structure

Based on the modeled wind circulation patterns of Hurricane Helene and the estimated direction of storm surge forces described earlier, the main structure was determined to have been displaced approximately 1,780 feet northeast of its original pre-Hurricane Helene location. To conclusively verify that the displaced structure corresponded to the subject property, a detailed visual and dimensional validation was conducted using multiple data sources, including aerial imagery and structural feature comparisons.

The first phase of verification involved analyzing the roof geometry and ventilation layout, features which were not observed in any of the surrounding buildings. As documented in the pre-Hurricane Helene imagery, the subject structure featured a distinctive roof configuration with a rectangular cut-out at the top-left corner, along with three evenly spaced roof vents. These features were found to match those of the displaced structure identified in the October 13, 2024, imagery taken after the passing of Hurricane Helene, strongly supporting the assertion that the same structure had been relocated by storm surge forces, as portrayed in **Figure 17**.

The second phase involved comparing roof area measurements before and after the passing of Hurricane Helene. Satellite imagery dated December 26, 2018, before the alleged date of loss (DOL), and October 13, 2024 (post-DOL), were used to estimate roof square footage. The original structure was found to have a roof area of approximately 1,737 square feet, while the displaced structure measured approximately 2,065 square feet — a difference of roughly 16%. While initially appearing to be a discrepancy, further investigation revealed the source of the additional area. A side-by-side comparison of right-side elevation images of both structures revealed a consistent alignment in architectural features, including window count, placement, and dimensions.

However, a protruding section at the rear elevation of the displaced structure, absent in the earlier satellite imagery, was identified as the cause of the increased roof area (light blue arrows in **Figure 17**). This extension, likely an enclosed or semi-enclosed addition to the rear balcony area noted in the pre-DOL aerial image, appears to have been constructed sometime after the 2018 imagery but prior to the passing of Hurricane Helene. A review of local building permit records yielded no documented approvals for such an addition. Nevertheless, visual evidence strongly suggests that an expansion was made to the rear of the property, as indicated by the green arrow in the pre-DOL imagery. This addition further confirms that the displaced structure matches the architectural characteristics and evolution of the original residence.

To further assess and better understand the magnitude of the forces that the structure was subject to during Hurricane Helene (e.g., wind- and surge-related forces), an estimation of forces was carried out, using engineering analysis and several assumptions, to shed light on the possible mechanisms of failure during the passing of Hurricane Helene.

First, an estimation of the structure's dead load was carried out following assumptions of material self-

Figure 16

(A) Estimated trajectory of debris due to Hurricane Helene forces [58] and (B) satellite image taken on October 13, 2024, after the passing of Hurricane Helene showing original property location and displaced property location (figures courtesy of Eagleview [54]).

weight from ASCE 7-22 (Chapter 3), which resulted in a total dead load of approximately 118 kips. Note this estimation was carried out by considering the roofing material, ceilings, flooring, exterior walls, interior partitions, mechanical-electrical-plumbing (MEP) components and fixed equipment based on the overall dimensions of the

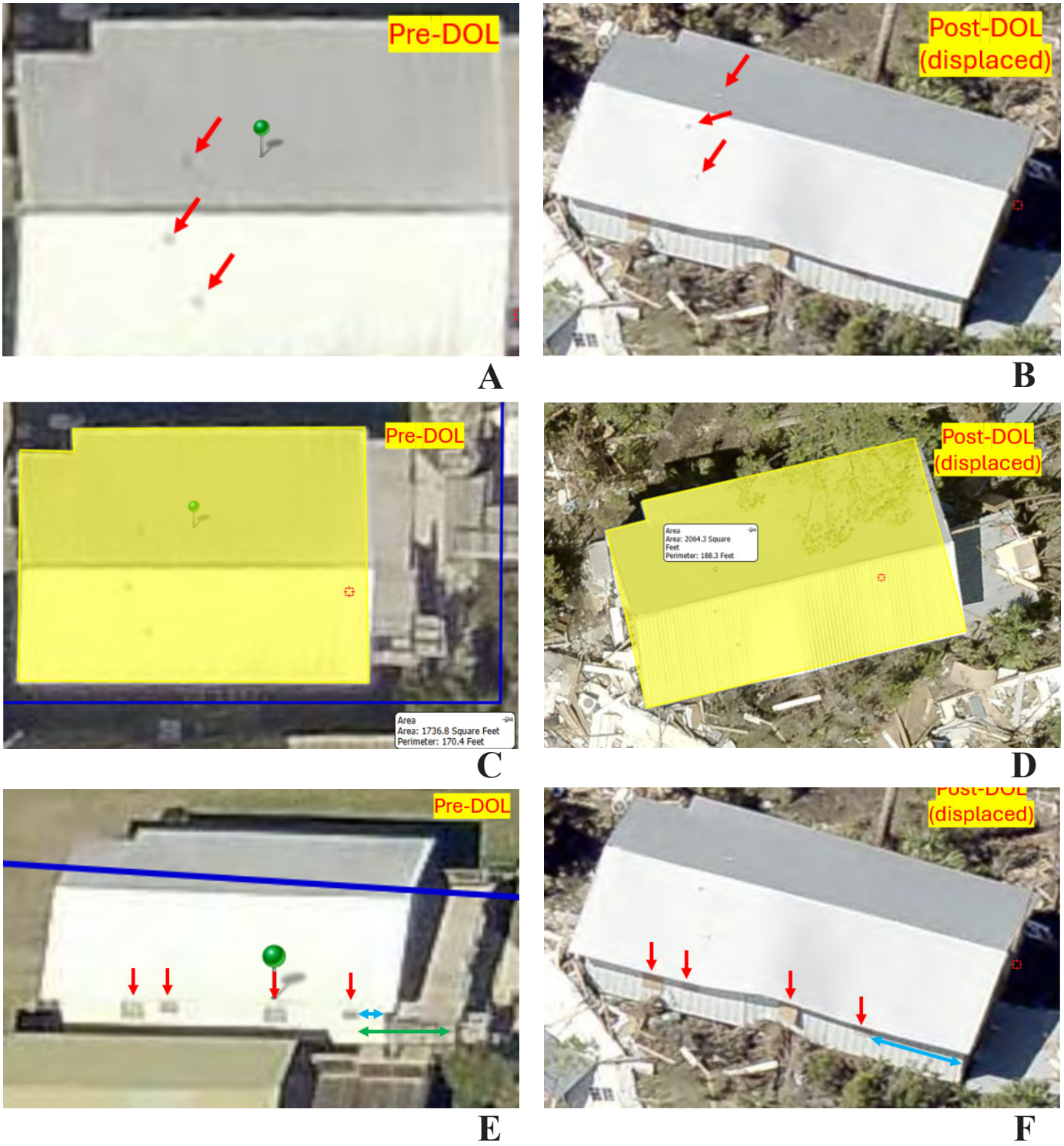

Figure 17

(A) Roof shape and appurtenances pre-DOL, (B) roof shape and appurtenances post-DOL, (C) roof estimated area pre-DOL, (D) roof estimated area post-DOL, (E) south elevation fenestration and details pre-DOL, and (F) south elevation fenestration and details post-DOL (all figures courtesy of Eagleview [54]).

structure (**Figure 18**). Also note that GWB stands for gypsum wall board.

Additionally, attempts to estimate the buoyant forces produced by stillwater onto the structure were estimated and ranged between 605 and 1,142 kips (about 5 to 10 times larger than the self-weight of the structure). This assumption is based on a storm surge height ranging between 12 and 16 feet above ground level, and with a 4.5 to 8.5 feet structure submersion (first-floor height was previously estimated at about 7.5 feet from ground level, and the calculations were conducted for a building with plan dimensions of 60 feet of length and 35 feet of width). Furthermore, the hydrodynamic forces induced on the structure were estimated to be approximately 9.3 kips, assuming a water flow velocity of 5 ft/s. Note that wave impact forces were not estimated [40]. Accordingly, the minimum buoyancy force acting on the structure, assuming about 12 feet of storm surge height, was about five times larger than the building self-weight alone including all the structural and architectural components.

Moreover, following ASCE 7-22 guidelines, the magnitude of the wind-induced forces, assuming 140-mph gusts, was estimated to be approximately 84 kips and 24 kips for lift and drag forces on the structure, respectively. Finally, an estimation of the overturning moment produced by wind-induced forces yielded about 2,600 ft-kip in contrast to the counter-overturning moment produced by the self-weight of the structure, which was estimated as 3,500 ft-kip. A diagram depicting the estimated wind-induced forces and associated overturning moment is shown in **Figure 19**. Note that F1 stands for the windward drag force, F2 is the leeward drag force, F3 stands for the lift force, and W is the associated self-weight of the structure.

Lastly, a visual assessment of the displaced structure revealed the roof covering sustained no discernible signs of missing, torn, displaced or damaged metal panel roofing components, as observed in **Figure 20**. Furthermore, a key finding during the authors' investigation was the deterioration of the columns and metal brackets, which showed clear signs of missing fasteners, wood rot and sectional reduction due to age-related deterioration of the columns/piers.

Based on the analysis of the conditions and the evidence observed at the inspection site discussed earlier, the following conclusions were made:

- The comprehensive forensic analysis of the subject property and the understanding of wind and storm surge effects on structures indicate that the total failure and displacement of the subject structure were caused by excessive storm surge levels and associated hydrodynamic forces, rather than by wind-induced forces. Multiple lines of evidence support this conclusion including structural assessments, engineering analysis, satellite imagery, and the conditions of Hurricane Helene before and after making landfall.

- The aerial imagery of the displaced structure revealed no significant damage to the roof cover-

Component	Dead Load (psf)	Area	Total Load (lbs)
Roof - Metal over Sheathing	10 psf	2,064 SQ FT	20,640
Ceiling - GWB + Joists	8 psf	2,064 SQ FT	16,512
Floor - wood subfloor	10 psf	2,064 SQ FT	20,640
Exterior Walls (wood frame, GWB inside, siding outside)	15 psf	1,508 SQ FT	22,620
Interior Partitions	10 psf	2,064 SQ FT	20,640
Mechanical, Electrical, Plumbing (MEP)	5 psf	2,064 SQ FT	10,320
Fixed Equipment (e.g., cabinets)	3 psf	2,064 SQ FT	6,192
		Total Dead Load (lbs)	**117,564**

Figure 18
Dead load estimates.

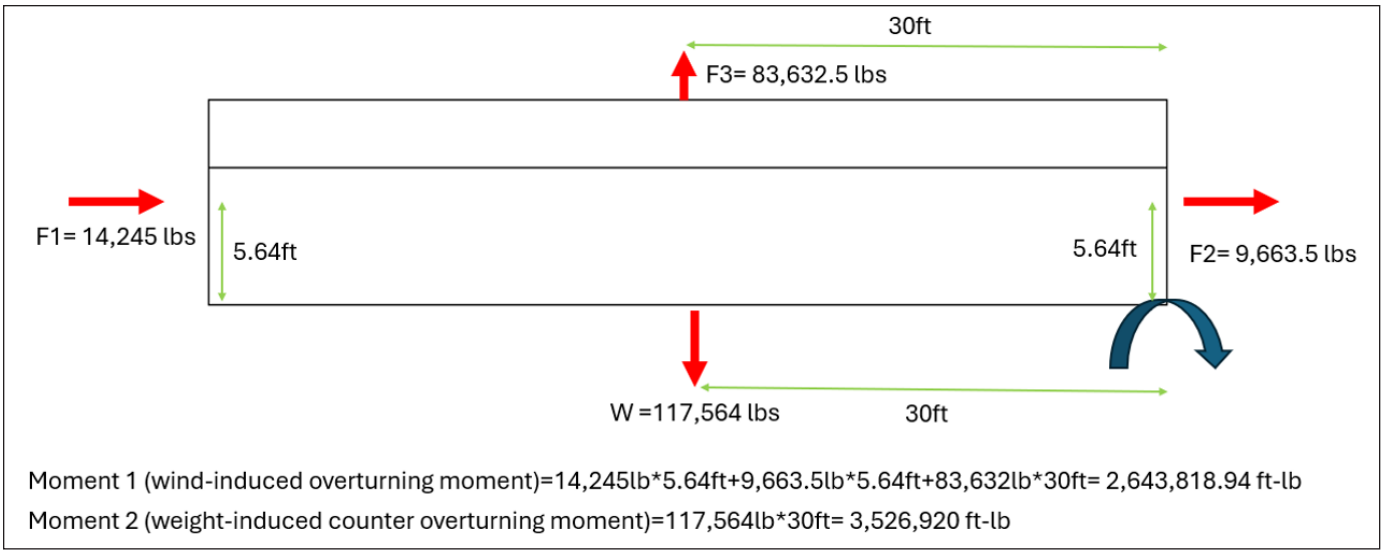

Figure 19
Estimated wind-induced forces diagram and accompanying moment calculations.

Figure 20
Displaced structure —– approximately 1,780 feet northeast from its original location: (A) right elevation view, (B) left elevation view, and (C) top view (all figures courtesy of Eagleview [54]).

ing or exterior siding, components typically susceptible to wind damage, indicating that the structure was not compromised by high wind pressures prior to or after its displacement. The structure was located approximately 1,780 feet northeast of its original location, mostly intact, in a direction consistent with modeled storm surge and tangential wind circulation patterns emanating from the path and trajectory of Hurricane Helene. This displacement aligns with the trajectory predicted by surge-induced water movement rather than chaotic windborne debris behavior.

Other Observations from Hurricane Helene

Although the earlier case study mainly focused on storm surge damage to a coastal structure in the town of Perry, Florida, including the combined effects of hydrostatic and hydrodynamic forces, field investigations of other structures revealed that numerous buildings did survive the elevated storm surge levels recorded at the time of the passing of Hurricane Helene. Such structures were noted with distinct wind-related damage as shown earlier in the manuscript. It was determined that a key factor in these structures withstanding the storm was their relatively recent construction, which followed updated versions of the local jurisdiction and state building codes. The assessment of the neighboring structures included obtaining permit histories and property appraiser reports, providing information pertaining to their year of construction as well as any recent roof replacement permits. This section summarizes the mechanisms of wind-induced damage observed in these surrounding structures and contrasts them with the damage patterns associated with storm surge.

Wind-induced damage during hurricane events is primarily driven by aerodynamic pressures acting on the building envelope and roof system. These pressures result from a combination of sustained wind flow, gust effects, turbulence, and flow separation around building geometries due to bluff-body aerodynamics. Elevated structures located outside the storm-surge inundation zone remain vulnerable to these forces, particularly at building corners, roof edges, ridges, and discontinuities in the envelope [50], [51], [65]. Additionally, due to the atmospheric boundary layer profile, structures with higher elevations have increased resiliency against surge-related forces but are exposed to increased wind-induced loading. Greater elevations result in increased forces to the lateral force resisting systems, such as foundation columns, imposing increased moment loading that the columns and their bracing connections must withstand, signifying an important aspect of the structure to analyze.

Suction (negative) pressures acting on roof coverings can exceed the attachment capacity of shingles, tiles, membrane systems as well as wall components leading to localized loss of roof or envelope covering materials. Once roof and/or wall coverings are compromised, increased internal pressurization may occur if envelope breaches develop, further amplifying uplift forces and accelerating progressive failure of the structure. Windborne debris impacts may additionally contribute to envelope breaches, particularly at wall claddings, soffits, fenestration systems, and garage doors [21].

As such, typical wind damage observations included partial loss of roof coverings, displaced or uplifted shingles, cracked or detached wall cladding, and damage to soffits as well as fascia boards. These damaged areas were generally localized in wind-critical zones and exhibited directional characteristics aligned with the prevailing wind field during the event.

The contrast between wind-induced damage in elevated structures and storm-surge–dominated damage in low-lying structures is significant for forensic attribution. Storm surge damage is characterized by lateral displacement of structural components, collapse or flotation of walls and floors, erosion or scour at foundations, and widespread water intrusion with associated sediment and debris patterns. In comparison, wind damage is generally more selective, affecting envelope components and roof systems without producing global structural instability in properly elevated buildings, as exhibited in **Figure 21** [21], [38], [48], [66]-[74].

The co-existence of these damage modes within the same geographic region underscores the importance of elevation, exposure, and load path continuity in determining damage causation. While both wind and storm surge are generated by the same meteorological event, the resulting damage mechanisms are distinct and must be evaluated independently to ensure accurate forensic conclusions. Representative photographs of wind-induced damage to elevated structures are included to illustrate typical envelope and roof failures attributable to aerodynamic loading (**Figure 22**). These photographs document roof covering displacement, localized wall cladding damage, and envelope breaches consistent with wind action, providing a visual contrast to the storm-surge–driven damage presented in the primary case

study. More information on wind flow around buildings as well as wind-related damage to residential roofs including shingle and tile roof coverings can be found in Azzi et al. [21].

Conclusion

Understanding the mechanisms by which hydrostatic and hydrodynamic loads interact with structural systems enables forensic engineers to more precisely differentiate

Figure 21
Coastal structure exhibiting: (A) warping of roof covering and (B) detachment of wall cladding.

Figure 22
Observed wind damage: (A) dislodging of metal panels in high suction pressure zones, (B) torn and partially torn shingles, (C) dislodging of soffits and roof fascia boards, and (D) warping of metal panels.

wind-induced damage from water-induced damage, mainly elevated storm surge levels. Hydrostatic and hydrodynamic actions primarily degrade structural elements at or near the foundation by inducing uplift, scour, and lateral fluid pressures. In contrast, wind loads produce their highest demand at elevated components such as roof coverings and components because wind velocity and corresponding aerodynamic pressures increase with height above the ground. Moreover, due to the substantially higher density of water relative to air (800:1), moving water can impart significantly greater momentum and lateral forces on structural members than wind, as shown in the aforementioned calculations section. Therefore, it is essential to accurately differentiate between wind and surge/flood damage in structural forensic investigations for the following reasons:

- Wind and flood damage are often differently insured. Establishing the correct peril is critical for fair claim resolution and policy compliance.

- Understanding the nature of damage informs future engineering standards and code compliance. For wind, this might include reinforced envelope components and impact-resistant fenestration design. On the other hand, for storm surge, strategies include increased elevation, foundation retrofitting, and breakaway construction in lower elevations of the property.

- Building codes and FEMA standards often rely on forensic assessments after the passing of extreme events to mandate peril-specific construction techniques in relevant geographical areas.

- Accurate assessment of wind versus storm surge damage guides emergency planning, regional development, and infrastructure upgrades.

- Urban planners, FEMA associates, and state agencies use forensic data to guide hazard mapping, land-use planning, and community resilience initiatives. Understanding true loss causation supports smarter investment in infrastructure and life-safety upgrades.

- Erroneous determination of causation can lead to unsafe reconstruction, legal disputes, and long-term vulnerability of coastal structures and communities.

Accurately distinguishing between wind and surge damage ensures technical, legal, financial, and ethical credibility in the aftermath of catastrophic storms. Literature, case studies, and expert practice all converge on the necessity of a rigorous, evidence-driven approach that protects property owners, supports infrastructure resilience, and maintains the credibility of the engineering discipline in general and the forensic engineering discipline in particular.

Acknowledgments

The authors greatly acknowledge the internal support provided by DDA Forensics and the engineering team. The contents of this paper reflect the views of the authors, who are responsible for the facts and the accuracy of the information presented herein.

References

[1] H. Masoomi, J. van de Lindt, M. Ameri, T. Do and B. Webb, "Combined Wind-Wave-Surge Hurricane-Induced Damage Prediction for Buildings," ASCE Journal of Structural Engineering, vol. 145, no. 1, 2018.

[2] M. Baradaranshoraka, J. Pinelli, K. Gurley, X. Peng and M. Zhao, "Hurricane Wind versus Storm Surge Damage in the Context of a Risk Prediction Model," ASCE Journal of Structural Engineering, vol. 143, no. 9, 2017.

[3] R. Pielke Jr., J. Gratz, C. Landsea, D. Collins, M. Saunders and R. Musulin, "Normalized Hurricane Damage in the United States: 1900–2005," ASCE Natural Hazards Review, vol. 9, no. 1, 2008.

[4] K. Quealy, "The Cost of Hurricane Harvey: Only One Recent Storm Comes Close," The New York Times, 1 September 2017. [Online]. Available: https://www.nytimes.com/interactive/2017/09/01/upshot/cost-of-hurricane-harvey-only-one-storm-comes-close.html?smid=pl-share. [Accessed 25 November 2025].

[5] N. D. O. Commerce, "Hurricane Harvey: A Look Back Seven Years Later," National Environmental Satellite, Data, and Information Service, 26 August 2024. [Online]. Available: https://www.nesdis.noaa.gov/news/hurricane-harvey-look-back-seven-years-later. [Accessed 25 November 2025].

[6] NOAA, “National Coastal Population Report: Population Trends from 1970 to 2020,” National Oceanic and Atmospheric Administration, 2017.

[7] K. Crosset, T. Culliton, P. Wiley and T. Goodspeed, “Population trends along the coastal United States 1980-2008,” National Oceanic and Atmospheric Administration (NOAA), Washington, DC, 2004.

[8] NOAA, “Natural hazard statistics,” National Oceanic and Atmospheric Administration, 2017.

[9] M. McCullough, A. Kareem, A. Donahue and J. Westerink, “Structural damage under multiple hazards in coastal environments,” Journal of Disaster Research, vol. 8, no. 6, pp. 1042-1051, 2013.

[10] T. Tomiczek, A. Kennedy and S. Rogers, “Collapse Limit State Fragilities of Wood-Framed Residences from Storm Surge and Waves during Hurricane Ike,” ASCE Journal of Waterway, Port, Coastal, and Ocean Engineering, vol. 140, no. 1, 2013.

[11] FEMA, “Mitigation Assessment Team Report: Hurricane Ike in Texas and Louisiana,” Federal Emergency Management Agency (FEMA), Washington, DC, 2009.

[12] D. Teasdale, "Field Evaluation of Damage from Wind and Flooding," in Structures Congress 2008: Crossing Borders, 2008.

[13] E. Roberts, “A Guide to Wind Versus Water Assessments for Property Damage Claims,” J.S. Held LLC, 2022.

[14] NIST, “Performance of Physical Structures in Hurricane Katrina and Hurricane Rita: A Reconnaissance Report,” National Institute of Standards and Technology, NIST Technical Note 1476, 2006.

[15] D. Prevatt, S. Kameshwar, D. Roueche, B. Rittelmeyer, T. Duarte, T. Heo, H. Ibrahim, S. Klepac, O. Lafontaine, T. Lin, L. Manuel, S. Pilkington, Y. Pinyochotiwong, J. Santiago-H, S. Strader, K. Gurley, T. Kijewski-Correa and K. Mosalam, “JOINT PRELIMINARY VIRTUAL AND EARLY ACCESS RECONNAISSANCE REPORT (PVRR-EARR),” National Science Foundation, Structural Extreme Events Reconnaissance (StEER), 2021.

[16] NHC, “Tropical Cyclone Report: Hurricane Harvey,” National Hurricane Center, 2018.

[17] FEMA, “Hurricane Irma in Florida: Building Performance Observations, Recommendations, and Technical Guidance,” Federal Emergency Management Agency, Mitigation Assessment Team Report, FEMA P-2023, 2018.

[18] M. Cortes, P. Arora, L. Ceferino, H. Ibrahim, D. Istrati, D. Reed, D. Roueche, A. Safiey, T. Tomiczek, I. Zisis, M. Alam, T. Kijewski-Correa, D. Prevatt and I. Robertson, “StEER: Hurricane Ian Preliminary Virtual Reconnaissance Report (PVRR),” Structural Extreme Events Reconnaissance (StEER) - Hurricane Ian, DesignSafe-CI, 2022.

[19] A. Kyprioti, J. Yuzbasi, H. Dang, A. Jana, S. Kameshwar, A. Diekmann, S. Garcia, P. Mohammadi, M. Gutierrez Soto, B. Webb and e. al., “EARLY ACCESS VIRTUAL RECONNAISSANCE REPORT (EARR),” National Science Foundation (NSF), Structural Extreme Events Reconnaissance (StEER), 2025.

[20] T. Do, W. Wang, M. Amini, A. Abdelhady, S. Xu, R. NEGRI, S. Kameshwar, C. Wang, H. Dang, A. Jana, E. Carter, M. Alam, T. Kijewski-Correa, D. Prevatt, D. Roueche and K. Wolohan, “StEER: Hurricane Milton Preliminary Virtual Reconnaissance Report (PVRR),” National Science Foundation (NSF), Structural Extreme Events Reconnaissance (StEER) - Hurricane Milton, DesignSafe-CI, 2025.

[21] Z. Azzi, K. Vutukuru and M. Matus, “Discerning Wind-related Damage to Residence Roofs,” Journal of the National Academy of Forensic Engineers, 990, 2026.

[22] Z. Azzi, F. Habte, A. Elawady, A. Chowdhury and M. Moravej, "Aerodynamic Mitigation of Wind Uplift on Low-Rise Building Roof Using Large-Scale Testing," Frontiers in Built Environment, vol. 5, no. 149, 2020.

[23] Z. Azzi, F. Habte, K. S. Vutukuru, A. G. Chowdhury and M. Moravej, "Effects of roof geometric details on aerodynamic performance of standing seam metal roofs," Engineering Structures, vol. 225, no. 111303, 2020.

[24] C. Feng, A. Chowdhury, A. Elawady, D. Chen, Z. Azzi and K. Vutukuru, "Experimental assessment of wind loads on roof-to-wall connections for residential buildings," Frontiers in Built Environment, vol. 6, no. 10, 2020.

[25] K. Alawode, K. Vutukuru, A. Elawady and A. Chowdhury, "Review of wind loading on roof to wall connections in low-rise light wood-frame residential buildings," Journal of Wind Engineering and Industrial Aerodynamics, vol. 236, no. 105360, 2023.

[26] ASCE/SEI-7, Minimum Design Loads and Associated Criteria for Buildings and Other Structures, Reston, VA, USA: American Society of Civil Engineers (ASCE), 2022.

[27] K. Vutukuru, M. Moravej, A. Elawady and A. Chowdhury, "Holistic testing to determine quantitative wind-driven rain intrusion for shuttered and impact resistant windows," Journal of Wind Engineering and Industrial Aerodynamics, vol. 206, 2020.

[28] K. Vutukuru, M. Moravej and A. Chowdhury, "Wind driven rain intrusion reduction for shuttered windows," in Proceedings of 15th International Conference on Wind Engineering (15ICWE), Beijing, China, 2019.

[29] K. Vutukuru, J. Erwin and A. Chowdhury, "Full-scale simulation of wind-driven rain and a case study to determine the rain mitigation effect of shutters," Wind & Structures, vol. 38, no. 3, pp. 171-191, 2024.

[30] T. Fujita, "Proposed characterizations of tornadoes and hurricanes by area and intensity," SMRP 91, 1971.

[31] J. McDonald, K. Mehta, D. Smith and J. Arn Womble, "The Enhanced Fujita Scale: Development and Implementation," in ASCE Forensic Engineering 2009: Pathology of the Built Environment, 2009.

[32] H. Saffir, "Hurricane Wind and Storm Surge," The Military Engineer, vol. 423, pp. 4-5, 1973.

[33] R. Simpson, "The Hurricane Disaster Potential Scale," Weatherwise, vol. 27, no. 169, pp. 169-186, 1974.

[34] T. P. Marshall, E. Brusky and J. Last, "Storm surge on Lake Butte des Morts during the 11 June 2001 bow echo event," in 21st Conference on Severe Local Storms, San Antonio, TX, 2002.

[35] FEMA, "Is it Wind or Water?" Federal Emergency Management Agency 46, 1989.

[36] T. Marshall, "Hurricane Ivan Damage Survey," in 27th Conference on Hurricanes and Tropical Meteorology, Monterey, CA, 2006.

[37] FEMA, "Hurricane Ivan in Alabama and Florida: Observations, Recommendations, and Technical Guidance," Federal Emergency Management Agency, Mitigation Assessment Team Report, 294, 2005.

[38] T. Marshall, W. Bunting and J. Wiethorn, "Procedure for assessing wind damage to wood-framed residences," in The Symposium on the Fujita Scale and Severe Weather Damage Assessment, 83rd Annual Meeting, Long Beach, CA, 2003.

[39] FEMA, "Hurricane Katrina in the Gulf Coast," Mitigation Assessment Team Report: Building Performance, Observations, Recommendations, and Technical Guidance, FEMA 549, 2006.

[40] FEMA, "Coastal Construction Manual: Principles and Practices of Planning, Siting, Designing, Constructing, and Maintaining Residential Buildings in Coastal Areas (Fourth Edition)," Federal Emergency Management Agency, FEMA P-55, 2011.

[41] A. Ewis and O. Nofal, "Leveraging national datasets for systematic socio-physical coastal flood risk assessment at the community level," Computer-Aided Civil and Infrastructure Engineering, vol. 40, no. 25, pp. 4132-4148, 2025.

[42] USGS, "Field manual for identifying and preserving high-water mark data," United States Geological Survey, 2017.

[43] T. Koenig, J. Bruce, J. O'Connor, B. McGee, R. Holmes, R. Hollins, B. Forbes, M. Kohn, M. Schellekens, Z. Martin and M. Peppler, "Identifying and preserving high-water mark data," United States Geological Survey, 2016.

[44] FEMA, "Flood Damage-Resistant Materials Requirements for Buildings Located in Special Flood Hazard Areas in accordance with the National Flood Insurance Program," Federal Emergency Management Agency (FEMA) Technical Bulletin 2, 2008.

[45] D. Peraza, W. Coulbourne and M. Griffith, Engineering Investigations of Hurricane Damage: Wind versus Water, American Society of Civil Engineers (ASCE), ISBN: 9780784413715, 2014.

[46] A. Mehrabi, S. Dolati, P. Malla, S. Farhangdoust and Z. Azzi, Non-destructive Testing for Inspection of Bridges and Buildings, Cambridge Scholars Publishing, ISBN: 9781036445287, 2025.

[47] Z. Azzi, H. Al Sayegh, O. Metwally and M. Eissa, "Review of Nondestructive Testing (NDT) Techniques for Timber Structures," Infrastructures, vol. 10(2), no. 28, 2025.

[48] A. Tolera, K. Mostafa, A. Chowhudry, I. Zisis and P. Irwin, "Study of wind loads on asphalt shingles using full-scale experimentation," Journal of Wind Engineering and Industrial Aerodynamics, vol. 225, 2022.

[49] F. Habte, M. Mooneghi, T. Baheru, I. Zisis, A. Chowdhury, F. Masters and P. Irwin, "Wind loading on ridge, hip and perimeter roof tiles: A full-scale experimental study," Journal of Wind Engineering and Industrial Aerodynamics, vol. 166, pp. 90-105, 2017.

[50] M. Matus, "Low-rise Irregular Shaped Buildings," FIU Electronic Theses and Dissertations, 5410, 2023.

[51] M. Matus and I. Zisis, "Wind-induced Pressure Distribution on Non-rectangular Shaped Low-rise Buildings," ASCE Journal of Structural Engineering (In production), 2025.

[52] T. Marshall, "Storm Surge Damage to Buildings," Haag Engineering Co., 2014.

[53] T. Marshall, "Hurricane Katrina Storm Damage Survey," Haag Engineering Co., Carrollton, Texas, 2005.

[54] Eagleview, "ConnectExplorer Pictometry Aerial Imagery," 13 October 2024. [Online]. Available: https://explorer.eagleview.com/index.php. [Accessed August 2025].

[55] Google, "Street View digital images, Google Maps," April 2021. [Online]. Available: https://maps.google.com. [Accessed August 2025].

[56] FEMA, "FEMA Flood Maps," 9 January 2025. [Online]. Available: https://hazards-fema.maps.arcgis.com/apps/webappviewer/index.html. [Accessed August 2025].

[57] NHC, "TROPICAL CYCLONE REPORT: HURRICANE HELENE," National Hurricane Center, 2025.

[58] Google, "Earth View digital images, Google Earth," 2025. [Online]. Available: https://earth.google.com/web/. [Accessed August 2025].

[59] NOAA, "NOAA Tides & Currents," [Online]. Available: https://tidesandcurrents.noaa.gov. [Accessed August 2025].

[60] USGS, "Streamflow Measurements for the Nation," [Online]. Available: https://waterdata.usgs.gov/nwis/measurements. [Accessed August 2025].

[61] G. Haddow, J. Bullock and D. Coppola, "Chapter 2: Natural and Technological Hazards and Risk Assessment," in Introduction to Emergency Management (Sixth Edition), Elsevier, 2017, pp. 33-77.

[62] H. Needham and B. Keim, "Correlating Storm Surge Heights with Tropical Cyclone Winds at and before Landfall," Earth Interactions, American Meteorological Society, vol. 18, pp. 1-26, 2014.

[63] R. Mattson, T. Frazer, J. Hale, S. Blitch and L. Ahijevych, "Florida Big Bend," in Seagrass Status and Trends in the Northern Gulf of Mexico: 1940–2002, USGS, 2007.

[64] R. Smith and M. Montgomery, Tropical Cyclones: Observations and Basic Processes, Elsevier, 2023.

[65] H. Sarma, M. Matus, S. Lee and I. Zisis, "Influence of Building Shape-factor on Wind Loads for Non-Rectangular Low-Rise Structures," Journal of Building Engineering, vol. 120, no. 115314, 2026.

[66] H. Snoke, "Asphalt-prepared roll roofings and shingles," National Bureau of Standards, Report BMS70, 1941.

[67] L. Sharara, J. Jordan and R. Kimble, "Residential Roofing Evaluation," in Fifth Forensic Engineering Congress, Washington, D.C., USA, 2009.

[68] J. Peterka, J. Cermak, L. Cochran, B. Cochran, N. Hosoya, R. Derickson, C. Harper, J. Jones and B. Metz, "Wind Uplift Model for Asphalt Shingles,"Journal of Architectural Engineering, vol. 3, no. 4.

[69] J. Koontz, "Shingle splitting problem," Western Roofing Magazine, 1990.

[70] T. Marshall, S. Morrison, R. Herzog and J. Green, "Wind Effects on Asphalt Shingles," Haag Engineering Co., Irving, TX, USA, 2010.

[71] T. Marshall, "Roof Damage Issues in Hurricanes," Haag Engineering Company, 2004.

[72] T. Marshall, "Curved Corner Fractures in Concrete Tile," Haag Engineering Company, 1990.

[73] Haag-Engineering, Field Guide to Residential Roof Damage Assessment, Haag Engineering Company, 2020.

[74] B. Bienkiewicz and Y. Sun, "Wind loading and resistance of loose-laid systems," Journal of Wind Engineering and Industrial Aerodynamics, vol. 72, no. 1, pp. 401-410, 1997.

[75] M. Noone and W. Blanchard, "Asphalt shingles — a century of success and improvement," in Tenth Conference on Roofing Technology, Gaithersburg, Maryland, USA, 1993.

[76] W. Cullen, "Research and performance experience of asphalt shingles," in 10th Conference on Roofing Technology, Gaithersburg, MD, USA, 1993.

Forensic Engineering Analysis of Roadway Geometry and Traffic Control

By Timothy B. McClure, PhD, PE, DFE (NAFE #1314A) and Jerry S. Ogden, PhD, PE, DFE (NAFE #561F)

Abstract

When evaluating evidence for causative factors contributing to a motor vehicle collision, consideration should be given to roadway geometric or traffic control factors. Roadway geometry, clear zone, safety features, visibility obstructions, and traffic control devices and their placement may influence drivers' behavior. Are the roadways involved properly designed and signed? The geometric design and traffic control requirements for special circumstances, such as highway construction zones, mixed-use paths, railway crossings, or low traffic volumes, may also present the potential for roadway issues. An evaluation of these potential contributing factors can open a Pandora's box of opportunities for errors when an improper engineering analysis follows. This paper explores the topics that guide proper engineering analysis of roadway geometry and traffic control, including determining which design standards, policies, or guidelines apply and the proper application of the semantics in these documents. Additionally, this paper addresses recommendations contained in research concepts or reports versus requirements for the designer, the constructor, or the roadway owner. The discussion includes examples from past cases addressing the topics presented, providing a systematic approach to evaluating permanent or temporary roadway geometric or traffic control design for factors contributing to a collision event.

Keywords

Roadway design, forensic engineering, civil engineering, forensic analysis, collision analysis, litigation, accident reconstruction, construction zone, temporary traffic control, road design, project development

Introduction

Forensic engineers analyzing collision events typically focus on the evidence from the aftermath of an incident when evaluating the progression and timing of events. The forensic engineer oftentimes relies on evidence that may include final rest locations of vehicles, tire and gouge marks, debris fields, and electronically imaged data. The most frequently identified contributing factors involve driver actions, vehicle mechanical condition, roadway features, traffic control, and the environment. Contributing factors may also include confusing, missing, or misleading information or roadside safety features.

The authors provide a general overview of the project development process and discuss several national highway design manuals, highlighting how this information can have an important influence on a collision investigation. This paper begins with a high-level overview of the design process from initial programming to construction. Next, it discusses the guiding documents provided to designers and agencies and how engineers use these standards and policies to make design decisions. The discussion then transitions to the semantics of the guiding documents, with the intent of highlighting where many forensic analyses go astray. The paper concludes with several case study examples in which design features, including both permanent and temporary ones, may contribute to collision events.

Process — Programming to Construction

Programming

Planning and programming of highway construction projects usually begin years, if not decades, before the first shovel breaks ground and normally involves individuals and agencies from the local level to the federal level.

Smaller local governments, regional agencies, and other stakeholders/groups with a vested interest in transportation combine to either form metropolitan planning

Tim McClure, PhD, PE, DFE, PO Box 64, Rossville, IN 46065, (317) 431-6997, tmcclure@nederveld.com

organizations (MPOs) or regional planning organizations (RPOs) at the local level. It is these MPOs and RPOs that are tasked with regional planning and programming for all modes of transportation. MPO and RPO operations are similar, with the major differentiator being population density and geographic boundaries (i.e., municipality, city, county, etc.) [1].

RPOs, according to the Federal Highway Administration (FHWA), can also be identified by other naming conventions, such as regional affiliations, councils of government, and others, but these organizations are generally referred to as RPOs. Currently, approximately 30 states have RPOs in place [2]. Regardless of the organization of local transportation planners, RPOs, and MPOs, they are tasked with working with state agencies to identify highway and transit projects.

From the federal level, the United States Department of Transportation (USDOT) oversees 11 operating administrations, including the FHWA, which "supports state and local governments in the design, construction, and maintenance of the nation's highway system (Federal Aid Highway Program) and various federally and tribal owned lands." [3] The FHWA provides financial and technical assistance to state and local governments.

A project must fulfill a need as defined by the National Environmental Policy Act (NEPA) for the identification and programming of the project to take place. Often, public welfare drives projects that aim to improve safety (e.g., when a roadway feature no longer functions as intended or newer technology becomes available). Whether traffic volumes exceed projections or a stop-controlled intersection, for example, is experiencing a high frequency of crashes, a need is identified, and a project is born.

Design

Once a project has the general parameters determined, it is ready for the design phase. Projects can be designed in-house by the respective agency or designed by a consultant working under contract with the agency. A senior-level PE provides oversight for a specific discipline or manages the project in its entirety, while less experienced engineers typically perform detailed design. For this reason, a designer's quality assurance/quality control (QA/QC) plan is fundamentally important for the production of transportation facilities that are safe enough for the traveling public.

The design process involves multiple submission and review cycles to evaluate the design against established design criteria, established early in the design development process. Comments and feedback are provided that require sufficient review and attention before approval is received for the respective submission.

Design Resources

Entry-level highway and traffic engineers graduate with a cursory understanding of national design guides and standards most frequently used in highway design. Very little, if any, of the baccalaureate academic career focuses on state-specific guides and standards. However, all state design guidance and standards are based on national standards, publications, guidance, and research.

This paper limits the discussion to three primary national documents that provide the policies or standards relied upon by highway design engineers:

- The American Association of State Highway Transportation Officials (AASHTO), *A Policy on Geometric Design of Highways and Streets* (Green Book)
- AASHTO's *Roadside Design Guide* (RDG)
- FHWA's *Manual on Uniform Traffic Control Devices for Streets and Highways* (MUTCD).

National Design Resources

Geometric — *Green Book*

The current version of the *Green Book* at the time of this paper's writing is the 7th Edition, dated 2018 [4]. Founded in 1914, AASHTO, then known as the American Association of State Highway Officials (AASHO), met for the first time [5], but it wasn't until 1965 that the first edition of the *Green Book* was published. However, prior to publishing the first *Green Book*, AASHO/AASHTO was involved in developing federal legislation from the group's inception.

A Policy on Geometric Design of Highways and Streets, commonly referred to as the "*Green Book*," is a publication produced by AASHTO that provides the policy by which states develop the standards for the design of roadways on the National Highway System (NHS). Each state may adopt the *Green Book* as standard, revise the *Green Book*, or develop its own that meets or exceeds the policy of the *Green Book*. Highway designers represent the target audience of the *Green Book* in the development of roadway geometric elements.

In the most recent versions of the *Green Book*, the text presents the concepts an engineer should understand regarding the relationships among the facets of geometric highway design, explains the development of the different concepts, and provides associated calculations. The *Green Book* also provides corresponding equations and adjustment factors for site-specific circumstances, such as grade. The results represent the minimum (or maximum) acceptable values that should be considered for design. For example, Table 3-1 provides the minimum design stopping distance for speeds ranging from 15 mph to 85 mph. With this type of presentation, the *Green Book* provides a pass/fail metric for evaluation, provided the person performing the evaluation properly applies the guidance.

With the *Green Book* developed for designers, the guidelines provide inherent challenges for the forensic engineer's evaluation of the as-built condition. The *Green Book* relies on holistic situational guidance requiring the engineer to evaluate a situation in a "connect-the-dots" systematic approach. The designer works from given parameters that define variables such as road type (freeway, arterial, collector, or local) and design speed, while the forensic engineer must determine the road type and consider the posted regulatory speed limit (PRSL). From there, the forensic engineer evaluates the design elements to determine whether the as-built conditions meet the design minimums (or maximums). It is also beneficial for a forensic engineer to be able to access and review project design records as part of the investigation, as discussed later in this paper.

Safety — *Roadside Design Guide*

Just as the *Green Book* provides design guidance for the roadway itself, designers use the *Roadside Design Guide* (RDG) as a resource guide for applying the clear zone concept and shielding the traveling public from roadside obstructions. A simple way to differentiate between the *Green Book* and RDG is to think of the *Green Book* as containing design guidance for everything a vehicle is intended to touch, while the RDG contains design guidance for elements a vehicle is not intended to touch. AASHTO published the 4th Edition of the RDG in 2011 [6], the current version as of the time of this writing. The RDG may be referenced directly by individual highway agencies or used as a basis for developing their respective guidelines and standards, and it functions in conjunction with other design resources, such as the *Green Book*.

According to the FHWA, the first edition of the RDG was adopted by FHWA and became effective on July 25, 1990 [7]. Many engineers may mistakenly refer to the RDG as a standard (as is the MUTCD discussed later) or policy (as is the *Green Book*), but it is neither. The RDG serves as a tool for designers, but ultimately the transportation agency soliciting the design should either maintain its own standard or adopt the document(s) as its standard. The RDG allows engineers and designers to establish a "clear zone" and identify obstructions located within.

The RDG includes a toolbox of options that designers and engineers can use for the selection of highway safety appurtenances to shield an obstruction. Transportation agencies can also use the RDG for developing their approved product list, respective design criteria, and standards. Many styles of roadside barrier, crash attenuators, end treatments, breakaway supports, and other options are presented in the RDG to facilitate establishing a proper clear zone.

As time progresses, it is inevitable that design standards and guidance are revised and updated, and the RDG is no different. A forensic investigation that includes an analysis of roadside grading and traffic barriers, for example, could identify features that may have been designed and installed appropriately and according to standards, but through time have lost the ability to meet the standards to which they were designed. Careful evaluation and documentation of the "non-traveled way" elements associated with an accident scene will aid a forensic investigation for causation.

Signage/Pavement Markings — *Manual on Uniform Traffic Control Devices for Streets and Highways*

The first release of the *Manual on Uniform Traffic Control Devices for Streets and Highways* (MUTCD) occurred in January 1927, as AASHO published the *Manual and Specifications for Manufacture, Display, and Erection of U.S. Standard Road Markers and Signs* [5]. At the time, however, the manual only included signage for rural areas. Signage for roadways located in urban areas was published by another agency. The rural and urban manuals were combined in 1932 when AASHO released the first official *Manual on Uniform Traffic Control Devices*. It wasn't until after the Highway Safety Act of 1966 that the FHWA became the agency responsible for the MUTCD, and it published its first version in 1971. Since 1971, FHWA has released updated versions of the MUTCD, with the most recent (11th edition) becoming effective on January 18, 2024.

The MUTCD was developed to establish a minimum standard that all transportation agencies must meet. Transportation agencies can either adopt the MUTCD as their standard, develop a state supplement to the MUTCD, or write their own version that meets or exceeds the federal MUTCD standards. The MUTCD provides standards for both permanent and temporary traffic control, but even with minimum standards defined, designers must use their engineering judgment and experience when applying them to each unique project or situation. States had until January 18, 2026, to adopt the 11th Edition of the MUTCD. It is important for engineers to know which edition the agency for which they are designing currently uses. As of the time of the writing of this report, 18 states have adopted the national MUTCD (2009 Edition), 22 states and two territories have adopted the national MUTCD (2009 Edition) along with a state supplement, and 10 states have adopted a State MUTCD (2009 Edition) [8].

The MUTCD functions very differently from the *Green Book* and RDG in how it provides information to designers. The MUTCD establishes minimum requirements for traffic control devices and provides additional commentary, including support, options, and guidance on when and where to use those devices. These semantics drive the use of the MUTCD and are discussed later in this paper.

Conversely, the AASHTO publications described in this paper define frequently encountered design situations and provide guidelines for developing and refining the design. For example, the *Green Book* provides the designer with guidance on how to balance the horizontal and vertical alignment by identifying the best locations for curves based on factors such as driver perception, comfort, and expectations. The *Green Book* builds upon that guidance and, in later chapters, provides minimum radii based on design speed, provides guidance on superelevation and rate, and so on. The *Green Book* provides flexibility such that multiple engineers may each have different solutions to a design, all of which may meet *Green Book* guidance. On the other hand, the MUTCD addresses site-specific features, such as signs and pavement markings. In the case of the horizontal curve design, the MUTCD will define under what conditions advance warning signs or additional pavement markings should be included.

Design/Contract Documents

Highway design contracts include more than just roadway and temporary traffic control plan sets. Teams of engineers responsible for the design will compile the bid package documents and submit them to the letting agency for contractor selection. Any number of items can be included in the bid package, and it is critically important that a designer understands the proper order (or hierarchy) of these documents. The order of the design documents may differ between transportation agencies. For example, according to the *2020 Standard Specifications for Construction*, the order of precedence for the Michigan Department of Transportation (MDOT) is as follows [9]:

1. All proposal material except the materials listed in subsections 104.06.B through 104.06.F;
2. Special provisions;
3. Supplemental specifications;
4. Project plans and approved working drawings;
5. MDOT standard plans; and
6. Standard specifications

The full list and most current order of MDOT documents should be referenced on MDOT's website.

It is important for engineers and designers to know the hierarchy of design documents. Likewise, a forensic engineer working to determine causation factors must understand this order when reviewing as-built or construction documents to determine which document controls in cases with conflicting information.

Construction

Typically, for public design/bid/build projects, the most common public highway construction contract procurement method, the project owner releases the contract documents for review and bidding and selects the lowest bidding contractor that meets all contractual requirements. Once awarded, the contractor and owner sign the contract, and the project progresses into the construction phase. While other contract procurement methods are available (A+B bidding, design-build, performance contracting, etc.), engineers must understand that design changes do occur during construction. No matter the method of contract procurement, any such changes should be stored with the project records by the owner. Forensic engineers should refer to as-built or as-constructed plan sets, if available, to ensure any design changes made during construction are included. Using or relying on as-designed plans may not paint the full picture required by the forensic engineer.

Waivers, Design Exceptions, and Variances

Designing for the natural environment can be challenging. Constraints, such as limited right-of-way, topographic changes, and sensitive environmental areas, are just a few examples of the many factors that can limit an engineer's design options, whether the design is a retrofit of an existing facility or an entirely new facility. In addition, when designing improvements to an existing facility, features that no longer meet current design criteria may need to be modified to meet current design standards and guidelines. In some situations, there may be no viable options within the scope of work that will allow an engineer to fully meet design requirements. The engineer must then, through his or her education, training, and experience, develop an engineering solution that best meets the requirements and document in the form of a design exception, variance, or waiver, how and why the selected design is optimal. The owner must maintain all approved waivers, variances, and/or design exception documentation with the respective project records.

Roadways of differing classifications and types may require different levels of waivers. For example, the FHWA requires a design exception to be developed and approved for any of 10 controlling criteria on National Highway System (NHS) roadways with a design speed greater than or equal to 50 mph [10]. The 10 controlling criteria follow:

1. Design speed,
2. Lane width,
3. Shoulder width,
4. Horizontal curve radius,
5. Superelevation rate,
6. Maximum grade,
7. Stopping sight distance,
8. Cross slope,
9. Vertical clearance, and
10. Design loading structural capacity.

While the FHWA requires the design exceptions for the listed criteria, other transportation agencies may require similar waivers or exceptions, or expand the listed criteria, for roadways under their jurisdiction. The Pennsylvania Department of Transportation (PennDOT), for example, requires an 11th controlling criterion for acceleration and deceleration lane length [11]. Another example of a frequently used waiver/exception would be for pedestrian facilities such as sidewalks, pedestrian curb ramps, driveway aprons, etc. For more than a decade, the *Proposed Draft Accessibility Guidelines for the Public Right-of-Way* were used by highway agencies in developing standard drawings and engineers to design pedestrian facilities within the public right-of-way. On August 8, 2023, the United States Access Board published the final rule on the minimum accessibility guidelines for pedestrian facilities within the public right-of-way. Pedestrian curb ramps, for example, are notoriously difficult to design and construct. Many highway agencies maintain their own type of waiver when pedestrian facilities do not meet accessibility requirements, which has been a focus of many lawsuits [12]. Well-documented design decisions, especially design exceptions, provide the forensic engineer valuable insight into reasoning for the chosen options, which may not be readily apparent post-construction and post-incident.

Semantics — "Words Have Meaning"

The subtitle "Words Have Meaning" summarizes the content of this section. The MUTCD divides its guidelines into four categories, with the definitions reprinted verbatim in the 2009 MUTCD [13]:

- **Standard** — a statement of required, mandatory, or specifically prohibitive practice regarding a traffic control device. All Standard statements are labeled, and the text appears in **bold** type. The verb "shall" is typically used. The verbs "should" and "may" are not used in Standard statements. Standard statements are sometimes modified by Options.

- *Guidance* — a statement of recommended, but not mandatory, practice in typical situations, with deviations allowed if engineering judgment or engineering study indicates the deviation to be appropriate. All Guidance statements are labeled, and the text appears in unbold type [italic]. The verb "should" is typically used. The verbs "shall" and "may" are not used in Guidance statements. Guidance statements are sometimes modified by Options.

- Option — a statement of practice that is a permissive condition and carries no requirement or recommendation. Option statements sometimes

contain allowable modifications to a Standard or Guidance statement. All Option statements are labeled, and the text appears in unbold type. The verb "may" is typically used. The verbs "shall" and "should" are not used in Option statements.

- Support — an informational statement that does not convey any degree of mandate, recommendation, authorization, prohibition, or enforceable condition. Support statements are labeled, and the text appears in unbold type. The verbs "shall," "should," and "may" are not used in Support statements.

Therefore, is a standard absolute? Not necessarily. Decisions must consider the situational context in which they are made. Section 1A.09 of the MUTCD [13] defines the following **Standard** text: **This Manual describes the application of traffic control devices, but shall not be a legal requirement for their installation.** *Directly followed by Guidance text stating: The decision to use a particular device at a particular location should be made on the basis of either an engineering study or the application of engineering judgment. Thus, while this Manual provides Standards, Guidance, and Options for design and applications of traffic control devices, this Manual should not be considered a substitute for engineering judgment. Engineering judgment should be exercised in the selection and application of traffic control devices, as well as in the location and design of roads and streets that the devices complement.*

It is unrealistic to expect a single guidance document or standard to be sufficient for all designs across the United States, and the MUTCD affords engineers flexibility to modify designs to fit specific situations. For example, sign placement guidelines from the MUTCD may be physically impossible to meet verbatim on a mountain road bounded by steep embankments. The designer then uses engineering judgment to determine an appropriate location. Note that appropriate documentation is important when deviating from any standard or guideline, as discussed earlier in this paper. In addition to decisions considering context, they must also be reviewed by qualified peers, as design typically requires a team process.

The MUTCD [13], [14] provides these definitions to convey very concise directives on when and how each term, Standard, Guidance, Option, and Support (SGOS) applies to the given topic. Even with these concise directives, disagreements in interpretation still develop. Semantics enters into discussion and lies as the root of many misinterpretations. Some examples include an engineer incorrectly interpreting guidance as a "must" rather than the defined "should," or assuming that because an option allows an action, the action should occur. These two examples result in Guidance and Options being "promoted" to a "Standard." Another common example occurs when no standard exists for a situation, and the engineer again "promotes" guidance to a standard. The editors of the MUTCD clearly defined the terms used and provided an allowance for engineering judgment. This promotion of guidance to standards often occurs when an engineer disagrees with the engineering judgment of a different engineer or does not fully understand the intention of the MUTCD authors' nomenclature. Supporting one's opinion with engineering principles may not be possible, making the "promotion" of Guidance or Options to a fictitious "Standard" the only option. The authors refer to situations in which an engineer makes a determination without directly citing supporting standards, as B.I.S.S. (Because I Said So). Keep in mind the forensic engineering analysis presents facts from a non-advocate position, and any B.I.S.S. statement appears to be from an advocatory position.

The SGOS structure of the MUTCD inherently leads engineers to grade traffic control with a common theme of "… should have done more," or "if only this option had been added, then the incident would not have occurred." A design either meets the MUTCD requirements or it does not. The grade is pass/fail — not A, B, C, D, F.

As stated previously, the presentation of the *Green Book* lends itself to a pass/fail analysis, while the MUCTD requires a much more "flowchart" (if-then) type of analysis. To further explain, Table 5-5 from the 2018 *Green Book* [4] presents minimum traveled way widths based on design speed and roadway volume, a very pass/fail, deterministic set of criteria.

The MUTCD includes prescriptive language but also contains inherent flexibility for engineers to customize designs to the specific location. Below the authors present Section 3B.01 Yellow Center Line Pavement Markings and Warrants from the 2009 MUTCD [13]:

> **Standard:**
> **Center line markings shall be placed on all paved urban arterials and collectors that have a traveled way of 20 feet or more in width and an ADT of 6,000 vehicles per day or greater. Center line markings shall also**

be placed on all paved two-way streets or highways that have three or more lanes for moving motor vehicle traffic.
Guidance:
Center line markings should be placed on paved urban arterials and collectors that have a traveled way of 20 feet or more in width and an ADT of 4,000 vehicles per day or greater. Center line markings should also be placed on all rural arterials and collectors that have a traveled way of 18 feet or more in width and an ADT of 3,000 vehicles per day or greater. Center line markings should also be placed on other traveled ways where an engineering study indicates such a need.
Engineering judgment should be used in determining whether to place center line markings on traveled ways that are less than 16 feet wide because of the potential for traffic encroaching on the pavement edges, traffic being affected by parked vehicles, and traffic encroaching into the opposing traffic lane.

The Standard "**shall"** contain a similar pass/fail, determinate set of criteria, while Guidance contains pass/fail criteria; the verb "*should*" applies to Guidance, which allows for engineering judgment to determine whether to install the centerline. Keep in mind that engineering judgment exceeds a single location and may require a holistic view. For example, consider the hypothetical situation of a 20-foot-wide, unstriped, two-way, collector roadway with 4,100 vehicles per day in a jurisdiction with three expensive new traffic signal installations scheduled and limited funds.

With the entirety of the information known, should a forensic analysis determine that the center lane markings were not required? The center line was not required (shall); it should be provided, and the budget situation explains the prioritization applied in the engineering judgment. Could any situation alter the findings? Regardless of the presented reasoning, the proper forensic analysis concludes the center line was not required. However, a proper analysis also notes that the MUTCD states the centerline should be installed. The forensic engineer may opine on the engineering judgment used to not install the centerline, but that guidance never becomes a standard. The trier of fact ultimately determines the sufficiency of the engineering judgment.

The engineering judgment used in making project decisions, even when well-documented and packaged with project records, may remain unavailable, making research important to the forensic analysis. Depending on the circumstances of the case being investigated, researching the historic ADT may present valuable information. Continuing with the same example, has the ADT been increasing and recently passed the 4,000 mark? How recently? Was there a closure of a parallel road, making the added ADT "detour traffic"? How quickly should a jurisdiction react to changing ADT? Has ADT decreased? Possibly an improvement to a parallel road. The answers to each of these example questions provide valuable insight into the engineering judgment used to decide whether to apply centerline pavement markings, but the Guidance never becomes a Standard.

Forensic Considerations

A forensic analysis of roadway design begins with the two primary factors, "when" and "where." One must consider that an incident that occurs "today" may happen on a roadway that was designed and constructed decades prior. One must ask "when" the agency constructed the roadway, rather than applying the latest design standards to a facility built and not improved since 1950, for example. The forensic engineer must research the roadway's construction history to determine whether and when the agency performed any intermediate improvements. The forensic engineer should also know the level of improvement to determine if the project triggered any additional modifications to be included in the improvement. Note: Recurring maintenance projects, such as pavement overlays, typically do not require updates to design features. The date of the latest improvement project provides the key to which design criteria apply to the design, thus also the analysis. The requirements for which features must be improved based on the work taking place in the construction process require an in-depth review of the design manuals in place at the time of design.

The "where" factor adds multiple components and must be broken down. First, consider the general location. As each state's guidelines may differ. Within each state, each political subdivision (e.g., county and city) may also develop its own guidelines. The forensic engineer must first determine the political subdivision in which the incident occurred, then determine which guidelines that political subdivision codified. Note that the code also defines which edition (the "when") of each guideline applies at the date of the design, as newly released guidelines may not have been adopted.

The next "where" factor considers the more precise

physical location and associated road classification. Roadway requirements differ significantly based on intended functionality. Consider low-volume rural roads, high-speed rural roads, urban residential streets, and urban arterials, each with its own functionality and requirements. Lane widths, cross-sectional elements, design speeds, alignments, and safety features differ significantly across different design speeds and traffic volumes, which relate to roadway functionality (classification).

Federal and state agencies continually seek to improve design to reduce the frequency and severity of vehicle collisions. With the discrete incremental introduction of design manuals, many state DOTs introduce new requirements through design memoranda that incorporate revisions in between releases of complete manuals. Along with design memoranda, agencies may seek to introduce new research into projects.

The introduction of current research requires very detailed engineering studies completed by the designers and/or the agency in control to implement new research. Consider the past evolution of roundabout design and the current evolution/implementation of continuous flow intersections. This concept introduces two important factors for the forensic engineer in these specific cases. First, the design criteria are in the design documentation, not necessarily in the published manuals. Second, the forensic engineer must not introduce new research not adopted by the agency in charge, nor introduce it into the design criteria through an engineering study. New research does not become a requirement until it is adopted.

Case Studies

Truck Runaway Ramp

The first case study involves an incident that occurred in the fall of 2018 with a semi-truck-trailer crashing into a structure located opposite a stop-controlled approach to an intersection. The intersection is located at the base of a long mountain downgrade. **Figure 1** displays a view of the route the truck had taken. As the semi entered the intersection, a security camera captured an image with visibly red-hot, overheated brakes. The forensic analysis consisted of several factors, including the design of the road reconstruction completed in the early 2000s, evaluation of the site for possible truck escape ramp (TER) locations, evaluation of the incident history, and review of other mitigation measures (i.e., signage and a brake check area).

With the construction taking place in the early 2000s, the 2001 *Green Book* and the 2001 MUTCD apply. The 2001 *Green Book* [16] (and still found in the 2018 *Green Book* [4]) references a technique called the "Grade Severity Rating System" (GSRS). The outdated DOS-based GSRS became unavailable in 1994. When reading the *Green Book* text: A technique for new and existing facilities available for use in analyzing operations on a grade, in addition to crash analysis, is the Grade Severity Rating System (45)…, the lack of availability of the GSRS becomes irrelevant as the *Green Book*'s intent is to determine the need for further evaluation. While the GSRS may have been useful for some situations, this specific project included an approximate 6-mile (approximately MP 492 to MP 498) downgrade average of 5.76% with no upgrades. A grade of this value and for this length should automatically trigger

Figure 1
Overview of route with milepost; re-construction project began at approximately MP 492 and ended at approximately MP 498 [15].

review for safety, specifically brake safety.

With the potential need for a TER established, evaluating the route for locations came next. The route contained 31 horizontal curves with the longest tangent between curves being 1,565 feet long. Note that at the time of design, Dragnet systems were in their infancy, and the *2002 Roadside Design Guide* [17] included them only as temporary options, leaving an arrestor bed TER as the only option. The grade dictates the length of the bed required. An arrestor bed requires 1,120 feet of length on a 0.5% downgrade (bed grade) and 1,421 feet of length for a 6% downgrade (bed grade). The only two tangents exceeding 1,000 feet occur in this corridor within 3 miles of the summit, where a TER could not be effective due to the physical location being closer to the summit and not being near the bottom of the grade. Further review of the aerial identifies some potentially viable locations between mileposts 497 and 498, prior to the end of the construction project, for additional examination. The side of the road adjacent to the downhill lane in any potentially viable location contained relatively narrow widths outside the shoulder and long steep slopes where costs to build an embankment alone approached the cost of the entire project. Note **Figure 1** shows a current TER location in this area as the state installed a dragnet type TER post incident. No accident history or traffic/safety studies for the reconstruction project were made available for forensic review. The authors are aware of a safety study that fell under undisclosable information. In this case, one must not confuse the availability of a study with a study not being completed. Regardless of the safety study, no viable location existed.

The reconstruction project was completed approximately 15 years prior to the incident. Therefore, consideration must be given to whether the site should have been evaluated for a TER for safety reasons. What would trigger a safety evaluation? Similar and potentially repeatable accidents involving overheated brakes and/or commercial vehicles. A 10-year accident review found only one somewhat similar incident; however, that incident involved a pickup truck with a trailer, not a commercial vehicle. The other commercial vehicle incidents resulted from many different factors that eliminated them from inclusion — factors such as weather conditions, improper loading, and a local commercial vehicle (dump truck), not a long-haul vehicle. Therefore, no event triggered a safety analysis.

The final part of the forensic analysis involved evaluating other safety features. The controlling design document (2001 Green Book [16]) contained the following regarding brake check areas.

> *Turnouts or pull-off areas at the summit of a grade can be used for brake-check areas or mandatory-stop areas to provide an opportunity for a driver to inspect equipment on the vehicle and to ensure the brakes are not overheated at the beginning of the descent. ... A brake-check area can be a paved lane behind and separated from the shoulder or a widened shoulder where a truck can stop. ...*

The MUTCD contained no brake check area signage until the 2009 edition. The construction plans contain a widened shoulder at the summit and a full rest area, complete with truck parking spaces, within 1 mile of the summit. Therefore, the as-built condition met the design standards for a brake check area at the time of the reconstruction design. Witness testimony and legal filings also indicate that the semi driver used the widened shoulder area to pull his truck over at the summit.

Section 2C.11 of the 2000 Edition of the MUTCD [14] recommends the following regarding supplemental posting of the W7-1 Hill Advanced Warning Sign on extended grades:

> *On longer grades, the use of the distance (W7-3a) plaque or the combination distance/grade (W7-3b) plaque at periodic intervals of approximately 1.6 km (1 mi) spacing should be considered.*

The subsequent 2009 Edition of the MUTCD [13] states the following in Section 2C.16 regarding the use of the W7-1, W7-1a and W7-2p signs on extended grades:

> *On longer grades, the use of the Hill sign with a distance (W7-3aP) plaque or the combination distance/grade (W7-3bP) plaque at periodic intervals of approximately 1-mile spacing should be considered.*

The state agency placed supplemental postings of the W7-1 along the grade at approximately 1-mile intervals as recommended by the MUTCD. Guidance statements within the MUTCD do not carry requirements or mandates for posting, but *recommended* practices for posting related Hill (W7-3P) signs on a grade. The designer can exercise engineering judgment to determine if a different W7-2p

suggested, but not **standar**d or *recommended*, sign should be posted. The state agency chose to reinforce USE LOW GEAR, which carries with it a greater and more specific message regarding the grade to a driver than simply the length of the grade. Section 2C.11 of the 2000 Edition [14], and Section 2C.16 of the 2009 [13] Edition of the MUTCD allows for the engineering judgment exercised by the engineer.

TTC Left-Turning Vehicle at Signalized Intersection

The second case study involves an active construction site with temporary traffic control in place. The location consisted of a signal-controlled intersection with the configuration as seen in **Figure 2**. A westbound driver made a left turn into the path of another vehicle. The client requested a review of the TTC for the required sight distance.

The 2018 AASHTO *Green Book* [4] applied based on date and location, which was used to calculate the appropriate sight distance. The *Green Book* contains seven possible cases (A-G) with some containing sub-cases for a total of 10 options. Case F (left turn from major road) applied. The authors used Equation 9-1 (ISD=1.47×Vmajor×tg) with Vmajor being the Posted Regulatory Speed Limit (PRSL) of the approaching road and tg being the time gap provided in Table 9.16 to calculate the ISD. Note that the forensic analysis uses actual case information — meaning that the calculation used 5.5 seconds for passenger cars from Table 9.16, based on the vehicles involved, and not the 6.5 seconds for single unit trucks, which would probably be the design vehicle based on road types. While the forensic analysis reviews design requirements, it also only applies collision-specific information.

The time gap given in Table 9-16 only accounts for passenger cars crossing one traffic lane with the requirement to add an additional 0.5 seconds per additional lane for passenger cars crossed.

The authors calculated the ISD by using the PRSL (40 mph) and the given first lane to cross (5.5 sec) plus two additional lanes (.5 sec each) = **3 total lanes** to cross during left turn:

$$ISD = 1.47 \times 40 \text{ mph} \times (5.5 + .5 + .5) = 382.2 \text{ feet}$$

The next step involved measuring the available sight distance. This case only involved horizontal issues for consideration because of existing infrastructure and topography. However, the *Green Book* contains specific guidance on eye and target elevations. Sight distance begins at the stop line and continues past any obstruction to the middle of the nearest approaching lane as described in Section 3.2.6.4 of the *Green Book* [4]. The question that remains is what is an obstruction? The *Green Book* Section 3.2.6.3 describes obstruction to sight lines as, "… *a crest vertical curve or it may be some physical feature* ***outside of the traveled*** *way (emphasis added), such as a longitudinal barrier, a bridge approach, fill slope, a tree, foliage, or the back slope of a cut section.*" Note that the *Green Book* makes no consideration for random or temporal conditions

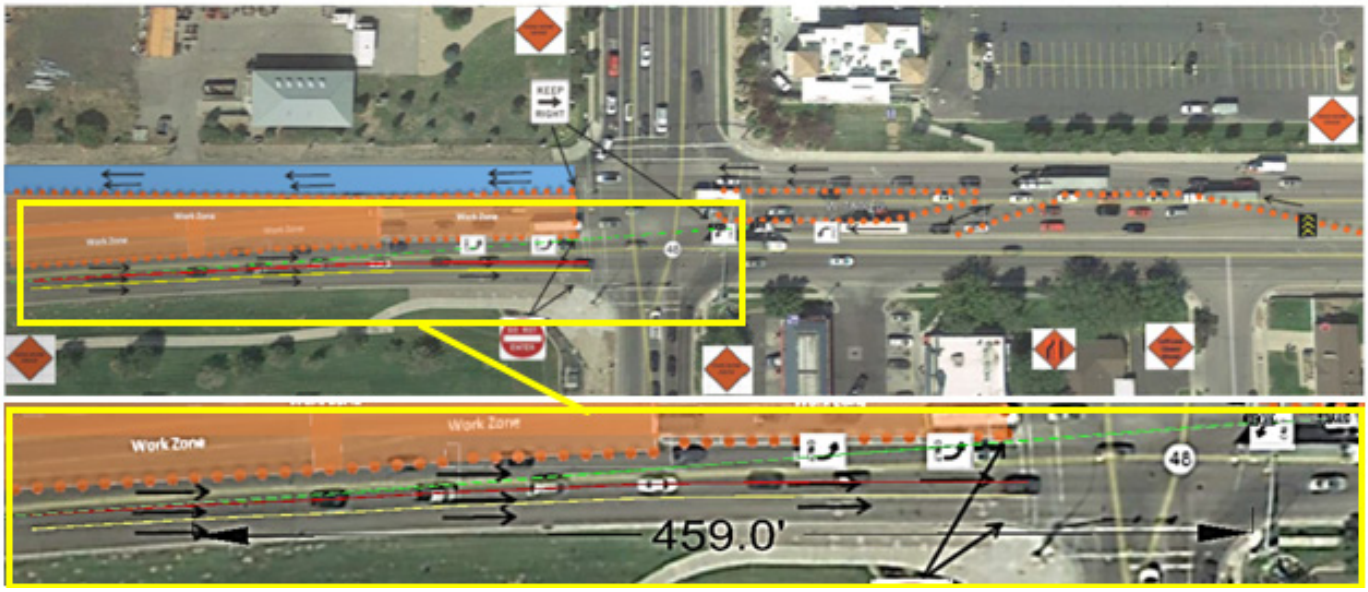

Figure 2
TTC plan with the ISD sight lines presented and then measured.

created by vehicles within the travel way, or for any other highly variable condition.

Figure 2 presents the available sight distance. The available 459 feet well exceeds the required 382 feet.

The idea of offsetting the westbound turn lane to be directly in line with the eastbound lane to further increase available sight distance came into question. Note the three lanes approaching the intersection from the west, with one of those lanes becoming the eastbound left turn lane. The fact of a travel lane transitioning to a turn lane (as opposed to adding a turn lane) introduces an increased potential for head-on collisions. With sufficient sight distance available, the authors found the as-placed configuration to be the better option.

TC Intersection Stop Sign Controlled

The third case study involves an incident in which a vehicle ran a stop sign and broadsided another vehicle. The 4-leg intersection contained a stop condition for the minor approaches. The litigant called into question the permanent signage and sight lines for the stop leg of the intersection. **Figure 3** presents an image of the viewshed experienced by the litigant, which is representative of the day of the incident. The stop sign at the right edge of the road remains visible past the trees in full foliage, but also note the supplemental stop sign on the left side of the road.

May the agency use a sign in this manner? Note that the state in which the collision took place chooses to use the federal MUTCD [13] with supplemental information.

Figure 3
Photograph taken during site visit with representative view available on day of collision, including traffic control.

The supplemental state MUTCD was used in the evaluation. Section 2A.16 Standardization of Location reads:

> *Option:*
> *Under some circumstances, such as on curves to the right, signs may be placed on median islands or on the left-hand side of the road. A supplementary sign located on the left-hand side of the roadway may be used on a multi-lane road where traffic in a lane to the right might obstruct the view to the right.*

With semantics in mind, an option represents a permissive condition and carries no requirement or recommendation but can be applied with appropriate engineering judgment. In general, additional information would only not be allowed when it introduces conflicting, confusing or too much information for a driver to process. None of these conditions exist; therefore, the MUTCD allows the additional stop sign on the left side of the road.

In deposition, the litigant stated he saw the stop sign on the left side of the road and believed it was for the crossing road. However, the agency also provided a properly placed and sized stop ahead sign on the approach to the intersection. The MUTCD [13] states the following regarding warning signs:

> **Section 2C.01 Function of Warning Signs**
> Support:
> Warning signs call attention to unexpected conditions on or adjacent to a highway, street, or private roads open to public travel and to situations that might not be readily apparent to road users. Warning signs alert road users to conditions that might call for a reduction of speed or an action in the interest of safety and efficient traffic operations.
> **Section 2C.02 Application of Warning Signs**
> **Standard:**
> **The use of warning signs shall be based on an engineering study or on engineering judgment.**
> *Guidance:*
> *The use of warning signs should be kept to a minimum as the unnecessary use of warning signs tends to breed disrespect for all signs. ...*

In deposition, the litigant also acknowledged seeing and recognizing the advance warning sign. In his acknowledgment of the sign, he also admitted to not

Figure 4
Site overview from RR to path entry with corresponding TTC plan and inset photo of actual path closure (Aerial photo [18]).

understanding or ignoring the basic function of the sign to warn of an imminent condition, and not some future condition farther away.

Closed Shared Use Path

The fourth case study involves the reconstruction of a railroad crossing, which required the closing of a local rural road and the adjacent shared-use path. A bicyclist proceeded on the closed shared-use path, rode off the path into the construction area, and wrecked, causing injury. **Figure 4** provides an aerial photo view of area — a portion of the approved TTC plan for the road — and a photo of the actual TTC in place. While small and difficult to read in the TTC plans, the "Sidewalk Closed" signs appear approximately 300 feet to 500 feet from the railroad tracks, with the closest entrance to the shared use path over 2,000 feet from the railroad tracks.

The state in which the incident occurred maintained standard TTC drawings developed using the guidance from the State's MUTCD that applied to the situation. **Figure 5** presents the standard drawing. Note 2 states that the closure of a sidewalk be at the last open business or residence, which equates to the last road crossing entrance in this case, as no businesses or residences exist. Also note, ADA guidelines do not allow sidewalk/paths to be open

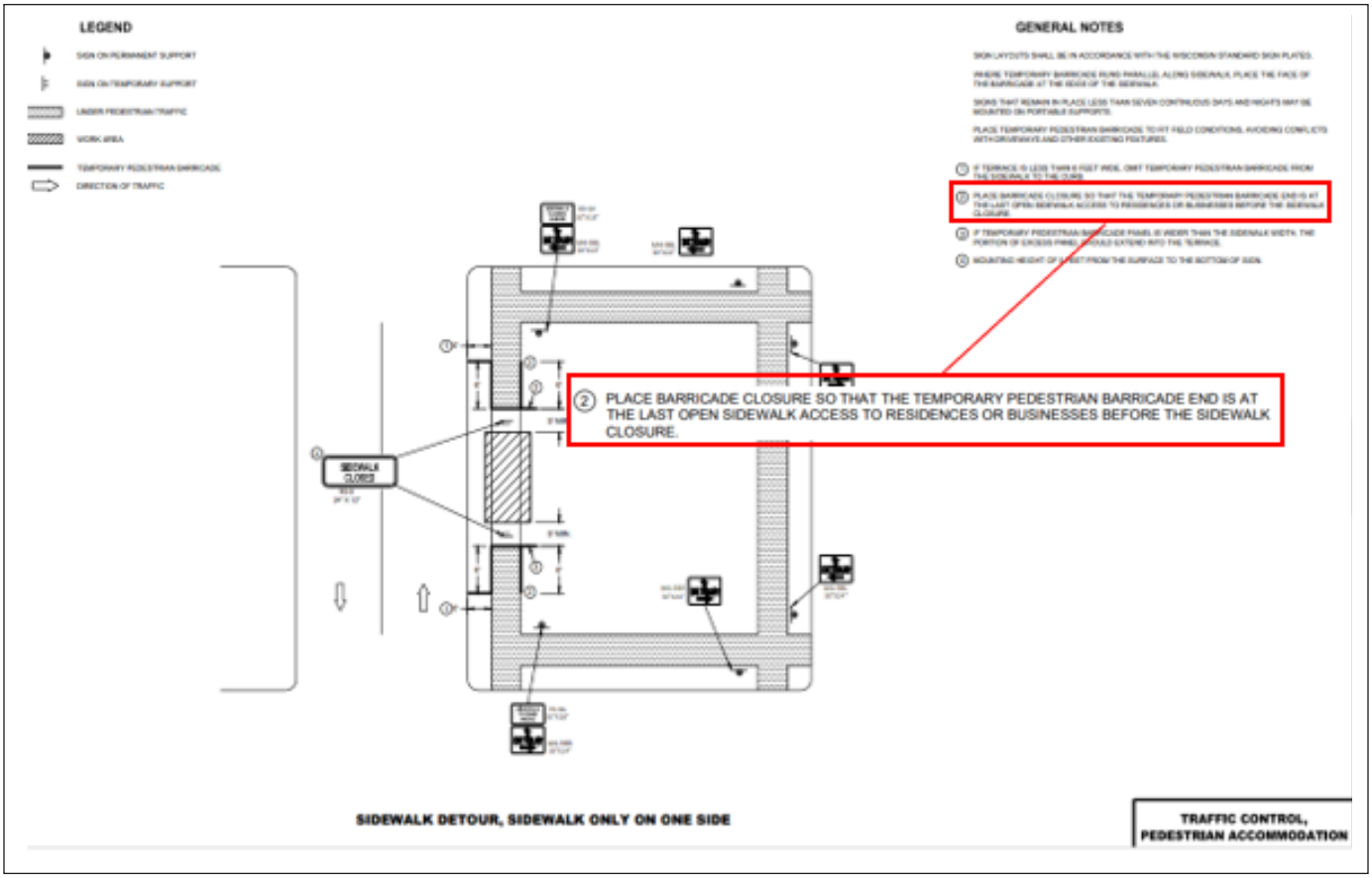

Figure 5
"State" Standard Drawing showing the appropriate sidewalk closure for the situation.

past the last access required (i.e., cannot lead to a dead-end. The TTC design does not meet the requirements of the standard drawing or the State MUTCD).

The inset photo in **Figure 4** shows the closure as it existed in the field at the entrance to the nearest road crossing. Therefore, the actual closure met the requirements of the standard drawing and the state MUTCD.

Another issue discussed was the lack of TTC near the railroad track, the actual location of the hazard. The incident occurred within an area closed to public entry or use, where no further TTC devices are required, recommended, or suggested by any applicable standards. Section 1A.13 of the state MUTCD defined traffic as:

> Traffic — pedestrians, bicyclists, ridden or herded animals, vehicles, streetcars, and other conveyances either singularly or together while using for purposes of travel any highway or private road open to public travel.

Note the "open to public travel" in the definition of traffic. With no traffic comes no traffic control, even though the closure occurs 2,000 feet from the actual construction area. Additional traffic control violates the MUTCD because it provides conflicting guidance by suggesting that a closed path (or road) is actually open.

Conclusion

Collision analysis, as it relates to design, construction, or temporary control measures, must be based on historical facts surrounding those activities. The forensic engineer's role when evaluating a collision is similar to that of a historian piecing together artifacts to determine the events and causes leading to a collision event. Using evidence from the scene, design records, and historical design manuals, the forensic engineer constructs a timeline of events and decisions that culminates in the identification of the cause of an accident. Determining and correctly applying the semantics of the guidance documents relevant to the situation is the single most important aspect of this type of forensic analysis. Words have meaning, and only the defined meaning matters.

Acknowledgments

Thanks to the Nederveld Collision Analysis team for their support on this paper and work on the case studies.

References

[1] Federal Highway Administration, "Transportation Planning and Capacity Building," U.S. Department of Transportation. [Online]. Available: https://www.planning.dot.gov/mpo/. Accessed: May 2024.

[2] Federal Highway Administration, "Integrating Safety in the Rural Transportation Planning Process," U.S. Department of Transportation. [Online]. Available: https://highways.dot.gov/safety/local-rural/integrating-safety-rural-transportation-planning-process/10-introduction#-footnotes. Accessed: May 2024.

[3] Federal Highway Administration, "About FHWA," U.S. Department of Transportation. [Online]. Available: https://highways.dot.gov/about/about-fhwa. Accessed: May 2024.

[4] American Association of State Highway and Transportation Officials, A Policy on Geometric Design of Highways and Streets. Washington, DC, USA: AASHTO, 2018.

[5] Federal Highway Administration, "Celebrating a Century of Cooperation," Public Roads, Sept./Oct. 2014. [Online]. Available: https://highways.dot.gov/public-roads/septemberoctober-2014/celebrating-century-cooperation. Accessed: May 2024.

[6] American Association of State Highway and Transportation Officials, Roadside Design Guide. Washington, DC, USA: AASHTO, 2011.

[7] Federal Highway Administration, "Memorandum: AASHTO Roadside Design Guide, 4th Edition," U.S. Department of Transportation, Jun. 26, 2012. [Online]. Available: https://highways.dot.gov/safety/rwd/reduce-crash-severity/memorandum-aashto-roadside-design-guide-4th-edition. Accessed: May 2024.

[8] Federal Highway Administration, "MUTCDs & Traffic Control Devices Information by State," U.S. Department of Transportation. [Online]. Available: https://mutcd.fhwa.dot.gov/resources/state_info/index.htm. Accessed: May 2024.

[9] Michigan Department of Transportation, 2020 Standard Specifications for Construction. Lansing, MI, USA: State of Michigan, 2020.

[10] Federal Highway Administration, "Guidance on NHS Design Standards and Design Exceptions," U.S. Department of Transportation, Mar. 6, 2019. [Online]. Available: https://www.fhwa.dot.gov/design/standards/qa.cfm. Accessed: May 2024.

[11] Pennsylvania Department of Transportation, Design Manual Part 1X. Harrisburg, PA, USA: State of Pennsylvania, 2023.

[12] M. O'Hagan, "Reluctant towns, cities and states are being dragged into court to fix sidewalks for people with disabilities," Time, Oct. 12, 2021. [Online].

[13] Federal Highway Administration, Manual on Uniform Traffic Control Devices for Streets and Highways. Washington, DC, USA: FHWA, 2012.

[14] Federal Highway Administration, Manual on Uniform Traffic Control Devices for Streets and Highways. Washington, DC, USA: FHWA, 2000.

[15] Google Earth Pro, imagery dated Jul. 26, 2016. [Online].

[16] American Association of State Highway and Transportation Officials, A Policy on Geometric Design of Highways and Streets. Washington, DC, USA: AASHTO, 2001.

[17] American Association of State Highway and Transportation Officials, Roadside Design Guide. Washington, DC, USA: AASHTO, 2002.

[18] Google Earth Pro, "Google Earth Pro," Mar. 6, 2024. [Online].

[19] American Association of State Highway and Transportation Officials, "Publication Detail: Roadside Design Guide, 4th Edition." [Online]. Available: https://store.transportation.org/Item/PublicationDetail?ID=1802. Accessed: May 2024.

Beyond the Building Code — Compliance and Forensic Failure Analysis of Retaining Walls

By Brian C. Eubanks, PE, DFE (NAFE #962S), Noel Janacek, PE, DFE (NAFE #1375M), Garrett Ryan, PE, DFE (NAFE #1125M), and Joseph Roberts, PE, DFE (NAFE #1354A)

Abstract

Retaining walls are structural walls that serve to laterally restrain earth at a desired elevation in order to shape the topography of a site by managing slopes and creating usable spaces for development and construction of the built environment. Common types of retaining walls include mass/gravity walls, cantilevered walls, pile walls, and mechanically stabilized earth (MSE) walls. The design and construction of such walls are not well covered in the International Residential Code (IRC) and/or the International Building Code (IBC). As structural elements subjected to applied soil forces, retaining walls cross engineering disciplines, and a successful design often requires careful coordination between geotechnical engineers and structural engineers. In addition, successful construction often requires field verification of expected geotechnical parameters and construction oversight to ensure compliance with design specifications. This paper will explore the different stability checks (e.g., internal stability, local stability, and global stability), as well as different factors of safety, required for the proper design of a retaining wall. In addition, it will use real-world case studies to explore failures of various retaining walls, highlighting differences between compliance analysis and forensic failure analysis to identify the root cause of the failure and the responsible party.

Keywords

Active pressure, at-rest pressure, compliance analysis, cosmetic distress, external stability, factor of safety, failure analysis, functional distress, global stability, internal stability, local stability, mass/gravity retaining wall, mechanically stabilized earth (MSE), passive pressure, reinforced zone, safety factor, scarp

Background and Common Types of Retaining Walls

The term "retaining wall" is a broad term that encompasses a family of structures that create vertical grade separation. In general, retaining walls fall into two categories based upon the mechanics of external resistance: gravity walls and cantilevered walls. Gravity retaining walls utilize the geometry and self-weight of the wall mass (as well as the vertical weight component of the overlying soil mass) to transfer the driving forces on the wall to vertical loads and frictional forces on the foundation soils. Cantilevered retaining walls utilize the strength/stiffness of a vertical element to transfer the driving forces on the wall to vertical loads, lateral loads, and frictional forces on the foundation soils. Both categories require the retaining wall structure to be capable of transmitting the external loads to the foundation soils for resistance. Examples of a cantilevered retaining wall system and a gravity retaining wall system are provided in **Figure 1**.

Gravity retaining walls rely primarily on mass, width, and friction interaction with the foundation soils to resist sliding, overturning, and soil bearing failures. The basic techniques used for these walls date back thousands of years to the use of stacked stones or soils reinforced with internal layers of materials capable of resisting tension forces. Advancements in concrete and steel have led to current gravity systems such as cast-in-place concrete, mechanically stabilized earth (MSE), precast block, soil nail, and gabion basket; however, the stacked/mortared-stone

Brian C. Eubanks, PE, DFE, 6275 W. Plano Parkway, Suite 140, Plano, Texas 75093, (469) 892-7520, info@pseglobal.com

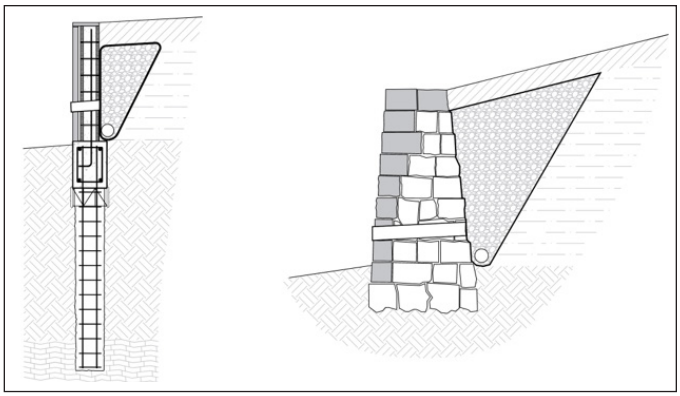

Figure 1
Exemplary cantilevered retaining wall (concrete masonry unit, CMU, stem on cast-in-place concrete beam on cast-in-place concrete piers, left) and gravity retaining wall (mortared stone, right).

wall is still instrumental in commercial and private development.

Common advantages of gravity walls include their relative ease of construction and control of materials. Wall components can often be placed by hand or with equipment already used for the construction of the project. The wall materials, as well as the backfill materials loading the wall, can be designed and specified by an engineer, and the foundation soils can be improved with limited additional effort. MSE, precast block, gabion, soil nail, and stacked/mortared-stone gravity retaining walls tolerate a greater degree of vertical and horizontal movement due to the fact that the components are not rigidly connected, and the individual components are relatively small with respect to the overall wall mass. For this reason, these types of gravity retaining walls are considered "flexible" in nature. The aforementioned types of gravity retaining wall structures continue to perform their intended function even with cracks/separations between elements of the wall and/or lateral/vertical movement of the wall from its original position. Challenges for gravity walls often include the width of the retaining wall mass, which can be greater than the height of the retaining wall in certain conditions, controlling the placement of fill materials and global stability.

Cantilevered retaining walls utilize relatively slender structural elements that are partially buried/embedded below grade, such that the soil at depth provides fixity for the base of the wall and the upper portion of the wall cantilevers upward to retain a mass of soil at a higher elevation. Cantilevered wall systems include reinforced concrete and/or concrete masonry unit (CMU) stem walls supported on piers, sheet pile walls, and pile walls. A cantilevered wall must be designed with adequate strength, stiffness, and rigidity to transfer the loads from behind the wall horizontally into the soil/rock in front of the wall.

Common advantages of cantilevered retaining walls include their relatively narrow footprint and the ability for some types to be installed before mass grading or excavation. Challenges include construction costs (specialized equipment and contractors are often required), practical limitations on height (though modifications exist to address this), and limited control of soils/drainage. Some cantilevered wall systems can be utilized for groundwater cutoff; however, this is also dependent upon the soil layering.

Governing Documents

The International Residential Code (IRC) typically governs the construction of single-family and townhouse-style residential dwelling structures as well as associated ancillary structures [1]. The International Building Code (IBC) typically governs the construction of all other structures intended for human use/occupancy (e.g., apartment complexes and commercial, industrial, educational, and institutional facilities) [2]. For the purpose of this discussion, the 2024 versions of the IRC and IBC will be considered.

Section R404.4 of the 2024 IRC includes provisions that require retaining walls to be designed in accordance with accepted engineering practice when: 1) the wall is not laterally supported at the top, and it retains in excess of 48 inches of unbalanced fill; or 2) the wall exceeds 24 inches in height and resists lateral loads, such as traffic surcharge, in addition to soil loads. In addition, the 2024 IRC explicitly requires that retaining wall designs consider stability against overturning, sliding, excessive foundation pressure, and water uplift.

Similar to the 2024 IRC, Section 1807.2.1 of the 2024 IBC explicitly requires that the design of retaining walls consider stability against overturning, sliding, excessive foundation pressure, and water uplift. Unlike the 2024 IRC, the 2024 IBC does not offer any exceptions to design/engineering requirements with respect to retaining walls that retain 48 inches or less of unbalanced fill without surcharge loads. The 2024 IBC includes prescriptive lateral soil loads that shall be used for the design of retaining walls unless such lateral loads are determined by a geotechnical investigation. Retaining walls in certain seismic locations require additional seismic loads to be applied; however, a discussion of seismic considerations is beyond the scope of this paper. Sections of the 2024

IBC applicable to the design and construction of retaining walls include Sections 1807.2, 1807.2.1, 1807.2.2, 1807.2.3, and 1807.2.4.

With respect to retaining walls, the factor of safety is defined as the load/pressure capacity of an element/component divided by the actual load/pressure applied to the element/component [3]. For example, if the sliding resistance (capacity) of a retaining wall is determined to be 12,000 pounds and the applied sliding force is determined to be 6,000 pounds, the factor of safety would be determined by dividing 12,000 pounds (capacity) by 6,000 pounds (actual load) to yield a factor of safety equal to 2.0.

The 2024 IRC specifies that retaining walls must be designed for a minimum factor of safety of 1.5 against lateral sliding and overturning. The 2024 IRC does not include minimum required factors of safety for bearing capacity of the soil or global stability. Similar to the 2024 IRC, the 2024 IBC also specifies that retaining walls must be designed for a minimum factor of safety of 1.5 against lateral sliding and overturning. The 2024 IBC also does not include a minimum required factor of safety for bearing capacity of the soil or global stability. A common factor of safety to consider for bearing capacity is 3.0, which is typically determined by the geotechnical engineer-of-record and reported in a site-specific geotechnical investigation report. A common factor of safety to consider for global stability is 1.5.

It should be noted that the 2024 IRC and the 2024 IBC do not include explicit requirements for geotechnical investigations for the design and/or construction of retaining walls. In the absence of a site-specific geotechnical investigation, a design engineer may be able to consider information and data from other sources, such as the Web Soil Survey by the United States Department of Agriculture (USDA) Natural Resources Conservation Services or data obtained from geotechnical investigations previously performed on nearby sites, if available [4].

While the IRC and IBC specify when a retaining wall must be designed in accordance with accepted engineering practice, the aforementioned codes do not provide any guidance for such engineering. Design guidance for a wide range of gravity and cantilevered wall types, including guidance for geotechnical investigations and design parameters, can be found in manuals published by the American Association of State Highway and Transportation Officials (AASHTO) and the Federal Highway Administration (FHWA). The current edition of these manuals, such as the *AASHTO LRFD Bridge Design Specifications*, Tenth Edition (2024) by AASHTO, utilizes load and resistance factor design (LRFD), which is a different methodology than the factor of safety previously described [5]. These manuals may be further adapted to specific state conditions through the state's department of transportation. Use of these design manuals and their associated construction specifications is common for state and municipal projects; however, implementation in commercial and residential projects varies based upon the engineer and contractors involved.

The *Design Manual for Segmental Retaining Walls*, 3rd Edition (Revised 2010) by the National Concrete Masonry Association (NCMA), as well as associated construction manuals, are typically used in commercial and residential projects [6]. These manuals specifically apply to walls utilizing precast facing elements with or without reinforced soils and precast modular block walls.

Retaining Wall Terminology

To facilitate the forthcoming discussion of retaining wall design, analysis, and forensic investigation, it is necessary to define basic retaining wall terminology. For orientation purposes, the side of the wall that is exposed at the change in grade elevation (i.e., the side facing the lower grade) is considered the front of the wall. The side of the wall that is contacted by the retained soil (i.e., the side facing the retained soil) is considered the back of the wall.

The **toe** of the wall is the portion of the foundation/footing near the front of the wall. The **heel** is the portion of the foundation/footing opposite the toe. **Active pressure** is the lateral earth pressure applied to the back of a retaining wall that is allowed to deflect away from the soil/surcharge load. **At-rest pressure** is the lateral earth pressure applied to the back of a retaining wall that is not allowed to deflect away from the soil/surcharge load (e.g., basement walls that are braced at the top by a floor system). **Passive pressure** is the lateral earth pressure typically applied to the front embedded portion of a retaining wall to resist sliding.

Backfill is the mass of soil placed against the back of a retaining wall. The **foundation zone** is the mass of soil and/or rock below the wall or adjacent to the embedded portion of a cantilevered wall. In general, this zone extends two times the wall height below the wall and up to two times the wall height beyond the horizontal limits of the wall. The interface between the foundation zone and the bottom of the wall is where sliding is typically analyzed. The foundation zone provides resistance to sliding,

bearing, and global failures. The **retained zone** is the mass of soil and/or rock that the wall is retaining. The retained zone generally extends upward from the heel of the wall to the ground surface at an angle (generally around 45 degrees) that is dictated by the nature of the soil/material being retained. The retained zone produces or transfers the majority of the lateral forces on the wall.

Soil reinforcements are structural elements embedded within a soil mass in a pattern to create a cohesive soil mass known as the **reinforced zone. Retaining wall facing** is a structural component that transfers limited soil loading proximal to the face into the soil reinforcing elements for MSE, segmental block, and/or soil nail walls.

A retaining wall **footing** is the component of a gravity retaining wall that interfaces with the foundation zone. For MSE, soil nail, and block walls, the retaining wall footing is the base of the wall mass, including the reinforced zone. A **shear key** is often added to the footing of retaining walls in order to increase the sliding resistance of a retaining wall. A **stem** is the vertical component of a cast-in-place wall or a gravity block wall that is primarily transferring the lateral loads to the footing/foundation.

The front face of a retaining wall may be vertical or exhibit a batter. A **batter** on a retaining wall is the slope of the front face toward the backfill.

Basic retaining wall terminology for a cantilevered cast-in-place concrete gravity retaining wall is graphically illustrated in **Figure 2**. This type of wall is often referred to throughout the industry as a cantilevered retaining wall due to the fact that it incorporates a cast-in-place concrete stem that is "cantilevered" from the footing; however, this type of wall is actually a gravity retaining wall system, unless it is constructed on piers, due to the fact that it relies upon the mass of the concrete wall and the vertical weight component of the soil on the footing for stability.

Basic retaining wall terminology for an MSE retaining wall is provided in **Figure 3**.

Common forensic failure terms that the reader should be familiar with include a scarp, failure wedge, and toppling. A **scarp** is a relatively steep surface produced by differential movements of soil on each side of a rupture in the ground surface [7]. A head scarp commonly develops during retaining wall failures when the retained soil rotates as a result of shear failure. A **failure wedge** is the mass of soil behind the wall that moves in response to lateral wall displacement during sliding or toppling, representing the retained zone that generates active earth pressure on the wall. **Toppling** is a rotational failure mode in which the wall rotates forward about its base; this may result in complete overturning or be limited to the upper portions of the wall failing before the entire wall mass becomes unstable.

Design and Construction Professionals

Retaining walls are used to increase the usable footprint of a development by creating stable grade separations over relatively short distances. Because retaining walls involve multiple disciplines, their successful implementation requires careful coordination among the parties involved. The **owner** or **developer** establishes site use, operational constraints, aesthetic expectations, and performance

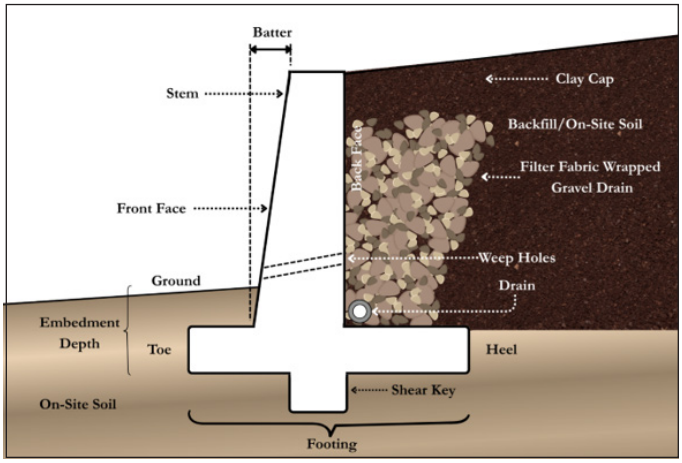

Figure 2
Basic retaining wall terminology for a typical battered cast-in-place cantilevered concrete gravity retaining wall.

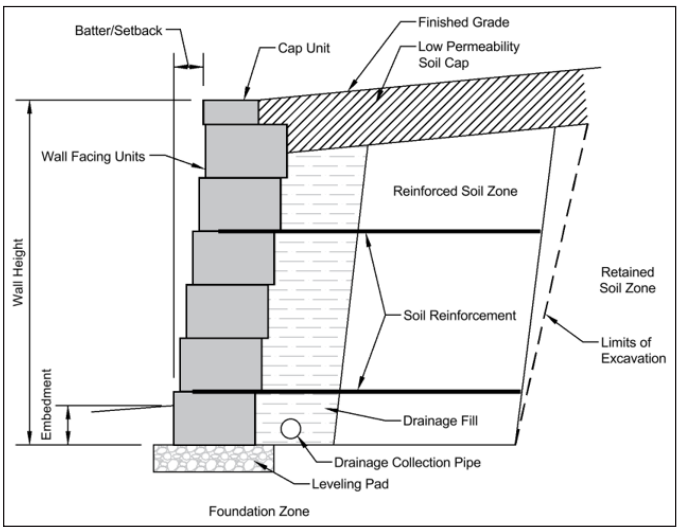

Figure 3
Basic retaining wall terminology for a typical mechanically stabilized earth (MSE) retaining wall.

expectations. The **civil engineer** and/or **landscape architect** defines the grading and drainage that establish wall location, geometry, exposed height, and adjacent conditions. The **geotechnical engineer** determines subsurface conditions and establishes appropriate soil parameters related to bearing capacity, settlement, applied soil pressures, and global stability, as well as recommendations for structural and reinforced fill materials. Using the combined information from the owner/developer, civil engineer, and geotechnical engineer, the **structural engineer** designs the wall to safely resist earth pressures, surcharge loads, and other applied forces, and to transfer those loads to the foundation soils. During construction, the **general contractor** coordinates all site activities, while the **wall subcontractor** constructs the wall and associated appurtenances. In deferred design contracts, a specialty **wall designer** provides the final structural design of proprietary wall systems. An **inspection and testing agency** observes construction and verifies that materials and workmanship comply with the approved plans and geotechnical recommendations.

Due to the fact that the responsibilities among the aforementioned parties are interdependent, coordination failures can occur during design development or construction. Common issues include retaining wall locations or heights that are not properly incorporated into the geotechnical investigation, which may result in incomplete soil data, missing settlement analyses, or missing global stability analyses. Changes in site grading may alter wall geometry or adjacent conditions and require redesign. Inadequate coordination of utilities can lead to field conflicts and differences between assumed and actual soil materials, particularly in deferred design scenarios or when fill sources change, which can compromise design assumptions if not communicated to the design team and inspection agency.

Wall Design/Stability Checks

To ensure that a retained soil mass remains stable behind a retaining wall, three stability requirements must be satisfied: internal stability, local/external stability, and global stability. Internal stability refers to the stability of the wall materials with respect to internal stresses that develop from the applied loads. Internal stability considerations include material strength, flexure/bending (i.e., moment), shear, reinforcement pull-out, tension, compression, and bond strength. Local/External stability refers to the stability of the retaining wall as a unit to resist external movement from the applied loads. Local/External stability considerations include sliding, overturning, and soil bearing. Global stability refers to the overall stability of the retaining wall system, including the retained soil mass, soil slopes, and surrounding site conditions. A global stability analysis evaluates potential slip planes that extend behind and/or below the retaining wall that may undermine the stability of the site. Refer to **Figure 4** for illustrations of different types of stability for a typical retaining wall.

Compliance Analysis Versus Failure Analysis

Compliance Analysis

A compliance analysis of a structure (e.g., retaining wall, building, pool, bridge, etc.) is an analysis that evaluates whether the structure was designed and/or constructed in accordance with the applicable requirements. A design-compliance analysis involves comparing the as-designed structure with applicable building codes, design standards, and/or geotechnical parameters. A construction-compliance analysis involves comparing the as-built structure with applicable construction documents, engineering designs, and/or industry construction standards. A design-compliance analysis may also be performed on an existing structure, in the absence of construction plans, to determine compliance with applicable provisions of a building code. In such cases, it might be possible to determine that a deficiency exists; however, it may not be possible to determine whether the deficiency constitutes a design deficiency or a construction deficiency.

With respect to retaining walls, one should consider that exact compliance with applicable building codes, construction documents, and/or industry standards may not be necessary in order to achieve a retaining wall that performs its intended function. Due to the degree of uncertainty associated with geotechnical science, in

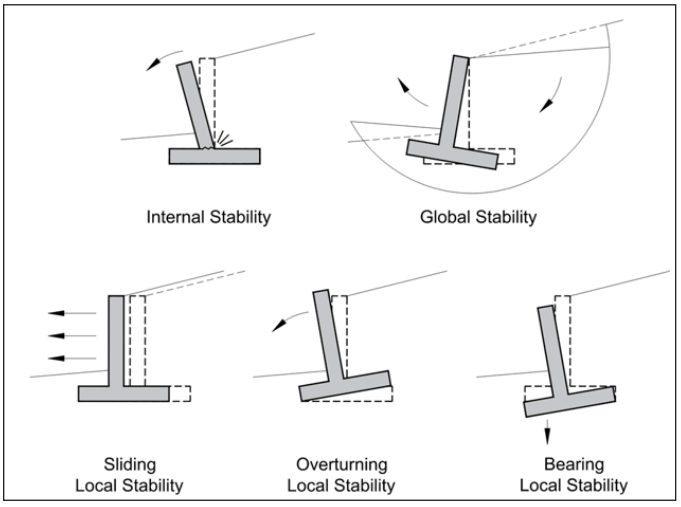

Figure 4
Different types of stability of a typical retaining wall.

conjunction with applied factors of safety, the presence of a design/construction variance relative to the applicable building codes, construction documents, and/or industry standards does not automatically equate to a retaining wall that will not perform its intended function.

When evaluating factors of safety, a value below the specified factor of safety does not establish the cause of a failure. Specifically, for failure mechanisms such as sliding, overturning, and bearing, only a factor of safety less than 1.0 suggests a potential correlation to a failure. For global stability, a factor of safety of less than 1.3 may suggest a potential correlation to failure. A compliance analysis can be performed even if a retaining wall does not exhibit any salient signs of distress or failure. This is commonly performed as a preventive measure to identify the potential presence of any latent deficiencies that could potentially affect long-term performance.

Failure Analysis

While a compliance analysis can identify potential shortcomings in the design and/or construction of a structure for consideration as potential causes of a failure, a failure analysis of a structure is an analysis that determines the actual cause of the failure. For example, a compliance analysis may indicate that a retaining wall was designed and/or constructed to yield a factor of safety less than the specified factor of safety in soil bearing, sliding, overturning, and/or global stability; however, the actual cause of the failure may have only been associated with one of the aforementioned mechanisms. A failure analysis can be useful to identify one or more parties responsible for the failure (and resultant damage) as well as to develop an appropriate scope of remediation. A failure analysis may include gathering background information, performing visual observations of the failed retaining wall, intrusive investigations, a forensic geotechnical investigation, materials testing, and/or engineering analyses.

Gathering background information may include obtaining the original construction documents, construction records, construction materials testing (CMT) reports, maintenance records, and/or a timeline of the failure.

Visual observations should attempt to document conditions consistent with a particular type of failure mechanism, such as soil bearing, sliding, overturning, internal stability, and/or global slope stability. In addition, observations should also document the drainage conditions in proximity to the retaining wall (i.e., positive drainage, negative drainage, ponding water, etc.), soil conditions (i.e., erosion, scour, saturated soil, dry soil, etc.), backfill conditions (i.e., drainage gravel, drainage system, general soil type, retained soil slope, etc.), measurements of wall geometry (i.e., cross-section dimensions, retained height of wall, embedment depth of wall, etc.), and measurements of movement (i.e., plumbness of wall face, plumbness of fence posts on top of the wall, relative elevations along the top of the wall, out-of-plane offset distance across cracks/separations).

Intrusive investigations may be necessary in order to obtain additional information. Test pit excavations, in which soil is removed near the toe of the wall or from behind the wall, are one form of intrusive investigation that may be necessary to determine backfill conditions and/or cross-sectional geometry of a retaining wall.

A forensic geotechnical investigation may be necessary to determine the soil properties and design parameters necessary to analyze the wall for internal stability, local/external stability, and global stability. A forensic geotechnical investigation should consider the different soil conditions that may affect the performance of a retaining wall, such as the backfill material, the material at the base of the wall, and any stratum of soil that may affect global stability.

Engineering analyses of the retaining wall should be performed utilizing information that closely resembles the state of the retaining wall and/or soil conditions at the time that the failure occurred. Typically, an analysis of the as-designed wall is beneficial to determine if the original design was acceptable, and an analysis of the as-built wall is beneficial to determine the actual cause of the failure.

Cosmetic Distress Versus Functional Distress

Distress in structures (e.g., retaining walls, buildings, pools, bridges, etc.) may be classified as cosmetic distress or functional distress. Cosmetic distress is that which may affect the appearance of the structure but does not affect the structural integrity or performance of the structure. Functional distress is that which affects the structural integrity and/or performance of the structure.

With respect to retaining walls, examples of cosmetic distress include mortar cracks/separations in a mortared-stone retaining wall as well as non-structural cracks/separations causally related to differential movement in concrete or CMU. Cracks/separations in mortar, concrete, and CMU can be related to a number of mechanisms, including, but not limited to, lateral yielding from applied

earth pressure, differential soil movement, and/or thermal expansion and contraction. Mortar cracks/separations in a mortared-stone retaining wall that are causally related to thermal expansion/contraction, differential soil movement, and/or nominal rotation are considered to be cosmetic distress and typically do not adversely affect the function of the retaining wall. Remediation of cosmetic mortar cracks/separations often includes repointing mortar joints and/or resetting displaced stones. Remediation of cosmetic distress should be expected, and it is typically considered a maintenance activity. There is oftentimes a trade-off between initial cost of construction and subsequent maintenance. For example, a mortared-stone retaining wall typically exhibits a lower initial cost of construction relative to a cantilevered wall; however, it may require periodic maintenance to maintain a desirable aesthetic appearance, whereas a cantilevered retaining wall typically exhibits a higher initial cost but may require less maintenance to maintain a desirable aesthetic appearance.

Functional distress includes resultant distress from movement mechanisms such as sliding, rotation/overturning, and bulging of the retaining wall beyond that which is expected by the nature of the design. A retaining wall may exhibit signs of functional distress without a catastrophic failure. Retaining walls that exhibit signs of functional distress, but have not yet experienced a catastrophic failure, can often be remediated in place rather than being removed and replaced. Remediation strategies typically focus on stabilizing the retaining wall, improving drainage, reinforcing soils, and/or mitigating erosion or scour. Stabilization of mortared-stone retaining walls typically includes the addition of mortared-stone to increase the mass of the wall, which reduces pressures on the underlying soil by spreading the load across a larger footprint, thereby increasing the factor of safety against soil bearing, sliding, and rotation/overturning.

Remediation of reinforced concrete/CMU retaining walls and MSE retaining walls typically includes the installation of soil anchors, tie-backs, or dead-man anchors. Drainage improvements, such as the installation of a drainage system, weep holes, and/or gravel backfill, help relieve hydrostatic pressure and reduce lateral load. Erosion and scour control measures, such as the addition of riprap, concrete footings, vegetative cover, and/or geotextile mats, help prevent undermining and surface erosion. These combined approaches can restore performance, extend service life, and mitigate future distress without full reconstruction.

Case Study #1: Failure of a Mechanically Stabilized Earth (MSE) Retaining Wall

A property located in north Texas was developed with a warehouse building as well as associated surface pavements for parking lots, driveways, and loading docks. The natural topography of the site generally sloped downward prior to construction, and development of the site required the construction of a retaining wall in order to create a more level building pad for the proposed improvements.

The retaining wall that is the subject of this matter is a mechanically stabilized earth (MSE) retaining wall comprised of dry-stacked masonry units (without mortar) connected by integrated shear keys and restrained by geosynthetic reinforcement grids (geogrid) that extend into the backfill behind the wall. The subject retaining wall is approximately 765 feet in length and ranges in height from approximately 1 foot to 20 feet tall (ground elevation differential plus footing). The ground surface behind the retaining wall (high side of wall) was specified to be graded with slopes that varied up to 1 unit vertical to 4 units horizontal (approximately 14 degrees). Approximately two-and-a-half years following completion of construction of the retaining wall, a portion of the wall, approximately 80 feet in length, failed when it translated toward the north (**Figure 5**).

The authors served as consultants for the engineer-of-record and were tasked with providing opinions regarding the design and construction of the subject retaining wall.

At the time of the initial site visit following the wall failure, scarps were observed behind the subject retaining wall (high side of wall), and portions of the subject retaining wall were observed to exhibit rotation, with the top of the wall leaning inward toward the backfill. In addition, weep mechanisms through the retaining wall were observed to be exposed by temporary excavations where they were previously blocked/occluded by soil prior to/during the failure of the retaining wall. The retaining wall exhibited the presence of bulging, with cracks in some of the blocks, and it also exhibited signs of sliding outward at the base.

Geotechnical Engineer-of-Record and Structural Engineer-of-Record

According to the original-construction geotechnical report issued for development of the subject property, the geotechnical engineer-of-record was aware that retaining walls were intended to be constructed on the property, and

Figure 5
Google Street View image of MSE retaining wall post-failure from April 2019 [8].

geotechnical borings were specifically located and identified as being applicable for the retaining walls; however, the geotechnical engineer-of-record did not provide site-specific soil parameters for the design of retaining walls within the report. As a result, the structural engineer-of-record for the subject retaining wall reportedly based the design upon expected soil parameters. The structural engineer-of-record for the retaining wall specified that the owner's representative bear responsibility to review and verify the applicability of the expected soil parameters with respect to the actual site conditions prior to construction. In addition, the structural engineer-of-record excluded global stability analysis from its scope of services.

Crushed Concrete Substitution for Drainage Gravel

The contractor who constructed the subject retaining wall reportedly installed crushed concrete instead of the specified drainage gravel behind the wall. Previously demolished concrete can be crushed and recycled for use in lieu of gravel in some construction applications; however, it is not always suitable for such uses. The pH value of crushed concrete can potentially cause degradation of the geogrid over time. Also, the use of crushed concrete aggregates is not typically considered suitable for drainage applications due to the potential for cementitious particles to rehydrate and harden when mixed with water, as well as the fact that excessive fines can cause reductions in hydraulic conductivity of the system over time.

Reinforced Zone Soil Material

After the failure of the subject retaining wall, site-specific soil samples were obtained by investigators for geotechnical laboratory testing. One of the aforementioned samples was obtained from the reinforced zone of the subject retaining wall. Based upon the tests of the soil obtained from the reinforced zone, it was reportedly determined that the soil exhibited a plasticity index (PI) of 25 percent and fines (material passing a No. 200 sieve) of 65.9 percent. The structural engineer-of-record for the subject retaining wall specified that the soil in the reinforced zone of the retaining wall was to exhibit a plasticity index less than or equal to 15 percent and fines less than 35 percent. As a result, the soil placed within the reinforced zone of the subject retaining wall was not compliant with the specifications for the design of the wall.

A relationship between the PI of a soil and its inherent swelling capacity was documented and qualitatively categorized by Terzaghi, Peck, and Mesri (1996) [9]. According to the plasticity index specified in the structural engineering drawings for the subject retaining wall (PI of less than 15), the shrink-swell potential of the material specified to be placed within the reinforced zone was classified as "medium." Based upon the reported plasticity index of the non-compliant soil that had actually been placed within the reinforced zone, the shrink-swell potential of the material was classified as "high." As a result, the additional swelling/expansion potential of the soil material from the addition of water would increase the lateral earth pressure applied to the retaining wall. In addition, due to the presence of an increased percentage of fines, the backfill material would not drain as easily and would not engage the geogrid as effectively as a soil material with fewer fines.

Rain Event

The failure of the subject retaining wall occurred in early January 2019. Dallas Love Field Airport, which is located approximately 5 to 6 miles from the subject retaining wall, recorded approximately 4.42 inches of rainfall over a period of nine days shortly before the wall failed. Near the toe of the subject retaining wall was a drainage channel/swale. Due to the presence of multiple rainfall events leading up to the date of the failure, the soils exhibited a softened state with a reduced shear capacity. Softened soil is characterized by a strength reduction due to a change in the moisture content [10].

Finished Grade Slope

The ground surface behind the retaining wall (high side of the wall) was specified by the civil engineer-of-record to be graded with slopes that varied up to approximately 14 degrees. During the investigation of the wall failure, a land surveyor performed a topographic survey, and the actual as-built slopes were found to range from 14.1 to 18.5 degrees, with an average slope of 16.2 degrees, in proximity to the portion of the subject retaining wall that experienced a failure. As a result, the finished grade at the top of the subject retaining wall exhibited a slope that was greater than the specified slope considered in the design. An increased slope of the soil behind the subject retaining wall yielded an increased lateral earth pressure applied to the retaining wall.

Global Stability

As part of the investigation into the failure of the subject retaining wall, a global (slope) stability analysis of the "as-designed" retaining wall was performed with consideration of the expected soil parameters identified in the retaining wall design drawings. Based upon the aforementioned analysis, it was found that the wall design yielded factors of safety that were compliant with the specified factors of safety for internal stability and local/external stability; however, it was also found that the retaining wall design yielded factors of safety that were lower than the specified factors of safety for global stability. Even if the retaining wall had been constructed in perfect compliance with the structural engineering design drawings, the retaining wall would still have been at risk of a global stability failure. As previously mentioned, the structural engineer-of-record excluded global stability analysis from its scope of services.

As part of the investigation into the failure of the subject retaining wall, a global (slope) stability analysis of the "as-built" retaining wall was also performed with consideration of the actual site-specific soil parameters as determined from the post-construction forensic geotechnical investigation following the wall failure. Based upon the aforementioned analysis, it was found that the as-built retaining wall yielded factors of safety that were generally compliant with the specified factors of safety for internal stability and local/external stability; however, it was also found that the as-built retaining wall yielded factors of safety that were lower than the specified factors of safety for global stability.

Construction-Phase Observations

According to construction documents and contract agreements, one of the subcontractors involved in the construction of the subject retaining wall had agreed to arrange, coordinate, and obtain all construction-phase inspections for its work. According to *The Design Manual for Segmental Retaining Walls*, 3rd Edition by the NCMA [6], soil in the reinforced zone should be checked to ensure it meets specifications similar to how concrete and steel in cast-in-place concrete construction are inspected. The aforementioned document by the NCMA stated that the wall contractor is responsible for quality control of the wall installation, which includes performing necessary observation and testing to verify that work performed meets the minimum standards. Typically, construction-phase observations are performed by a representative of the structural engineer-of-record, as the structural engineer-of-record is the most familiar with the requirements of the design. It was found that the structural engineer-of-record for the subject retaining wall was never contacted during construction to perform any such construction-phase observations.

Findings

Based upon a design-compliance analysis, consultants identified pullout of geogrid, global stability, and/or sliding as potential failure mechanisms; however, based upon the observed mode of failure, in conjunction with a failure analysis, it was found that the cause of the failure was primarily related to global stability. The global stability failure was causally related to a lack of coordination between the owner, the geotechnical engineer-of-record, and the structural engineer-of-record as well as a lack of site-specific geotechnical design values. Contributory factors to the failure included non-compliant reinforced zone backfill material, non-compliant aggregates utilized in the drainage system, increased hydrostatic pressure from rain events and reduced drainability, and a lack of adequate construction-phase observations. Based upon the investigation, remediation of the as-built retaining wall was warranted. Remediation of

the subject retaining wall included a complete rebuild of the portions of the wall that failed and the addition of tie-backs to the non-failed portions of the wall.

Case Study #2: Evaluation and Remediation of a Mortared-Stone Retaining Wall

A residential development for hundreds of residential properties in north Texas included thousands of linear feet of mortared-stone retaining walls. The retaining walls were constructed within the subject development during the original mass grading activities on the land circa 2005 to create more-level building pads for the residential properties. According to governing documents, the owner's association for the subject development reportedly bears responsibility for maintenance and upkeep of the retaining walls. The subject retaining walls range in height from 1 foot, 0 inches to 5 foot, 6 inches tall above grade.

The authors served as consultants for the owner's association and were tasked with performing an evaluation of the retaining walls throughout the development in order to provide recommendations for remediation of the retaining walls, if necessary.

An initial site visit related to the mortared-stone retaining walls was performed on October 14, 2022. At the time of the initial site visit, portions of the subject retaining walls exhibited signs of bulging in the face of the wall, delaminated face stone, leaning/rotation/overturning, sliding, mortar separations, and separations at abutments with adjacent structures (i.e., monument sign structure, masonry column footings/pier caps, etc.).

A majority of the retaining walls were found to be performing as intended, with only signs of cosmetic distress consistent with distress that is to be expected in mortared-stone retaining wall construction. When the mass/geometry of a mortared-stone retaining wall is not being called into question, remediation of cosmetic distress in a mortared-stone retaining wall can be accomplished by having a mason clean out cracks/separations and repoint the mortar to achieve a more aesthetically pleasing appearance.

At locations where separations occurred between the mortared-stone retaining walls and adjacent structures, it was recommended to apply an elastomeric sealant to mitigate any water from flowing through the separation while still accommodating differential movement between the two structures.

Some portions of the mortared-stone retaining walls exhibited signs of bulging that appeared to be related to delaminated face stone, as shown in **Figure 6**. The aforementioned condition is considered to be cosmetic in nature; however, it can also pose a safety hazard due to the fact that a stone can fall off the face of the retaining wall. As a result, it was recommended that such conditions be remediated by the removal and reinstallation of the face stone at such locations.

In consideration of the portions of the mortared-stone retaining walls that exhibited signs of leaning/rotation/overturning and/or sliding, the walls were evaluated on a case-by-case basis. It was recommended to monitor portions of retaining walls that exhibited an inward lean with the top leaning toward the retained soil. In addition, it was recommended to perform additional investigation for retaining walls that exhibited an outward lean, with the top leaning away from the retained soil, in order to determine contributory factors associated with the lean/rotation/overturning and to provide remedial recommendations.

Some engineering judgment may be required to determine acceptable limits/thresholds at which mortared-stone retaining walls should be remediated versus monitoring. There was only one wall that exhibited a lean/rotation of a degree, such that it exhibited a reverse batter with the top of the wall away from the soil that it was retaining (**Figure 7**). The aforementioned retaining wall varied in

Figure 6
Photographs of mortared-stone retaining wall with bulge related to delaminated face stone.

Figure 7
View of mortared-stone retaining wall that exhibited a reverse batter (lean/rotation with the top away from the retained soil).

height from 2 feet to 5 feet tall, and it was approximately 185 feet in length. The aforementioned retaining wall will be considered the subject retaining wall for the remainder of this case study.

Exploratory test pit excavations were performed behind the subject retaining wall, as well as near the toe of the retaining wall, in proximity to the tallest portion of the wall, to establish the as-built cross-sectional geometry of the wall such that it could be modeled and analyzed. It should also be noted that the exploratory test pit excavation revealed that the backfill soil retained by the wall appeared to consist of on-site clay soil (i.e., not imported material).

A post-construction forensic geotechnical investigation was also performed to identify the in-situ soil properties and conditions to determine the geotechnical parameters necessary for evaluation of the retaining wall design/construction. Based upon the geotechnical investigation, the geotechnical engineer specified an allowable bearing pressure of 2,000 pounds per square foot, a minimum embedment depth of 24 inches, an equivalent fluid pressure of 65 pounds per cubic foot (pcf) for active conditions of on-site soil, an equivalent fluid pressure of 40 pcf for at-rest conditions of a free-draining gravel wedge backfill, an equivalent fluid pressure of 225 pounds pcf for passive conditions of on-site soil for resistance against sliding, and a coefficient of friction of 0.3 between the base of the retaining wall and the underlying clay soil.

As previously mentioned, the subject retaining walls were constructed circa 2005, and the subject investigation began in 2022. As a result, the original engineered design drawings were not available for review as part of the investigation. As such, a design-compliance and a construction-compliance analysis with respect to any original engineered design drawings could not be performed.

A compliance analysis was performed for the as-built retaining wall with respect to code-prescribed factors of safety for sliding and rotation, as well as allowable bearing pressures for the soil based upon the aforementioned geotechnical investigation. Based upon the compliance analysis, the as-built retaining wall did not provide adequate factors of safety for sliding or overturning, and the applied pressure on the soil beneath the base of the wall exceeded the allowable bearing pressure. In addition, trees that had been planted immediately behind the subject retaining wall likely exerted additional pressure upon the wall as the root systems of the trees increased in volume over time as the trees grew.

Due to the fact that mortared-stone retaining walls utilize their mass and geometry to resist applied forces, additional mortared stone can typically be added to an existing mortared-stone retaining wall to increase the mass and/or change the geometry as necessary to achieve an acceptable design. Based upon an analysis of the subject retaining wall, additional mortared stone would be necessary to increase the mass of the wall. In addition, it was necessary to replace the existing clay soil backfill with free-draining gravel backfill in order to reduce the lateral pressure on the wall and achieve an acceptable design. In order to implement the aforementioned remediation, the soil (and trees) behind the existing retaining wall would need to be excavated such that additional mortared stone could be added to increase the cross-sectional geometry, and the excavated backfill would need to be replaced with a wedge of gravel behind the retaining wall.

Findings

A compliance analysis determined that the as-built retaining wall did not achieve adequate/compliant factors of safety for sliding or overturning, and the applied pressure on the soil beneath the base of the wall exceeded the allowable bearing pressure. A failure analysis ruled out that the failure was causally related to sliding due to the fact that the footing/toe was restrained by a concrete sidewalk, and there were no salient signs of sliding. Based upon the mode of movement, which was rotation/overturning, a failure analysis determined that the failure

of the wall to perform as intended was causally related to lack of overturning/local stability and/or a bearing capacity failure. An analysis of the subject retaining wall found that it could be salvaged with modifications to the wall geometry and backfill; however, it was removed and replaced due to other considerations not related to the wall's performance.

Summary

Due to the fact that retaining walls involve multiple disciplines, the successful implementation of a retaining wall requires careful coordination amongst all parties involved, including but not limited to the owner/developer, landscape architect, civil engineer, geotechnical engineer, structural engineer, general contractor, specialty wall subcontractor, wall designer (for proprietary wall system), and/or inspection/testing agency.

The first case study presented herein offered an example of a wall failure that occurred primarily due to a global (slope) stability failure associated with a lack of site-specific geotechnical design parameters and the omission of a global (slope) stability analysis during the original design, which was exacerbated by multiple construction deficiencies associated with non-compliant reinforced zone backfill material, non-compliant aggregates utilized in the drainage system, increased hydrostatic pressure from rain events and reduced drainability, and a lack of adequate construction-phase observations.

The second case study presented herein offered an example of a wall failure that occurred due to local stability failures (overturning and/or bearing capacity) associated with the as-built geometry of the wall. An analysis of the retaining wall found that it could have been salvaged with modifications to the wall geometry and backfill; however, it was removed and replaced due to other considerations not related to the wall's performance.

Conclusion

A compliance analysis of a retaining wall is an analysis that evaluates whether the retaining wall was designed and/or constructed in accordance with the applicable requirements. While a compliance analysis can identify potential shortcomings in the design and/or construction of a retaining wall for consideration as potential causes of a failure, a failure analysis of a retaining wall is an analysis that determines the actual cause of the failure. A failure analysis of a retaining wall should be performed utilizing information that closely resembles the state of the retaining wall and/or soil conditions at the time the failure occurred.

Distress in retaining walls may be classified as cosmetic distress or functional distress. Remediation of cosmetic distress should be expected, and it is typically considered a maintenance activity. A retaining wall may exhibit signs of functional distress without a catastrophic failure. Retaining walls that exhibit signs of functional distress, but have not yet experienced a catastrophic failure, can often be remediated in place rather than being removed and replaced.

References

[1] International Code Council, *International Residential Code (IRC)*, 2024 ed. Falls Church, VA, USA: International Code Council, 2024.

[2] International Code Council, *International Building Code (IBC)*, 2024 ed. Falls Church, VA, USA: International Code Council, 2024.

[3] B. M. Das, *Principles of Foundation Engineering*, 6th ed. Stamford, CT, USA: Cengage Learning, 2007.

[4] U.S. Department of Agriculture, Natural Resources Conservation Service, "Web Soil Survey." [Online]. Available: https://websoilsurvey.nrcs.usda.gov/app/

[5] American Association of State Highway and Transportation Officials (AASHTO), *AASHTO LRFD Bridge Design Specifications*, 10th ed. Washington, DC, USA: AASHTO, 2024.

[6] National Concrete Masonry Association, *Design Manual for Segmental Retaining Walls*, 3rd ed., 5th printing. Herndon, VA, USA: National Concrete Masonry Association, Jan. 2012.

[7] L. Highland and P. Bobrowsky, *The Landslide Handbook: A Guide to Understanding Landslides*. Reston, VA, USA: U.S. Geological Survey, Nov. 15, 2008.

[8] Google, "Street View image of MSE retaining wall post-failure," Apr. 2019. [Online]. Available: https://maps.google.com

[9] K. Terzaghi, R. B. Peck, and G. Mesri, *Soil Mechanics in Engineering Practice*, 3rd ed. New York, NY, USA: John Wiley & Sons, 1996.

[10] S. G. Wright, J. G. Zornberg, and J. E. Aguettant, "The Fully Softened Shear Strength of High Plasticity Clays," Feb. 2007.